



**UCGE Reports
Number 20168**

Department of Geomatics Engineering

**Implementation and Analysis of GPS Ambiguity
Resolution Strategies in Single and Multiple Reference
Station Scenarios**

(URL: <http://www.geomatics.ucalgary.ca/links/GradTheses.html>)

by

Junjie Liu

January 2003



THE UNIVERSITY OF CALGARY

**Implementation and Analysis of GPS Ambiguity Resolution Strategies in Single and
Multiple Reference Station Scenarios**

by

Junjie Liu

A THESIS

SUBMITTED TO THE FACULTY OF GRADUATE STUDIES
IN PARTIAL FULFILMENT OF THE REQUIREMENTS FOR THE
DEGREE OF MASTER OF SCIENCE

DEPARTMENT OF GEOMATICS ENGINEERING

CALGARY, ALBERTA

January 20, 2003

© Junjie Liu 2002

ABSTRACT

The Global Positioning System (GPS) double-difference (DD) operations can effectively reduce or eliminate many errors innate to raw undifferenced carrier-phase observables, such as the atmospheric effects and satellite orbital error. Although the DD carrier phase is a much more precise observable than the pseudorange, it is ambiguous because of the constant, but unknown, initial integer number of carrier cycles. In order to fully exploit the carrier phase observable to achieve centimetre-level accuracy, this ambiguity needs to be resolved. For most real-time kinematic (RTK) applications, the main obstacle to successful ambiguity resolution is the DD ionospheric error. This issue is more notable during the time of a solar maximum when the DD ionospheric error may increase by a factor of three. Ambiguity resolution under the influence of the ionosphere has been under extensive investigation for the past decade, and numerous resolution strategies have been proposed.

In this research, several representative ambiguity-resolution strategies are compared. As a result, eight different ambiguity resolution strategies are implemented and investigated with an emphasis on the impact of the ionospheric error on positioning accuracy and ambiguity resolution. These eight strategies include the L1-only ambiguity resolution, widelane (WL) ambiguity resolution, combined L1 and L2 ambiguity resolution, ambiguity resolution using of ionosphere-free (IF) combination, and stochastic ionosphere modelling ambiguity resolution. All eight strategies are tested on three baselines ranging from 13 km to 43 km. In general, strategies that take the ionospheric

error into account in their estimation models give much better position and ambiguity results than those that do not, and the stochastic ionosphere modelling ambiguity resolution strategies give best performance in both the ambiguity and position domains. The impact of the different parameterization schemes is also investigated and it is found that parameterizing the L1 and L2 observables with respect to L1 and WL ambiguities versus L1 and L2 ambiguities does not bring significant gain in the ambiguity domain, while it does in the position domain.

ACKNOWLEDGEMENTS

First, I would like to express my deepest gratitude to my supervisor, Dr. Elizabeth Cannon. Her continuous encouragement and confidence in me are greatly appreciated. Without her support, both academic and financial, this thesis would not have been possible.

Second, I would like to thank my friends and fellow graduate students, Rakesh Nayak, Mark Petevello, Xiaobing Shen, Glenn Macgougan, Paul Alves, Kongze Chen, Kyle O’Keefe, Changlin Ma, Lei Dong, Xiaohong Zhang, Luiz Fortes, and Andrew Huang, to name a few, who provided a lot of valuable input to my research.

Third, I would like to thank Dr. Gerard Lachapelle for some financial support and good advice.

Fourth, I would like to thank Lance De Groot for helping with the data processing and experiments. He reminds me of how valuable and helpful an excellent intern can be. I also would like to thank Mr. Giovanni Pugliano of Università Degli Studi Di Napoli “Parthenope”, for making the Campania, Italy, data, available for analysis in this thesis.

Last, and most of all, I would like to thank my parents, sister and especially my Jian, who makes everything meaningful.

TABLE OF CONTENTS

ABSTRACT	iii
ACKNOWLEDGEMENTS.....	v
TABLE OF CONTENTS.....	vi
LIST OF TABLES.....	viii
LIST OF FIGURES	x
NOTATION.....	xiii
1.0 INTRODUCTION.....	1
1.1 Background and Objectives	1
1.2 Thesis Outline.....	7
2.0 GPS OBSERVABLES AND ERROR SOURCES.....	9
2.1 Basic GPS Observables	9
2.2 GPS Error Sources	13
2.2.1 Satellite Orbital Error	13
2.2.2 Tropospheric Error	15
2.2.3 Ionospheric Error	17
2.2.4 Multipath.....	21
2.2.5 Measurement Noise.....	22
2.3 Phase Combinations	22
2.3.1 Widelane Combination (WL)	24
2.3.2 Narrowlane Combination (NL).....	25
2.3.3 Ionosphere-free Combination (IF).....	26
3.0 GPS AMBIGUITY RESOLUTION	32
3.1 Introduction.....	32
3.1.1 Float Filter Procedure.....	33
3.2 Ambiguity Resolution.....	40
3.2.1 LAMBDA Method.....	41

3.2.2 Bootstrapping Method.....	42
3.3 Tests and Results.....	44
3.3.1 Results with LAMBDA.....	44
3.3.2 Results with Bootstrapping.....	46
3.4 Suggested Ambiguity Resolution Method.....	48
4.0 AMBIGUITY RESOLUTION STRATEGIES.....	53
4.1 Introduction.....	53
4.2 Strategy Formulation.....	54
4.2.1 Strategy 1 (use CP_1 , CP_2 and P):.....	55
4.2.2 Strategy 2 (use CP_1 , CP_2 and P):.....	56
4.2.3 Strategy 3 (use CP_1 , CP_2 and P):.....	57
4.2.4 Strategy 4 (use CP_1 , CP_2 and P):.....	58
4.2.5 Strategy 5 (use CP_1 , CP_2 and P):.....	59
4.2.6 Strategy 6 (use CP_1 , CP_2 and P):.....	61
4.2.7 Strategy 7 (use CP_1 , CP_2 and P):.....	62
4.2.8 Strategy 8 (use CP_1 , CP_2 and P):.....	63
4.3 Software Realization.....	64
5.0 SINGLE AND MULTIPLE REFERENCE STATION TESTS AND RESULTS..	69
5.1 Introduction.....	69
5.2 Single Reference Station Tests and Results.....	69
5.2.1 Results.....	73
5.3 Multiple Reference Station Tests and Results.....	112
5.3.1 Test Setup.....	115
5.3.2 Results.....	118
5.4 Summary.....	125
6.0 CONCLUSIONS AND RECOMMENDATIONS.....	127
REFERENCES.....	132
APPENDIX: QUALITY CONTROL IN GPS CARRIER PHASE POSITIONING.....	142

LIST OF TABLES

Table 2.1 Baseline Errors due to Residual Tropospheric Error	16
Table 2.2 L1/L2/WL/NL/IF Combination Properties	27
Table 2.3 RMS Position Errors (cm) with Bernese Ambiguities, 26 km Baseline	28
Table 3.1 LAMBDA and Bootstrapping Comparison	48
Table 4.1 Strategy Summary	55
Table 4.2 Software Functionality.....	65
Table 5.1 Observation Standard Deviations	72
Table 5.2 24-hour-run Position Estimate RMS (cm) for Test Baseline 1	75
Table 5.3 Percentage of Ambiguities Resolved Correctly (%).....	75
Table 5.4 600-second-run Statistics, 13 km Baseline	85
Table 5.5 Position RMS (cm) for 600-second-run, 13 km Baseline.....	86
Table 5.6 24-hour-run Position Estimate RMS (cm) for Test Baseline 2	88
Table 5.7 Percentage of Ambiguities Resolved Correctly (%), 26 km Baseline.....	88
Table 5.8 600-second-run Statistics, 26 km Baseline	98
Table 5.9 Position RMS (cm) for 600-second-run, 26 km Baseline.....	99
Table 5.10 24-hour-run Position Estimate RMS (cm) for Test Baseline 3	100
Table 5.11 Percentage of Ambiguities Resolved Correctly (%), 43 km Baseline	100
Table 5.12 900-second-run Statistics, 43 km Baseline.....	111
Table 5.13 RMS Position (cm) for 900-second-run, 43 km Baseline	112
Table 5.14 RMS Position Errors, Strategy 1.....	119

Table 5.15 RMS Position Errors, Strategy 2.....	120
Table 5.16 RMS Position Errors, Strategy 3.....	121
Table 5.17 RMS Position Errors, Strategy 4.....	122
Table 5.18 RMS Position Errors, Strategy 7.....	123
Table 5.19 RMS Position Errors, Strategy 8.....	124
Table A1 Carrier Phase Cycle Slips Detection Summary	147
Table A2 Simulated Cycle Slips	147
Table A3 Detected Cycle Slips.....	148

LIST OF FIGURES

Figure 1.1 Typical DGPS Configuration.....	2
Figure 2.1 Double Differencing Concept	11
Figure 2.2 Orbit Error vs. Baseline Lengths for Certain SV Orbit Induced Error Thresholds	15
Figure 2.3 DD Ionospheric Error on L1 for a 21.6 km Baseline in Italy.....	28
Figure 2.4 L1 Position Errors	30
Figure 2.5 L2 Position Errors	30
Figure 2.6 WL Position Errors	31
Figure 2.7 IF Position Errors	31
Figure 3.1 DD Carrier Phase Positioning Flowchart (Cannon, 2002)	33
Figure 3.2 Linearized Kalman Filter Loop (Brown and Hwang, 1992)	34
Figure 3.3 Position Errors with LAMBDA Method.....	45
Figure 3.4 Ambiguity Difference between LAMBDA and Bernese Approaches	45
Figure 3.5 Position Errors with Bootstrapping Method.....	46
Figure 3.6 Ambiguity Differences between Bootstrapping and Bernese Approaches.....	47
Figure 4.1 Tropospheric Delay Model Classes.....	67
Figure 4.2 Data Handling Class	68
Figure 5.1 Test Set-up	71
Figure 5.2 DD Ionospheric Errors on L1, 13 km Baseline.....	73
Figure 5.3 Position Errors and Ambiguity Comparison, Strategy 1	76

Figure 5.4 Position Errors, Strategy 2	77
Figure 5.5 Position Errors and Ambiguity Comparison, Strategy 3	78
Figure 5.6 Position Errors and Ambiguity Comparison, Strategy 4	79
Figure 5.7 Position Errors, Strategy 5	80
Figure 5.8 Position Errors, Strategy 6	81
Figure 5.9 Position Errors, Strategy 7	82
Figure 5.10 Position Errors, Strategy 8	83
Figure 5.11 DD Ionospheric Errors on L1, 26 km Baseline	87
Figure 5.12 Position Errors and Ambiguity Comparison, Strategy 1	89
Figure 5.13 Position Errors, Strategy 2	90
Figure 5.14 Position Errors and Ambiguity Comparison, Strategy 3	91
Figure 5.15 Position Errors and Ambiguity Comparison, Strategy 4	92
Figure 5.16 Position Errors, Strategy 5	93
Figure 5.17 Position Errors, Strategy 6	94
Figure 5.18 Position Errors, Strategy 7	95
Figure 5.19 Position Errors, Strategy 8	96
Figure 5.20 DD Ionospheric Errors on L1, 43 km Baseline	99
Figure 5.21 Position Errors and Ambiguity Comparison, Strategy 1	101
Figure 5.22 Position Errors, Strategy 2	102
Figure 5.23 Position Errors and Ambiguity Comparison, Strategy 3	103
Figure 5.24 Position Errors and Ambiguity Comparison, Strategy 4	104
Figure 5.25 Position Errors and Ambiguity Comparison, Strategy 5	105
Figure 5.26 Position Errors, Strategy 6	106

Figure 5.27 Position Errors and Ambiguity Comparison, Strategy 7	108
Figure 5.28 Position Errors and Ambiguity Comparison, Strategy 8	109
Figure 5.29 A GPS MultiRef Network.....	114
Figure 5.30 Real Time Test Flow Chart.....	115
Figure 5.31 Calgary MultiRef Network Configuration	117
Figure 5.32 Real Time Position Errors with Strategy 1	118
Figure 5.33 Real Time Position Errors with Strategy 2.....	120
Figure 5.34 Real Time Position Errors with Strategy 3.....	121
Figure 5.35 Real Time Position Errors with Strategy 4.....	122
Figure 5.36 Real Time Position Errors with Strategy 7.....	123
Figure 5.37 Real Time Position Errors with Strategy 8.....	124
Figure A1 Linearized Kalman Filter Loop.....	144
Figure A2 Sky Plot	146
Figure A3 Test Statistics t^k versus GPS Time.....	146

NOTATION

i) Symbols

c	speed of light (m/s)
$C_{\hat{N}}$	variance covariance matrix of the float ambiguities
CP	carrier phase observable (cycle)
$C_{\hat{v}}$	innovation sequence variance-covariance matrix
dT_u^0	receiver clock offset (s)
dT_0^s	satellite clock offset (s)
e	combined effect of measurement noise, multipath and residual tropospheric delay after applying a tropospheric model
E	satellite elevation angle ($^\circ$)
F	cumulative distribution function of a normal Gaussian distribution
h	ellipsoidal height (metre)
\dot{h}	vertical velocity (m/s)
H	design matrix
I	ionospheric delay (m)
L1	GPS signal transmitted at a frequency of 1575.42 MHz
L2	GPS signal transmitted at a frequency of 1226.70 MHz
m	number of observations
N	phase ambiguity (cycle)
\hat{N}	float-valued DD phase ambiguity (cycle)

\tilde{N}	integer-valued DD phase ambiguity (cycle)
P	pseudorange observable (m)
Q	noise variance-covariance matrix
r	degree of freedom
sp	spectral density
T	tropospheric delay (m)
T_u	time of reception (s)
T^s	time of transmission (s)
T_0	time constant of a first-order Gauss-Markov process
u	number of unknowns
w	system driving noise
z	observation vector
r	true geometric range (m)
dr	satellite orbital error (m)
l	GPS carrier wavelength (m)
$\nabla\Delta$	double differencing operator
e_{CP}	the combined effect of carrier multipath and receiver measurement noise in cycles
e_p	the combined effect of pseudorange multipath and receiver measurement noise in metres (m)
d	ratio threshold

Φ	transition matrix
j	latitude (rad)
l	longitude (rad)
\dot{j}	latitude rate (rad/s)
\dot{l}	longitude rate (rad/s)

ii) Acronyms

C/A	Coarse Acquisition
DD	Double Difference
DGPS	Differential GPS
GM	Gauss-Markov
GPS	Global Positioning System
IF	Ionospheric Free
IP	Internet Protocol
LAMBDA	Least Squares Ambiguity Search Adjustment
MDB	Minimum Detectable Bias
MPC	Modulated Precision Clock
MultiRef	Multiple Reference
NL	Narrowlane
NMEA	National Marine Electronics Association
P-Code	Precise Code
PPS	Precise Positioning Service

PRN	Pseudorandom Noise
RMS	Root Mean Square
RTK	Real Time Kinematic
SA	Selective Availability
SD	Single Difference
SPS	Standard Positioning Service
STD	Standard Deviation
TCP	Transmission Control Protocol
TEC	Total Electron Content
VC	Variance Covariance
VRS	Virtual Reference Station
WAAS	Wide Area Augmentation System
WGS84	World Geodetic System of 1984
WL	Widelane

CHAPTER 1

INTRODUCTION

1.1 Background and Objectives

The Global Positioning System (GPS) Standard Positioning Service (SPS) provides positioning accuracies of approximately 13 m in the horizontal and 22 m in the vertical at a 95% probability level (U.S. Department of Defense, 2001). However, many civil applications such as dredging, harbour guidance, and offshore oil exploration require accuracies in the metre to sub-metre levels (Lachapelle, 2000). This cannot be met by the SPS of GPS.

To meet the aforementioned accuracy specifications, differential GPS (DGPS) is used in which relative positioning between two GPS receivers using GPS pseudorange observables is performed. The differencing operation in DGPS effectively removes many errors from the raw GPS pseudorange observables since most of these errors are highly correlated between receivers. As a result, the accuracy and precision of the SPS can be dramatically increased. Figure 1.1 shows the usual configuration of a DGPS system. The reference GPS station and the rovers (e.g. ship, surveyor) all track the same satellites. The error can be computed for the reference station observable to each satellite if the coordinates of the reference station are known. The rover observables will have

approximately the same level of error as those at the reference station because the error sources between the reference station and the rover station are strongly correlated. The reference station then transmits the computed errors (corrections) to the rover to compensate for the errors in the rover's observations. This results in a better position solution. DGPS greatly enhances the accuracy that a user can obtain with GPS.

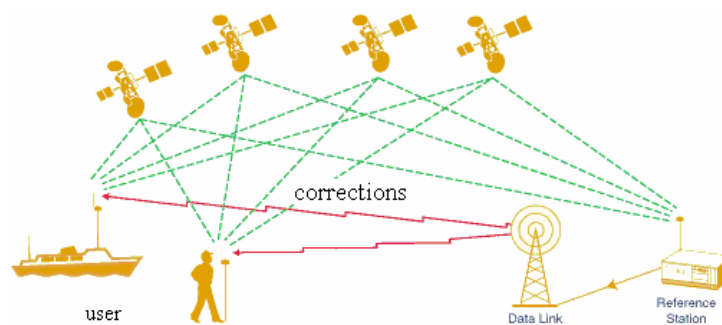


Figure 1.1 Typical DGPS Configuration

More civil communities are no longer satisfied with the performance of pseudorange-based DGPS and are requiring higher accuracies at the centimetre level. For example, dam deformation monitoring and earthquake prediction both require the positioning accuracy to be at the centimetre or even millimetre level (Behr and Hudnut, 1998), and 3-Dimensional navigation in navigation channels requires better than 10-centimetre positioning accuracy (Lachapelle, 2000). The pseudorange-based DGPS cannot meet these stringent accuracy requirements due to the accuracy limitations of the pseudorange observables (Langley, 1996).

In order to achieve centimetre or millimetre level accuracies, the double-differenced (DD) carrier phase observable must be used, which means that the DD integer carrier phase ambiguities need to be resolved. Unlike pseudorange-based DGPS, where the dominant accuracy-limiting factor is code multipath and receiver noise, the dominant accuracy-limiting factor for carrier phase based positioning is the differential ionospheric error, the differential tropospheric error, the differential satellite orbital error and multipath.

The tropospheric delay is caused by the Earth's troposphere and can generally be well modelled using most tropospheric delay models (Spilker, 1994). The residual tropospheric error for baselines ranging up to 30 to 40 km may be negligible and the differential satellite orbital error also tends to cancel for short to medium baselines. The real difficulty lies in the differential ionospheric error because, unlike the troposphere, the ionosphere cannot be easily modelled (Klobuchar, 1996).

The differential ionospheric error is dependant on baseline length and the level of the ionospheric activity. For very short baselines, the differential ionospheric errors tend to cancel and L1 or L2 ambiguity resolution is straightforward. With an increase of the baseline length, the differential ionospheric error tends to increase as well, thus making it difficult or sometimes impossible to resolve the DD carrier phase integer ambiguities. The resolution of the ambiguities is likely to be successful as long as the distance to the nearest reference receiver is less than 10-30 km, depending on geographic location, time of day, and location in the 11-year sunspot cycle (Colombo, 1998).

Ambiguity resolution under the influence of the ionosphere has long been a fertile research topic, particularly during a solar maximum, which is the case at the time of this thesis. A lot of research has been carried out in this field to ensure correct ambiguity fixing under active ionospheric conditions. As a result, many ionospheric models have been developed. Klobuchar (1986) introduced an ionospheric error model that is being used by the GPS control centre as part of the navigation message broadcast by the GPS satellites. This model consists of a cosine representation of the diurnal ionospheric error curve, which will vary in amplitude and period depending on the user's latitude. It has been shown to be effective in removing around 50% of the total RMS (root-mean-square) error. Applying this model will obviously help the SPS performance. However, to reach centimetre level positioning performance, this model is not sensitive enough. Another model is the global ionosphere map produced by the Centre for Orbit Determination in Europe (CODE) (Schaer, 1999). These maps are only available for postprocessing and cannot be used in real time. Other models include the United States Wide Area Augmentation System (WAAS) ionospheric grid model. This model estimates the ionospheric error at the fixed grid points in real time, using a Kalman filter technique (Skone, 1998). Unfortunately, this grid model still does not have sufficient sensitivity to provide centimetre-level positioning performance (FAA, 1997).

Other research efforts examine the use of frequency combinations to combat the increased ionospheric effect. One countermeasure to a high ionospheric effect is to form the widelane (WL) observable since the WL has a much smaller ionosphere/wavelength ratio than L1 or L2 so it is more resistant to ionospheric error. Examples can be found in

Hatch (1982, 1989), Allison (1991), Euler and Landau (1992), Goad (1992), and Seeber (1993). Other well-known countermeasures include forming the ionosphere-free combinations to remove the first order ionospheric effect (Blewitt, 1989). Teunissen (1997) proposed an original method that estimates the ionospheric error explicitly through stochastic modelling.

With so many methods for ambiguity resolution, it is sometimes difficult to determine which method best fits an application. It is not clear whether these methods have the same ambiguity resolution and positioning performance or whether one is significantly better than the others, depending on the conditions. Even with the same ambiguity resolution method, different parameterization schemes may be used. For example, it is popular practice to parameterize the dual frequency carrier phase observable with respect to the L1 and WL ambiguities in contrast to the L1 and L2 ambiguities, e.g. Goad (1992), Bock (1996), and Liu (2001). The reasons and benefits (if any) for this practice are not clear.

Another emerging technique to facilitate successful ambiguity resolution under a severe ionosphere is to use a network of GPS reference stations to model the ionospheric error explicitly. The University of Calgary has developed a very promising approach called MultiRefTM (Multiple Reference Station) (Raquet, 1998; Fortes, 2002). This approach can model and correct differential errors (mainly the ionospheric error) between various reference stations for transmission to a user in the network. With less residual differential errors, ambiguity resolution performance can be improved.

Based on these developments, the following objectives form the basis of the thesis research:

- Implement various ambiguity resolution strategies. These strategies include the well known ionosphere-free combination ambiguity resolution strategy, stochastic ionospheric modelling strategy, widelane ambiguity resolution strategy and L1 only ambiguity resolution strategy.
- Investigate the implemented ambiguity resolution strategies to assess how the selection of observation types and combinations, different parameterization schemes, and estimation model impact the ambiguity resolution and positioning performance.
- Evaluate the impact of the ionospheric error on ambiguity resolution and positioning performance.
- Implement a real-time system to evaluate the MultiRefTM approach when using various ambiguity resolution strategies.

Considering that ambiguity resolution is a very broad and complicated topic that depends on many different factors such as rover dynamics, baseline length etc., the scope of this thesis is restricted to normal RTK practice. Normal RTK practice means that the baseline separation is usually less than 50 km, and the rover receiver is assumed to be in kinematic mode.

In fulfilling the above objectives, the author has significantly enhanced the University of Calgary software FLYKINTM. The latest FLYKIN+TM and FLYKINRT+TM software can

operate in both post mission and real-time modes within a single software package. It can process the data in either static or kinematic mode with various ambiguity resolution strategies that will be discussed in detail in this thesis.

1.2 Thesis Outline

Chapter 2 describes the general differential GPS positioning concepts. The basic equations relating DD GPS observables and their unknown parameters are presented. Various differential error sources are introduced, and the impact of the ionosphere on relative carrier phase positioning is investigated.

Chapter 3 discusses ambiguity resolution techniques. Centimetre positioning accuracy can be achieved only when the integer carrier phase ambiguities are correctly fixed. Ambiguity resolution is the core of the carrier phase relative positioning. There are various ambiguity resolution techniques available, and this chapter investigates several commonly used ones.

Chapter 4 is the core of this thesis. It contains two parts. The first part investigates various ambiguity resolution strategies utilizing different carrier phase combinations, parameterizations, and estimation models. The observation equations for these strategies are presented in this chapter. Test results for these strategies are shown in Chapter 5. The second part of this chapter discusses the software realization of these ambiguity resolution strategies, namely the development process of the FLYKIN+TM software. Most

of the research work done for this thesis is on the development of FLYKIN+TM, so it is relevant to discuss some issues related to the software development. The general software functionality and architecture are presented in this chapter.

In Chapter 5, results for the various ambiguity resolution strategies introduced in Chapter 4 are shown for single and multiple reference station scenarios. The test methodology and parameters are presented. The performance is compared in terms of positioning, time to ambiguity resolution, and percentage of correctly resolved ambiguities. Finally, advantages and disadvantages of various ambiguity resolution strategies are outlined.

Chapter 6 concludes the thesis and envisages further research.

CHAPTER 2

GPS OBSERVABLES AND ERROR SOURCES

2.1 Basic GPS Observables

Many GPS receivers output two primary GPS observables: pseudorange and carrier phase.

The pseudorange observable is generated by measuring the difference between the transmission time and reception time of the GPS Pseudo-Random Noise (PRN) signal. The observation equation relating the pseudorange observable P in metres and unknown parameters is expressed as (Parkinson, 1996):

$$P = r = c (T_u - T^s) \quad (2.1)$$

where $r = \sqrt{(x^s - x)^2 + (y^s - y)^2 + (z^s - z)^2}$ (the true range between the GPS satellite and receiver antenna phase centre), (x^s, y^s, z^s) is the satellite coordinate, and (x, y, z) is the receiver antenna phase centre coordinate which is to be estimated. Both satellite and receiver coordinates are referred to the Earth-Centred-Earth-Fixed reference frame (WGS84). T_u is the time of reception in seconds, T^s is the time of transmission in seconds, and c is the speed of light in metres per second.

Equation (2.1) holds only in theory. In practice the GPS signal is corrupted by many error sources. These error sources include satellite clock error, satellite coordinate error, and atmospheric effects (including tropospheric and ionospheric components); therefore the complete equation relating the pseudorange in metres and unknown parameters is expressed as

$$P = \mathbf{r} + d\mathbf{r} + T + I + c(dT_u^0 - dT_0^s) + \mathbf{e}_p \quad (2.2)$$

where $d\mathbf{r}$ is the satellite orbital error in metres, T is the tropospheric delay in metres, I is the ionospheric delay in metres, dT_u^0 is the receiver clock offset in seconds, dT_0^s is the satellite clock offset in seconds, and \mathbf{e}_p is the combined effect of pseudorange multipath and receiver measurement noise in metres.

Similarly, the observation equation for the carrier phase observable, CP , in cycles is defined as

$$CP = [\mathbf{r} + d\mathbf{r} + T - I + c(dT_u^0 - dT_0^s)] / \mathbf{I} + N + \mathbf{e}_{CP} \quad (2.3)$$

where \mathbf{I} is the L1 or L2 carrier wavelength in metres, N is an arbitrary number representing the unknown, but constant, initial phase ambiguity, and \mathbf{e}_{CP} is the combined effect of multipath and receiver measurement noise in cycles. The carrier phase observation equation is very similar to that of the pseudorange except that it contains an extra parameter, N . The ionospheric error for the carrier phase observable is the same as the pseudorange observable in units of metres but they differ in sign, as the ionosphere causes an advance to the carrier and a delay to the pseudorange (Klobuchar, 1996). In the context of this thesis, the double differenced (DD) processing technique is used. The

double differenced observable equation and error sources are therefore discussed in more detail.

Figure 2.1 depicts a typical DD set-up. By taking the difference between observations to the same satellite from the rover and reference GPS receiver, the satellite clock error, tropospheric error, ionospheric error, and satellite orbital error are significantly reduced. The amount of reduction depends on the spatial separation between the reference and rover GPS receivers. The derived observable is known as the single difference (SD) observable between receivers. By further differencing the SD observable between satellites (see Figure 2.1), the receiver clock errors are eliminated completely. DD processing is performed to reduce the errors in Equations (2.2) and (2.3).

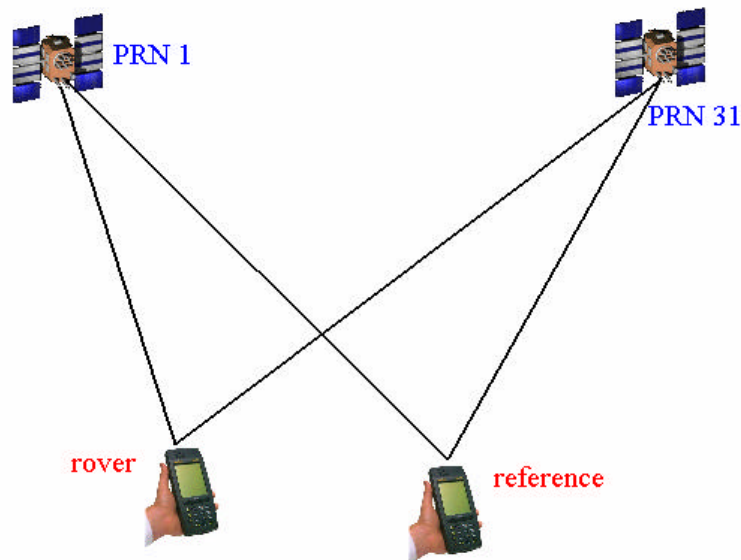


Figure 2.1 Double Differencing Concept

The DD pseudorange and carrier phase observation equations are respectively expressed as:

$$\nabla\Delta P = \nabla\Delta\mathbf{r} + \nabla\Delta d\mathbf{r} + \nabla\Delta T + \nabla\Delta I - \nabla\Delta dT_0^s + \nabla\Delta\mathbf{e}_p \quad (2.4)$$

$$\nabla\Delta CP = [\nabla\Delta\mathbf{r} + \nabla\Delta d\mathbf{r} + \nabla\Delta T - \nabla\Delta I - \nabla\Delta dT_0^s] / \mathbf{I} + \nabla\Delta N + \nabla\Delta\mathbf{e}_{CP} \quad (2.5)$$

where $\nabla\Delta$ is the double differenced (DD) operator.

Double differenced observables have many advantages over undifferenced observables. First, the receiver clock offset is removed. Second, it is well known that the satellite clocks are highly stable (Kaplan, 1996), thus the value $\nabla\Delta dT_0^s$ tends to cancel as long as the observations are differenced at approximately the same time at both reference and rover stations. That means Equations (2.4) and (2.5) can be further simplified as:

$$\nabla\Delta P = \nabla\Delta\mathbf{r} + \nabla\Delta d\mathbf{r} + \nabla\Delta T + \nabla\Delta I + \nabla\Delta\mathbf{e}_p \quad (2.6)$$

$$\nabla\Delta CP = [\nabla\Delta\mathbf{r} + \nabla\Delta d\mathbf{r} + \nabla\Delta T - \nabla\Delta I] / \mathbf{I} + \nabla\Delta N + \nabla\Delta\mathbf{e}_{CP} \quad (2.7)$$

Third, the scales of the DD tropospheric error, DD satellite orbital error, and DD ionospheric error are much smaller than the undifferenced values.

The double difference observable has some disadvantage over the undifferenced observable. The most significant effect is that the noise level of the DD observable increases since it is a linear combination of the carrier phase observable.

To fully understand Equations (2.6) and (2.7), it is worthwhile to look at the individual terms on the right-hand side of the two equations, especially the double differenced error terms.

2.2 GPS Error Sources

The DD errors can be classified into two categories, spatially correlated and non-spatially correlated. Spatially correlated errors are those that tend to cancel between a reference receiver and a rover receiver but increase in relation to the baseline length. These errors include

- Satellite orbital error
- Tropospheric error
- Ionospheric error

Non-spatially correlated errors are those that are unique to each receiver or its environment. They are not related to the baseline length and therefore will not cancel through DD processing. These errors are

- Multipath
- Measurement noise

All of the above mentioned error sources are discussed in detail later in this thesis.

2.2.1 Satellite Orbital Error

In order to compute a receiver position using GPS measurements, the coordinates of the GPS satellites must be known. These coordinates are normally expressed in terms of an ephemeris, which gives a mathematical description of where a satellite is at a given time (Roulston et al., 2000). In order to provide users with an ephemeris for real-time

applications, the GPS design group came up with what is known as broadcast ephemeris, which is in the form of a navigation message that is modulated on the L1 and L2 carrier that are transmitted to users (Seeber, 1993). The satellite orbital error is a result of the discrepancy between the computed coordinate using the broadcast ephemeris and its actual value. According to IGS (2001), the satellite orbital computed from the broadcast ephemeris has an RMS error of 2 m. However according to Wells et al. (1986), in differential positioning, the following general rule holds:

$$\frac{db}{b} = \frac{d\mathbf{r}}{\mathbf{r}} \quad (2.8)$$

where db is the total error in the length of the baseline b , $d\mathbf{r}$ is the total error in the coordinates of a satellite position, and \mathbf{r} is the mean distance from the stations to the satellite.

Equation (2.8) shows that the actual influence of the satellite orbital error on the baseline is limited. Assuming an RMS satellite orbital error of 2 m and an average satellite-receiver range of 20200 km, the contribution of the orbital error to the differential positioning error budget is at 0.19 ppm. Figure 2.2 shows the relationship between admissible SV orbital errors $d\mathbf{r}$ with respect to baseline length b for the given baseline error thresholds $db = 0.5$ cm and 1 cm. From this figure, it can be concluded that the baseline error caused by satellite orbital errors is less than 1 cm for baselines up to 50 km, and is negligible assuming a nominal satellite orbital error of 2 m.

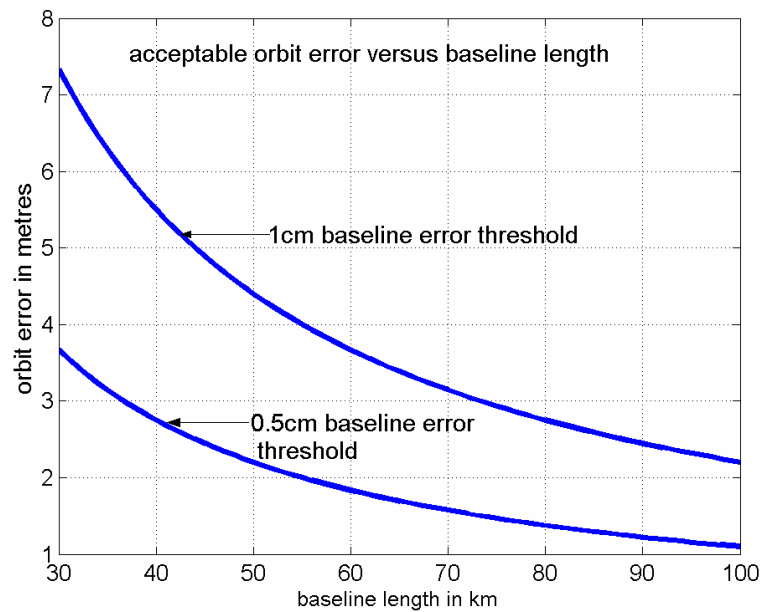


Figure 2.2 Orbit Error vs. Baseline Lengths for Certain SV Orbit Induced Error Thresholds

2.2.2 Tropospheric Error

The troposphere is the portion of the atmosphere extending up to 60 km above the Earth's surface. When the GPS signal travels through the troposphere, its path will bend slightly due to the refractivity of the troposphere. The change of the refractivity from free space to the troposphere causes the speed of the GPS signal to slow down, which causes a delay in the GPS signal. This tropospheric delay is a function of temperature, pressure, and relative humidity. Measurement of these quantities at widely spaced monitoring stations would be ineffective owing to their short spatial correlations (Kaplan, 1996).

The atmosphere consists of dry and wet components. These components affect the propagation delay of the radio frequency signals quite differently. The dry component causes a delay around 2.3 m in the zenith direction which varies with local temperature

and pressure. The dry component induced delay is quite constant and may vary only 1% in a few hours. This dry zenith delay can be predicted very well using existing models. The wet component of the zenith delay is generally much smaller, between 1 and 80 cm at the zenith, and is very unpredictable. It may change by as much as 10% to 20% in a few hours (Spilker, 1994).

Generally, tropospheric delay can be modelled very well. It was found that the contribution of the troposphere to the differential positioning error budget varies typically from 0.2 to 0.4 parts per million (ppm), after applying a model (Lachapelle, 2000). Assuming a nominal value of 0.4 ppm, the baseline errors after applying a model are tabulated below for different baseline lengths. From Table 2.1 one can conclude that for baselines beyond 25 km, the residual tropospheric delay is larger than 1 cm. For a baseline of 100 km, the residual tropospheric error is as high as 4 cm. In order to achieve a one-centimetre level of positioning accuracy, either the residual tropospheric delay must be modelled explicitly or corrections have to be made to compensate for it.

Table 2.1 Baseline Errors due to Residual Tropospheric Error

Baseline length (km)	Baseline errors (cm)
5	0.2
10	0.4
25	1.0
50	2.0
100	4.0
500	20.0

There are quite a number of tropospheric delay models available, e.g. Hopfield (1970, 1972), Saastamoinen (1972), and Lanyi (1984). The Hopfield tropospheric delay model and Saastamoinen tropospheric model are the most frequently used and they give comparable results in most situations. For low elevation satellites, the Saastamoinen model produces slightly better results than the Hopfield model (Spilker, 1994).

2.2.3 Ionospheric Error

The ionosphere is the layer of the atmosphere that extends from 60 to over 1000 km of height above the Earth's surface. The ionosphere is an important source of range and range-rate errors for users of the GPS who require high-accuracy measurements. At times, the range errors of the troposphere and the ionosphere can be comparable, but the variability of the earth's ionosphere is much larger than that of the troposphere, and it is more difficult to model (Klobuchar, 1996). The first-order carrier phase error I (in metres) caused by the ionosphere is given as (Skone, 1998):

$$I = -\frac{40.3}{f^2} \text{TEC} \quad (2.9)$$

where 40.3 is an empirically derived constant with units of $\text{m}^3/\text{s}^2/\text{electrons}$, TEC represents the Total Electron Content along the signal path in units of $\text{electrons}/\text{m}^2$, and f is the L1 or L2 carrier frequency. From Equation (2.9), it can be seen that the magnitude and variability of the ionospheric error is a function of TEC. The TEC values depend on the rate of ionization, recombination and transport processes (Skone, 2001). The rate of ionisation in a global sense is a function of the solar activity, which follows cycles of approximately 11 years in duration (Klobuchar, 1996). The TEC values have

been observed to increase by a factor of three during a solar maximum versus a solar minimum (Klobuchar et al., 1995). In addition to the large-scale global increase in the absolute value of TEC during solar maximum, an increase in the frequency and magnitude of magnetic storms accompanies the enhanced solar flare activity (Skone, 1998). The latest solar maximum occurred during the year 2000-2001. The data set used in this thesis is collected in early 2002, one year after the solar maximum, which means there is still a strong ionospheric signature in the data.

The pseudorange and carrier phase measurements include ionospheric range errors of equal magnitude in metres and opposite sign (Skone, 1998). This causes trouble to users of single frequency GPS receivers who want to smooth the pseudorange with the carrier phase observation, as the smoothing process must be restarted at certain intervals to avoid the divergence caused by the ionosphere on pseudorange and carrier phase.

There are some ionospheric models available. Klobuchar (1986) introduced a model that is being used by the GPS control centre as part of the navigation message broadcast by the GPS satellites. This model consists of a cosine representation of the diurnal ionospheric error curve which will vary in amplitude and period depending on the user's latitude. It has been shown to be effective in removing around 50% (RMS) of the total error. Applying this model will help the SPS performance. However, to reach centimetre-level positioning performance, this model is not sensitive enough. One such effort tries to develop efficient global ionosphere maps. The most representative of these maps are the Global Ionosphere Maps produced by the Centre for CODE (Schaer, 1999). These maps

are only available for post processing and cannot be used in real-time. Other models include the United States WAAS ionospheric grid model. This model estimates the ionospheric TEC values at the fixed grid points in real time using a Kalman filter technique. Estimates are made of satellite and receiver L1-L2 interchannel biases, which must be included in ionospheric delay calculations, in addition to parameters characterizing the vertical TEC. Model parameters are generally approximated as Gauss-Markov or random walk stochastic processes (Skone, 1998). Unfortunately, this model still does not have sufficient sensitivity to provide centimetre level positioning performance.

Although the ionospheric error is hard to compensate for by applying models like the troposphere, there are several good properties about the ionospheric error that enable its direct estimation from the carrier phase and pseudorange measurements. The first property is that the ionosphere is a dispersive medium (Klobuchar, 1996). From Equation (2.9), it can be seen that L1 and L2 will encounter different ionospheric errors. Skone (1998) showed estimation of the ionospheric error on L1 through data from a dual frequency receiver. This dispersive property also allows forming a very important carrier phase combination, the ionosphere-free combination. The ionospheric error is removed in this combination.

Another property of the ionospheric error is that it has very good temporal characteristics. Skone (1998) has shown that a first order Gauss-Markov process is consistent with the

observed temporal correlations in TEC. The following system model was employed to describe the evolution of the TEC.

$$VTEC(t_{j+1}) = e^{\frac{-dt}{T_0}} VTEC(t_j) + w(t_j) \quad (2.10)$$

where VTEC is the TEC content in the zenith direction, T_0 is the correlation time and $dt = t_{j+1} - t_j$. This property allows estimation of the ionospheric error through a Kalman filter. This approach will be demonstrated in Chapter 4.

The contribution of the ionosphere to the differential positioning error budget is estimated to be at 1-2 ppm (Seeber, 1993), and this figure is generated at the time of a solar minimum. In time of solar maximum, the contribution of the ionosphere to the differential positioning error budget increases by a factor of three. This figure can be even higher in regions of frequent magnetic storms which cause a sharp increase of the TEC value. Wanninger (1993) reported up to 40 ppm DD ionospheric error in the equatorial regions. In addition, the ionospheric scintillation (Wanninger, 1993) which may also be severe in equatorial regions (geomagnetic equator $\pm 15^\circ$) can easily cause semicodeless receivers to lose tracking of the L2 carrier signals (Hegarty et al., 2001), and this will cause additional difficulty to those semicodeless dual frequency receiver users. In practice, the ionospheric error is usually the most detrimental error source for medium to long baseline carrier phase positioning.

2.2.4 Multipath

Multipath is the interference of a reflected GPS signal with the line-of-sight GPS signal. It distorts the signal modulation and thus degrades the measurement accuracy (Braasch, 1996). For a system using GPS pseudorange observables, signal degradation attributable to multipath can be very severe as the magnitude of the multipath error is usually not insignificant. Multipath is not spatially correlated since it is highly dependent on the local receiver environment. Multipath sources that affect a reference station do not necessarily cause errors in the rover receiver provided that they are not spaced very close to each other. Similarly, multipath sources that affect the rover receiver do not necessarily affect the reference station. The C/A pseudorange multipath can be half of a C/A code chip, which is equivalent to 150 m. The carrier phase multipath is much smaller than that of the pseudorange, with a maximum magnitude of one quarter of a carrier wavelength, i.e 5 cm for L1 and 6 cm for L2 (Cannon, 2002). However, in practical applications, the reflected signal is attenuated to some extent and the typical phase multipath values are more on the order of 1 cm or less (Lachapelle, 2000). To reduce the impact of multipath, the simplest way is to carefully select the antenna site to avoid any potential reflectors.

On very short baselines such as the case in attitude determination, where the spatially correlated errors (ionospheric error, tropospheric error, orbital error) are mostly removed by double differencing, multipath is the major error source for carrier phase based positioning (Lu, 1995). Compared to the ionospheric error, multipath is not assumed to be a major error source in this research since the shortest baseline used in this thesis is over 10 km.

2.2.5 Measurement Noise

Measurement noise is generated by the receiver in the process of taking code or phase measurements. The noise is primarily due to tracking loop “jitter” (Raquet, 1998). For moderate to strong signals, the standard deviation of the C/A pseudorange measurement noise is around 1 m, and this figure can be reduced to 0.4 m or less for receivers which use narrow correlators; the standard deviation of the L1 carrier phase measurement noise is 0.2 mm (Langley, 1996). The measurement noise can be effectively estimated through the use of a zero-baseline test (Cannon, 2002). In this test, the GPS signal from one antenna is split to two receivers. All the error sources are eliminated in the double differencing process except the measurement noise. The satellite-receiver geometry term is also absent as a common antenna is used. The double differenced measurement can be used as an efficient observable to estimate the magnitude of the measurement noise.

2.3 Phase Combinations

For most carrier-phase relative positioning applications with short to medium baseline separation, the satellite orbital error tends to cancel completely and the tropospheric error after applying a troposphere model is generally negligible. Yet, there is no effective and reliable model at this stage to effectively compensate or reduce the ionospheric error. Since the work of this research is done under the “short to medium baseline” assumption, the ionosphere is then considered to be the only remaining dominant error source. Thus Equation (2.7) can be rewritten as

$$CP = [\mathbf{r} - \mathbf{I}] / \mathbf{I} + N + e \quad (2.12)$$

where e contains mainly noise, multipath, and residual tropospheric error. The DD operator $\nabla\Delta$ in above equation has been omitted for simplicity.

Following Equation (2.12), the observation equation for the L1 and L2 carrier phase observables can be written as:

$$\begin{aligned} CP_1 &= [\mathbf{r} - I_1] / I_1 + N_1 + e_1 \\ CP_2 &= [\mathbf{r} - I_2] / I_2 + N_2 + e_2 \end{aligned} \quad (2.13)$$

where I_1, I_2 are the ionospheric errors in units of metres on L1 and L2, respectively.

Because the ionosphere is dispersive, the following relationship holds between I_1 and I_2 :

$$I_2 = \left(\frac{I_2^2}{I_1^2}\right) I_1 \quad (2.14)$$

So Equation (2.13) can be rewritten as

$$\begin{aligned} CP_1 &= \frac{\mathbf{r}}{I_1} - \frac{I_1}{I_1} + N_1 + e_1 \\ CP_2 &= \frac{\mathbf{r}}{I_2} - \left(\frac{I_2}{I_1}\right) \frac{I_1}{I_1} + N_2 + e_2 \end{aligned} \quad (2.15)$$

It is also possible to form phase combinations using the basic L1 and L2 carrier phase observations. Assume that both double differenced L1 and L2 carrier phase observables, CP_1 and CP_2 , are available, then a generic linear phase combination can be formed as (Seeber, 1993):

$$CP_{i,j} = iCP_1 + jCP_2 \quad (2.16)$$

The wavelength of $CP_{i,j}$ is expressed as

$$I_{i,j} = \left(\frac{i}{I_1} + \frac{j}{I_2}\right)^{-1} \text{ with ambiguity } N_{i,j} = iN_1 + jN_2 \quad (2.17)$$

where I_1 and I_2 are the wavelengths of L1 and L2 in metres, and N_1 and N_2 are the L1 and L2 integer carrier phase ambiguities in cycles. Thus, CP_1 can be seen as a special case of $CP_{i,j}$ with $i=1, j=0$, while CP_2 has $i=0, j=1$.

Following Equation (2.12), the observation equation for $CP_{i,j}$ can be written as

$$CP_{i,j} = \frac{\mathbf{r}}{I_{i,j}} + N_{i,j} - (i + j \frac{I_2}{I_1}) \frac{I_1}{I_1} + e \quad (2.18)$$

where I_1 is the ionospheric bias on L1 (in metres).

There are many possible carrier phase combinations. The following section will discuss several popular combinations. These are the widelane, narrowlane, and ionosphere-free combinations.

2.3.1 Widelane Combination (WL)

The observation equation for the WL observable ($i=1, j=-1$) (Seeber, 1993) is:

$$\begin{aligned} CP_{WL} &= CP_1 - CP_2 \\ N_{WL} &= N_1 - N_2 \\ CP_{WL} &= \frac{\mathbf{r}}{I_{WL}} + N_{WL} + \frac{17}{60} \frac{I_1}{I_1} + e \end{aligned} \quad (2.19)$$

The wavelength of the widelane phase observable is $\frac{I_1 I_2}{-I_1 + I_2}$ (0.86 m). As can be seen,

the ionospheric error in units of cycles has been reduced to $\frac{17}{60}$ of a wavelength. To

illustrate the advantages of this, assume there is an ionospheric bias equivalent to one L1 cycle, then the corresponding error for the WL observable would only be 17/60 of a cycle. It is therefore clear that the widelane combination is more resistant to ionospheric

error (in cycles) than L1 and thus, it is more reliable to resolving widelane ambiguities under adverse ionospheric conditions. Another property of the widelane observable is that it is also more resistant to position errors. For example, it takes a minimum position error of only 19 cm to introduce a one-cycle error on L1, but a minimum position error of 86 cm to introduce a one-cycle error for widelane.

Although the widelane combination reduces the impact of the ionospheric bias in cycles, it actually amplifies its effect in metres, which is the unit used for position estimation.

Specifically, the ionospheric bias for the widelane in metres is $\frac{17}{60} \frac{I_1}{I_1} I_{WL} = \frac{77}{60} I_1$. The

noise is also amplified in the widelane observable compared to the L1 and L2 raw observables in metres. Thus it is expected that the position estimate derived using the widelane linear combination will have a higher position error than the position errors determined with the L1 observable, assuming the integer ambiguities are resolved correctly for both.

2.3.2 Narrowlane Combination (NL)

The observation equation for the narrowlane combination ($i = 1, j = 1$) (Seeber, 1993) is:

$$\begin{aligned} CP_{NL} &= CP_1 + CP_2 \\ N_{NL} &= N_1 + N_2 \\ CP_{NL} &= \frac{\mathbf{r}}{\mathbf{I}_{NL}} + N_{NL} + e \end{aligned} \tag{2.20}$$

The wavelength of the narrowlane combination is $\frac{I_1 I_2}{I_1 + I_2}$ (10.7 cm). This wavelength is

much shorter than that of the WL. Narrowlane has the same magnitude of noise as WL

does in cycles. However, due to its relatively short wavelength, narrowlane has lower noise compared to L1, WL or IF in metres. As a result, the narrowlane should give better positioning results than L1, WL and IF does, provided the ionospheric error is negligible. However, narrowlane has the same amount of ionospheric error as WL does in metres. So in situations when the ionospheric error is not negligible, the narrowlane suffers from the ionosphere the same as the widelane does. Furthermore, the short wavelength also makes it difficult to resolve the narrowlane ambiguities. In this research, all data have strong ionospheric signature, thus the narrowlane is not investigated further.

2.3.3 Ionosphere-free Combination (IF)

The observation equation for the ionosphere-free combination ($i=1, j=-\frac{I_1}{I_2}$) (Raquet, 1998) is:

$$\begin{aligned}
 CP_{IF} &= CP_1 - \frac{I_1}{I_2} CP_2 \\
 N_{IF} &= N_1 - \frac{I_1}{I_2} N_2 \\
 CP_{IF} &= \frac{\mathbf{r}}{I_{IF}} + N_{IF} + e
 \end{aligned} \tag{2.21}$$

The main advantage of the ionosphere-free combination is the removal of the first order effects of the ionosphere. As a result, the level of ionospheric activity is of less significance. The disadvantage of this combination is that the IF ambiguity is no longer an integer. Also the IF combination is noisier than L1 and L2 since it is a combination of L1 and L2.

Table 2.2 summarizes the magnitude of the ionosphere and noise errors for the undifferenced L1, L2, WL, NL and IF observables in both metres and cycles. In this research, two combinations are examined extensively in addition to L1 and L2. One is the widelane combination and the other is the ionosphere-free combination as both have shown good performance in combating the ionospheric error.

Table 2.2 L1/L2/WL/NL/IF Combination Properties

Combination	i	j	$I_{i,j}$ (cm)	$N_{i,j}$	Ionospheric Error		Noise (1-sigma)	
					m	cycle	m	cycle
L1	1	0	19	N_1	I_1	$\frac{I_1}{I_1}$	$19s_1$	s_1
L2	0	1	24	N_2	$\left(\frac{77}{60}\right)^2 I_1$	$\frac{77}{60} \frac{I_1}{I_1}$	$24s_1$	s_1^*
WL	1	-1	86	$N_1 - N_2$	$-\frac{77}{60} I_1$	$\frac{17}{60} \frac{I_1}{I_1}$	$12s_1$	$1.41s_1$
NL	1	1	10.7	$N_1 + N_2$	$\frac{77}{60} I_1$	$\frac{137}{60} \frac{I_1}{I_1}$	$15s_1$	$1.41s_1$
IF	1	$-\frac{I_1}{I_2}$	48	$N_1 - \frac{I_1}{I_2} N_2$	0	0	$60s_1$	$1.26s_1$

* Assume the standard deviation (1-sigma) of the observation noise on L2 carrier is the same as L1 in units of cycles.

To demonstrate the impact of the ionospheric error on different carrier phase and phase combinations, a medium distance baseline (21.6 km) from a network in Italy has been processed with the four scenarios in Table 2.2. The data is 24hour long with a 1 Hz sampling rate, collected in February, 2002. The DD ionospheric error on L1 is depicted in Figure 2.3. It is clear that the ionospheric error is high between 08:00-16:00 local time.

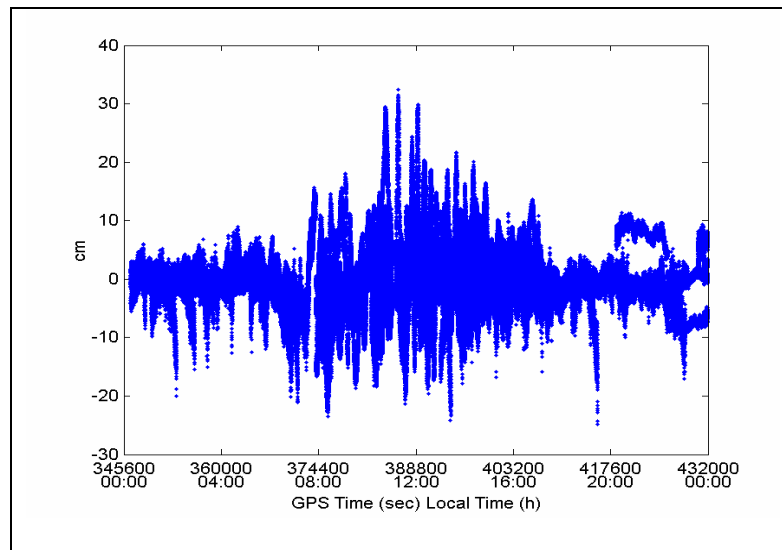


Figure 2.3 DD Ionospheric Error on L1 for a 21.6 km Baseline in Italy

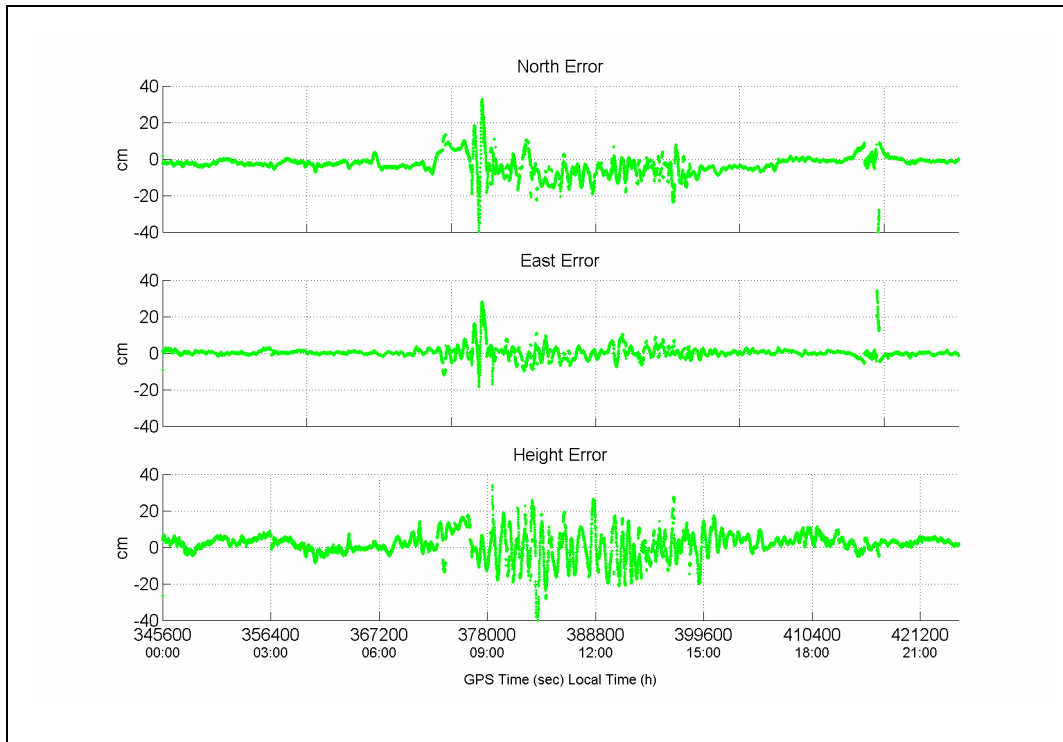
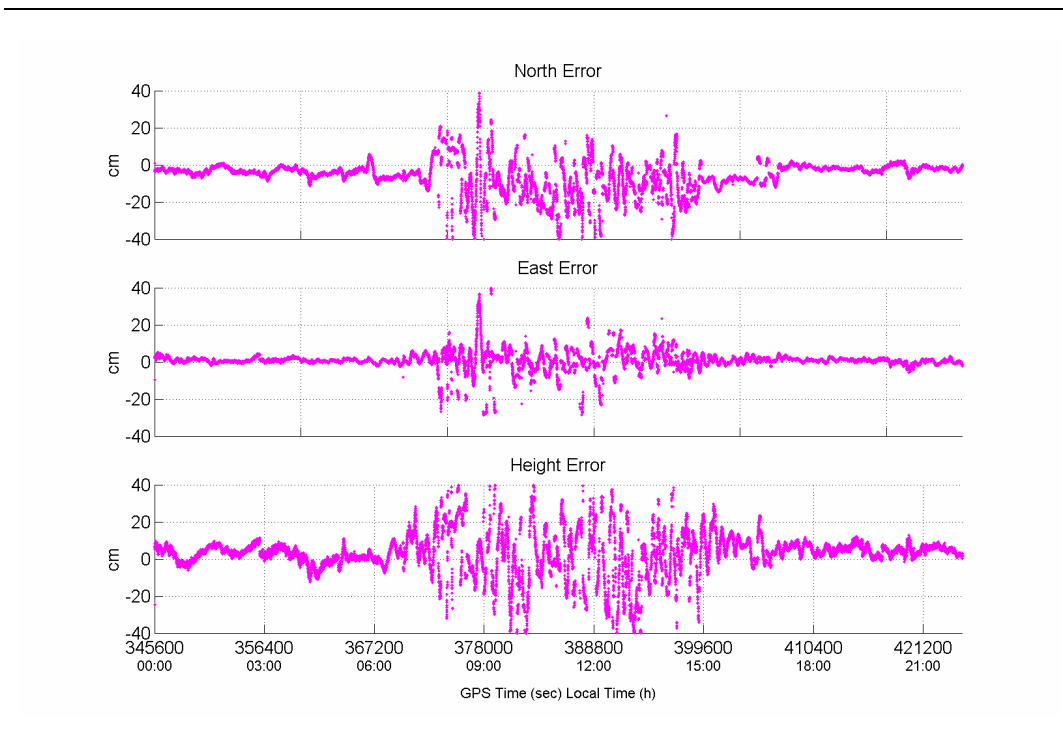
The data is processed at a 1 Hz interval to determine position estimates but with ambiguity parameters constrained to known values that had been determined a priori. This was done so that the positioning accuracies of the various approaches could be directly compared. Therefore only the baseline components were estimated. Table 2.3 shows the RMS position errors for all four combinations. It can be seen that the IF combination gives the smallest RMS error for all three axes. This indicates that the ionospheric error is the dominant error source for this baseline data.

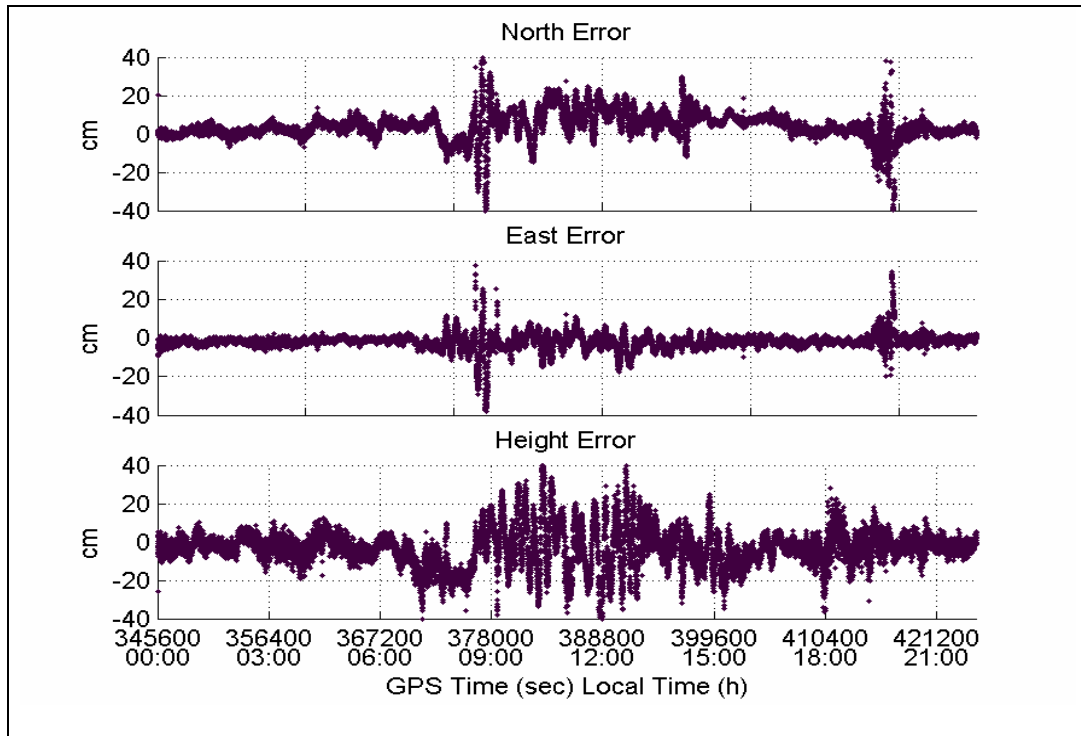
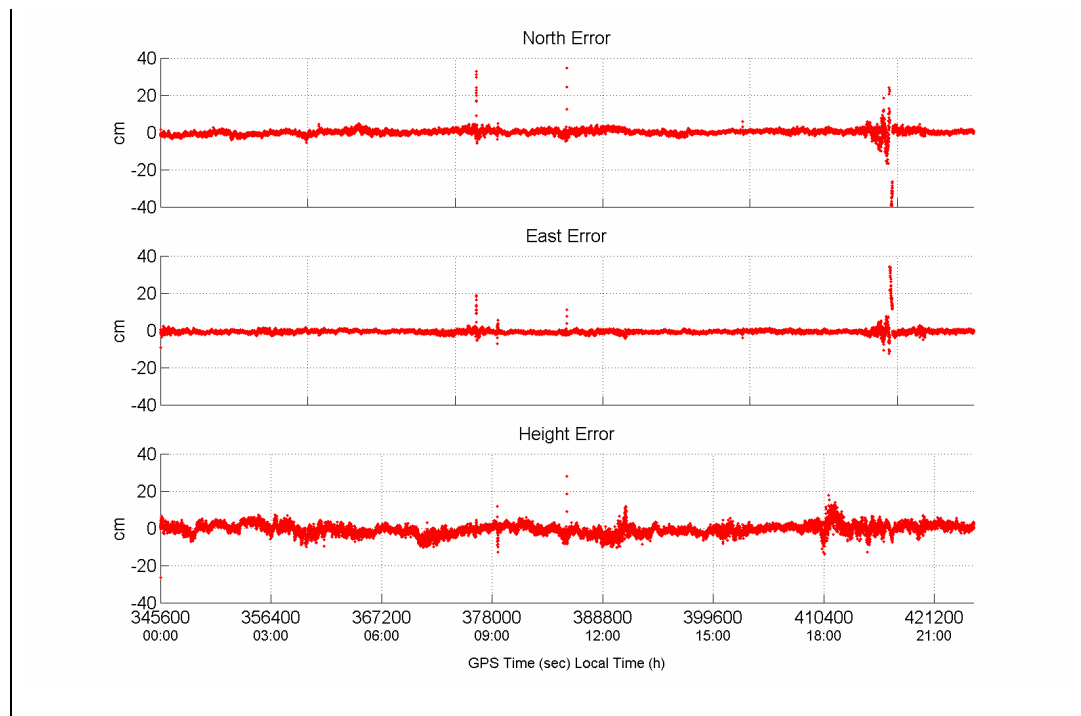
Table 2.3 RMS Position Errors (cm) with Bernese Ambiguities, 26 km Baseline

Component	Combination			
	L1	L2	WL	IF
East	7	12	9	5
North	4	6	5	2
Height	10	18	14	8

Figures 2.4 to 2.7 show the position error for the four different combinations. The ionospheric impact on the position is evident in Figures 2.4, 2.5 and 2.6. All three figures show large position errors in the middle of the data set when the ionosphere is very active. The position error is small at the beginning and end of the data set when the ionospheric activity is low. It is interesting that the position error using L2 is worse than the WL combination for this data set, even though the WL combination is five times noisier than L2. This is because L2 contains more ionospheric error than WL as L2 is a lower frequency. The ambiguities are resolved using the Bernese Software (Universität Bern, 2000). This software does not solve all the ambiguities at some epochs due to certain internal software mechanisms, in which case a reduced geometry results, which has caused several large spikes in Figures 2.4 to 2.7.

Based on the above results, the following conclusion can be drawn: Assuming that both L1, L2 and WL ambiguities are correctly resolved, then the L1 phase only solution will always give better positioning RMS than the WL because L1 contains less ionosphere and noise in centimetres than WL does; whether L2 can give a better position RMS than WL depends on the DD ionospheric error. Further details on various ambiguity resolution strategies that use the L1, L2 and/or WL observations are presented in the following chapter.

**Figure 2.4 L1 Position Errors****Figure 2.5 L2 Position Errors**

**Figure 2.6 WL Position Errors****Figure 2.7 IF Position Errors**

CHAPTER 3

GPS AMBIGUITY RESOLUTION

3.1 Introduction

Before discussing various ambiguity resolution strategies that involve various frequency combinations, parameterization schemes, and modelling methods, it is worthwhile to investigate basic ambiguity resolution techniques. From Equation (2.12) in the previous chapter, the DD carrier phase observation equation is

$$CP = [\mathbf{r} - \mathbf{I}] / \mathbf{I} + N + e \quad (3.1)$$

where \mathbf{r} is the DD satellite-receiver range containing the baseline information that is to be estimated, and N is the unknown DD integer carrier phase ambiguity. In order to solve the baseline component, the ambiguity term, N , has to be solved first. The process of estimating the correct carrier phase integer ambiguity is called GPS ambiguity resolution. Successful ambiguity resolution is the key to high precision positioning using the carrier phase observable. In order to reach centimetre level positioning accuracies, this ambiguity term must be determined correctly.

Figure 3.1 shows the flowchart for using the DD carrier phase observable in GPS positioning. In general, there are three procedures involved. These are the float filter

procedure ([1] in Figure 3.1), ambiguity resolution ([2a] in Figure 3.1) and validation procedure ([2b] in Figure 3.1), and the fixed solution procedure ([3] in Figure 3.1).

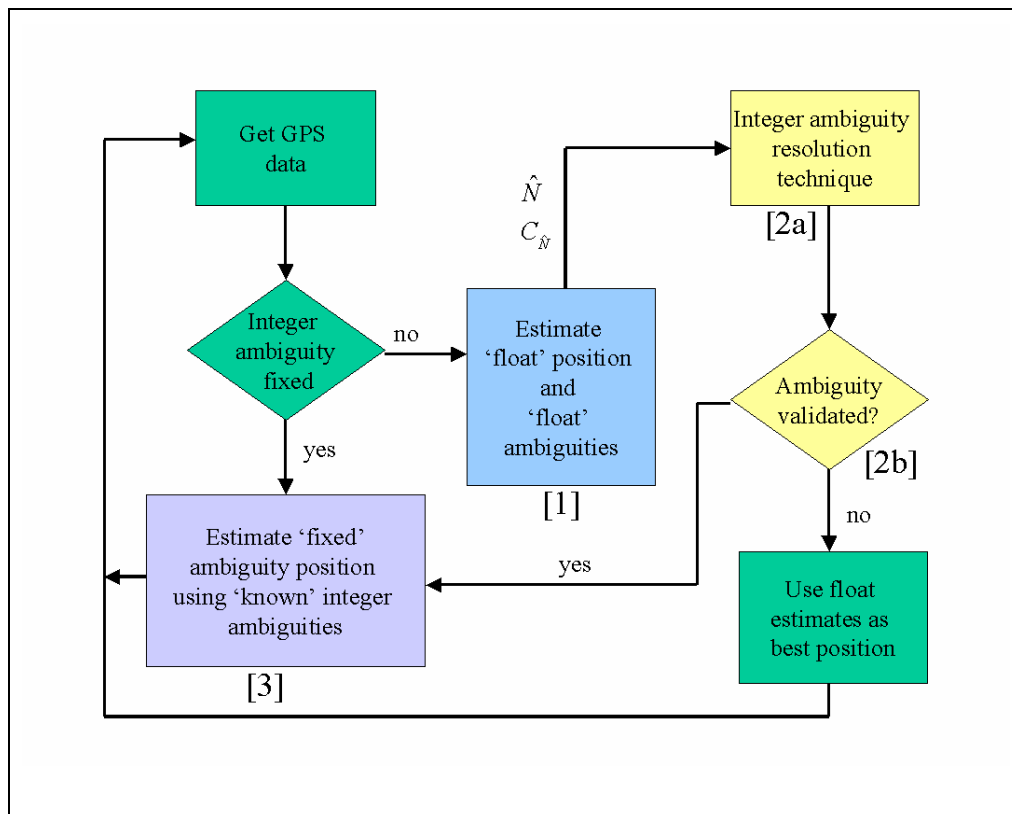


Figure 3.1 DD Carrier Phase Positioning Flowchart (Cannon, 2002)

3.1.1 Float Filter Procedure

The float filter procedure is usually implemented through a Kalman filter and Figure 3.2 shows the usual steps. Kalman filtering usually contains four steps: prediction, computation of the innovation sequence, computation of the Kalman gain, and update. In Figure 3.2, x_k is the state vector estimated at epoch k , C_k is the variance-covariance matrix of the state vector x_k at epoch k , z_k is the observation vector at epoch k , Φ is the transition matrix, Q_k is the system process noise matrix at epoch k , R_k is the variance

covariance matrix of the observation vector z_k , I is an identity matrix, and H is the design matrix which is the matrix computed by taking the derivatives of the observables with respect to the estimated states. The $-$ sign is used with any matrix or state vector before the “Update” step, while the $+$ sign is used with any matrix or state vector after the “Update” step. More on Kalman filtering can be found in Brown and Hwang (1992).

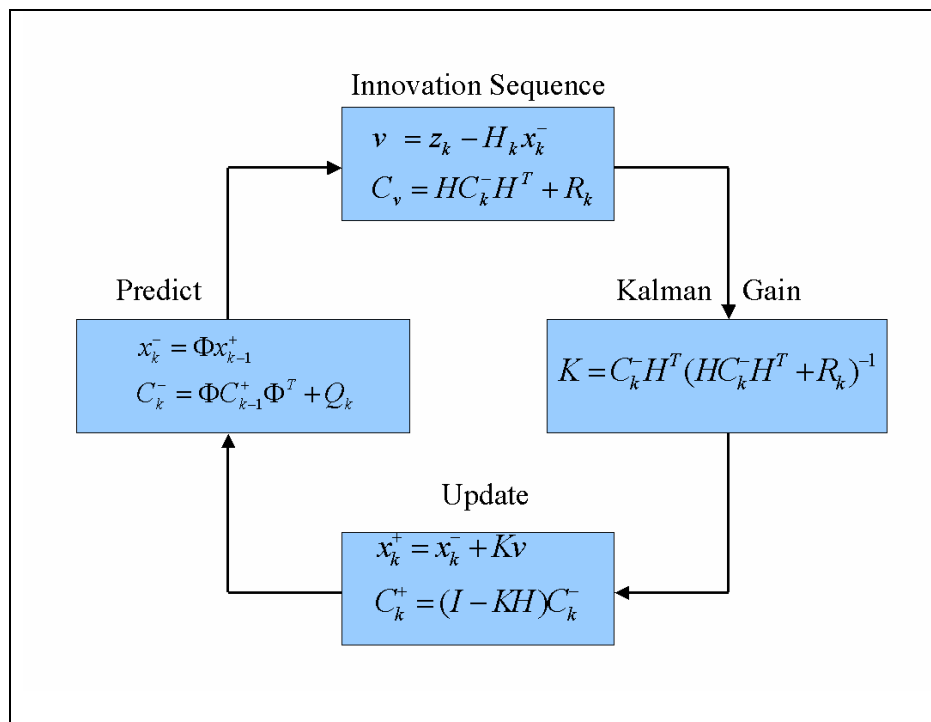


Figure 3.2 Linearized Kalman Filter Loop (Brown and Hwang, 1992)

A Kalman filter contains two sets of models (Axelrad et al., 1996). The first one is a dynamic model that describes how the state vector transforms from one epoch to the next, and how the variance covariance matrix of the state vector evolves from one epoch to the next. The other one is a measurement model that relates the observations to the state vector through the design matrix H . These two models are described below.

3.1.1.1 Kalman Filter Dynamic Model

Specific to DD carrier phase-based GPS RTK positioning, the state vector usually contains the three position states $(\mathbf{j}, \mathbf{l}, h)$ (latitude in units of radians, longitude in units of radians, height in units of metres, respectively), three velocity states $(\dot{\mathbf{j}}, \dot{\mathbf{l}}, \dot{h})$ (latitude rate in units of radians per second, longitude rate in units of radians per second, and height rate in units of metres per second, respectively), and the DD ambiguity state \hat{N} (in units of cycles) for each satellite-receiver pair. Assuming n DD ambiguities are available, the complete state vector is

$$x = (\mathbf{j}, \mathbf{l}, h, \dot{\mathbf{j}}, \dot{\mathbf{l}}, \dot{h}, \hat{N}_1, \hat{N}_2, \hat{N}_3, \dots, \hat{N}_n) \quad (3.2)$$

For most navigation problems, the dynamics of the system are modelled using a random walk model or a Gauss-Markov model, thus the transition matrix is easily obtained (Brown and Hwang, 1992). Assume a random walk model for the velocity state $(\dot{\mathbf{j}}, \dot{\mathbf{l}}, \dot{h})$ with corresponding driving noise vector (w_j, w_l, w_h) , the transition matrix for the position and velocity state vector is derived as

$$\Phi_1 = \begin{bmatrix} 1 & 0 & 0 & dt & 0 & 0 \\ 0 & 1 & 0 & 0 & dt & 0 \\ 0 & 0 & 1 & 0 & 0 & dt \\ 0 & 0 & 0 & 1 & 0 & 0 \\ 0 & 0 & 0 & 0 & 1 & 0 \\ 0 & 0 & 0 & 0 & 0 & 1 \end{bmatrix} \quad (3.3)$$

where dt is the transition time interval in seconds. The equations relating the white driving noise and the three velocity states are as follows:

$$\begin{aligned}
\dot{\mathbf{j}} &= w_j \\
\dot{\mathbf{l}} &= w_l \\
\dot{\mathbf{h}} &= w_h
\end{aligned} \tag{3.4}$$

Assume a spectral density for the driving noise vector of (sp_j, sp_l, sp_h) (all in units of m^2/s^3), the subsystem noise matrix for the position and velocity state vector is derived as

$$Q_1 = \begin{bmatrix} \frac{sp_j}{3} dt^3 & 0 & 0 & \frac{sp_j}{2} dt^2 & 0 & 0 \\ 0 & \frac{sp_l}{3} dt^3 & 0 & 0 & \frac{sp_l}{2} dt^2 & 0 \\ 0 & 0 & \frac{sp_h}{3} dt^3 & 0 & 0 & \frac{sp_h}{2} dt^2 \\ \frac{sp_j}{2} dt^2 & 0 & 0 & sp_j dt & 0 & 0 \\ 0 & \frac{sp_l}{2} dt^2 & 0 & 0 & sp_l dt & 0 \\ 0 & 0 & \frac{sp_h}{2} dt^2 & 0 & 0 & sp_h dt \end{bmatrix} \tag{3.5}$$

The ambiguity states are modelled as random constants since ambiguity states will not change unless there is a loss of phase lock. So the transition matrix for the ambiguity state vector is derived as

$$\Phi_2 = \begin{bmatrix} 1 & 0 & 0 & 0 & 0 & 0 \\ 0 & 1 & 0 & 0 & 0 & 0 \\ 0 & 0 & 1 & 0 & 0 & 0 \\ 0 & 0 & 0 & 1 & 0 & 0 \\ \vdots & \vdots & \vdots & \vdots & \ddots & \vdots \\ 0 & 0 & 0 & 0 & 0 & 1 \end{bmatrix} \tag{3.6}$$

The subsystem noise matrix for the position and velocity state vector is derived as

$$Q_2 = \begin{bmatrix} 0 & 0 & 0 & 0 & 0 & 0 \\ 0 & 0 & 0 & 0 & 0 & 0 \\ 0 & 0 & 0 & 0 & 0 & 0 \\ 0 & 0 & 0 & 0 & 0 & 0 \\ \vdots & \vdots & \vdots & \vdots & \ddots & \vdots \\ 0 & 0 & 0 & 0 & 0 & 0 \end{bmatrix} \quad (3.7)$$

The complete transition matrix is

$$\Phi = \begin{bmatrix} \Phi_1 & 0 \\ 0 & \Phi_2 \end{bmatrix} \quad (3.8)$$

and the complete system noise matrix is

$$Q = \begin{bmatrix} Q_1 & 0 \\ 0 & Q_2 \end{bmatrix} \quad (3.9)$$

The above derivations show the equations for the basic system dynamic model in GPS RTK positioning. In case the user wants to estimate additional states, like the DD ionospheric errors, the state vector can be expanded as follows:

$$x = (\mathbf{j}, I, h, \mathbf{j}, \dot{I}, \dot{h}, \hat{N}_1, \hat{N}_2, \hat{N}_3, \dots, \hat{N}_n, I_1, I_2, I_3, \dots, I_n) \quad (3.10)$$

where I_i is the DD ionospheric error in metres between the i th satellite-receiver pair.

Assuming a first order Gauss-Markov process for the DD ionospheric error state I_i with a driving noise w_i of spectral density sp_i in units of m^2/s , and time constant T_0 in seconds, the continuous state-space equation for I_i is derived as

$$\dot{I}_i = -\frac{1}{T_0} I_i + w_i \quad (3.11)$$

The discrete form of the above equation is

$$I_i^{k+1} = e^{-\frac{dt}{T_0}} I_i^k + w_i^{k,k+1} \quad (3.12)$$

where $w_i^{k,k+1} = \int_{t^k}^{t^{k+1}} e^{-\frac{1}{T_0}(t^{k+1}-t)} w(\mathbf{t}) d\mathbf{t}$, $d\mathbf{t} = t^{k+1} - t^k$, and the variance of the discrete white

noise $w_i^{k,k+1}$ is $\frac{sp_i T_0}{2} [1 - e^{-\frac{2}{T_0} d\mathbf{t}}]$.

The subtransition matrix for the complete DD ionospheric error state vector $(I_1, I_2, I_3, \dots, I_n)$ is then derived as

$$\Phi_3 = \begin{bmatrix} e^{-\frac{d\mathbf{t}}{T_0}} & 0 & 0 & 0 & 0 \\ 0 & e^{-\frac{d\mathbf{t}}{T_0}} & 0 & 0 & 0 \\ 0 & 0 & e^{-\frac{d\mathbf{t}}{T_0}} & 0 & 0 \\ \vdots & \vdots & \vdots & \ddots & \vdots \\ 0 & 0 & 0 & 0 & e^{-\frac{d\mathbf{t}}{T_0}} \end{bmatrix} \quad (3.13)$$

The subsystem noise matrix for the DD ionospheric error state vector is derived as

$$Q_3 = \begin{bmatrix} \frac{sp_1 T_0}{2} [1 - e^{-\frac{2}{T_0} d\mathbf{t}}] & 0 & 0 & 0 & 0 \\ 0 & \frac{sp_2 T_0}{2} [1 - e^{-\frac{2}{T_0} d\mathbf{t}}] & 0 & 0 & 0 \\ 0 & 0 & \frac{sp_3 T_0}{2} [1 - e^{-\frac{2}{T_0} d\mathbf{t}}] & 0 & 0 \\ \vdots & \vdots & \vdots & \ddots & \vdots \\ 0 & 0 & 0 & 0 & \frac{sp_n T_0}{2} [1 - e^{-\frac{2}{T_0} d\mathbf{t}}] \end{bmatrix} \quad (3.14)$$

In the expanded state vector case, the complete transition matrix is denoted as

$$\Phi = \begin{bmatrix} \Phi_1 & 0 & 0 \\ 0 & \Phi_2 & 0 \\ 0 & 0 & \Phi_3 \end{bmatrix} \quad (3.15)$$

and the complete system noise matrix is derived as

$$Q = \begin{bmatrix} Q_1 & 0 & 0 \\ 0 & Q_2 & 0 \\ 0 & 0 & Q_3 \end{bmatrix} \quad (3.16)$$

3.1.1.2 Kalman Filter Measurement Model

The dynamic model in a Kalman filter describes the evolution of the states. The measurement model relates the state vector to the GPS observations through the design matrix H . For information on how to compute the design matrix H , see Cannon (1991). Regular updates by the measurement into the state vector is crucial as the system will diverge if there is no measurement provided over a long period of time, driven by the system input noise. These observations for the float filter can be DD carrier phase observables (CP) only, or DD carrier phase plus DD pseudorange observables (CP and P). The pseudorange observables are used most of the time because the position states are not directly observable by the DD carrier phase observable because of the existence of the DD ambiguity terms, but they are directly observable by the DD pseudorange observations. Providing the DD pseudorange observation can reduce the time for the Kalman filter to converge. In this thesis, DD C/A pseudorange P is used in every ambiguity resolution strategy to speed up the filter convergence. The selection of the carrier phase observable is a little complicated, and more on this topic is covered in Chapter 4.

3.2 Ambiguity Resolution

The output of the float filter procedure is the current position component estimates, the velocity component estimates, and the float-valued DD ambiguities \hat{N} (the Kalman filter does not take the integer property of the DD ambiguities into account in the float filter procedure, so the estimated DD ambiguities are floating valued), and the variance covariance matrix $C_{\hat{N}}$ for \hat{N} .

The second procedure in Figure 3.1 is the ambiguity search or resolution and validation procedure. It is in this procedure that the integer property of the DD ambiguities is applied in certain search algorithms to find the correct DD integer ambiguities. Usually these search algorithms are carried out in the ambiguity domain, based on the output of the float filter procedure, \hat{N} and $C_{\hat{N}}$. To date, there are numerous ambiguity search methods available. The most prominent methods among them are:

- Ambiguity function method (Counselman et al., 1981)
- Least-squares ambiguity search technique (Hatch, 1990; 1991)
- Fast ambiguity resolution approach (FARA) (Frei, 1991)
- Least-squares ambiguity decorrelation adjustment method (LAMBDA) (Teunissen, 1993)
- Fast ambiguity search filter (FASF) (Chen and Lachapelle, 1994)
- Sequential integer rounding (Bootstrapping Method) (Blewitt, 1989; Teunissen, 1998a)

In this research, two ambiguity resolution schemes are investigated thoroughly. They are the Bootstrapping method and the LAMBDA method. Although the ambiguity search algorithm in the FASF is more complicated and robust than the Bootstrapping method, they both utilize the basic techniques; even though FASF does “bootstrapping” recursively. Thus, in this chapter, only the LAMBDA and Bootstrapping methods are discussed.

3.2.1 LAMBDA Method

LAMBDA stands for Least-squares Ambiguity Decorrelation Aadjustment. It was proposed by Teunissen (1993). Assuming an n -dimensional ambiguity state vector, the LAMBDA ambiguity resolution method is based on the following principle

$$\min(\hat{N} - N)C_{\hat{N}}^{-1}(\hat{N} - N)^T, \text{ with } N \in Z^n \quad (3.17)$$

where Z^n means an n -dimensional integer space. Equation (3.17) tries to find the integer ambiguity vector \tilde{N} that makes the above quadratic product minimum. Teunissen (1998a) has proven that the success rate of using the LAMBDA method to estimate integer ambiguities is always greater than or equal to any other integer ambiguity estimator.

Another important procedure in carrier phase positioning is the ambiguity validation, shown in Figure 3.1. With the LAMBDA method, a set of integer ambiguities can always be generated that satisfy Equation (3.17). However, the biggest limitation for LAMBDA is not whether an ambiguity solution can be generated, but instead how the ambiguities generated from Equation (3.17) can be validated. Usually this validation process is done

by a ratio test that compares the smallest sum of squared ambiguities residuals to the second smallest. The ratio test is (Han and Rizos, 1996a):

$$ratio = \frac{(\hat{N} - N_2)C_{\hat{N}}^{-1}(\hat{N} - N_2)^T}{(\hat{N} - N_1)C_{\hat{N}}^{-1}(\hat{N} - N_1)^T} \geq \mathbf{d} \quad (3.18)$$

where N_1 is a set of integer ambiguities that makes Equation (3.17) result in the smallest sum of squared ambiguities residuals, N_2 is another set of integer ambiguities that makes Equation (3.17) result the second smallest sum of squared ambiguities residuals. Usually the value of the ratio, \mathbf{d} , is dependant on the dimension of the ambiguity vector; the larger the dimension of the ambiguity vector, the smaller the value of \mathbf{d} . At this stage, there is no better measure than this ratio test to validate the resolved integer ambiguities.

3.2.2 Bootstrapping Method

The simplest way of integer ambiguity resolution is to round the float ambiguity to its closest integer regardless of the ambiguity variance-covariance matrix. The integer bootstrapping is very similar to integer rounding except that it takes the correlation between ambiguities into account. The bootstrapping method follows from a sequential conditional least squares adjustment and it is computed as follows. If n ambiguities are available, the bootstrapping method starts with the first ambiguity \hat{N}_1 , and rounds its value to the nearest integer. Having obtained the integer value of this first ambiguity, the real-valued estimates of all remaining ambiguities are then corrected by virtue of their correlation with the first ambiguity. Then the second, but now corrected, real-valued ambiguity estimate is rounded to its nearest integer, and the real-valued estimates of all remaining $n-2$ ambiguities are again corrected, but now by virtue of their correlation

with the second ambiguity. The process is continued until all ambiguities are considered.

The components of the bootstrapped ambiguities are given as (Teunissen, 1998a):

$$\begin{aligned}
 N_1 &= [\hat{N}_1] \\
 N_2 &= [\hat{N}_{2|1}] = [\hat{N}_2 - \mathbf{s}_{\hat{N}_2, \hat{N}_1} \mathbf{s}_{\hat{N}_1}^{-2} (\hat{N}_1 - N_1)] \\
 &\vdots \\
 N_n &= [\hat{N}_{n|n-1}] = [\hat{N}_n - \sum_1^{n-1} \mathbf{s}_{\hat{N}_n, \hat{N}_{i|I}} \mathbf{s}_{\hat{N}_{i|I}}^{-2} (\hat{N}_{i|I} - N_i)]
 \end{aligned} \tag{3.19}$$

where the shorthand notation $\hat{N}_{i|I}$ and $\mathbf{s}_{\hat{N}_{i|I}}$ stands for the i th least squares ambiguity and its standard deviation obtained through conditioning on the previous $I = \{1, \dots, (i-1)\}$ sequentially rounded ambiguities. The success rate of any bootstrapped ambiguity can be computed as (Teunissen, 1998a):

$$S(\hat{N}_i = N_i) = 2F\left(\frac{1}{2\mathbf{s}_{\hat{N}_{i|I}}} - 1\right) \tag{3.20}$$

$$\text{with } F(x) = \int_{-\infty}^x \frac{1}{\sqrt{2\mathbf{p}}} \exp\left(-\frac{1}{2}y^2\right) dy \tag{3.21}$$

where $F(x)$ is the cumulative distribution function of a normal Gaussian distribution. It can be seen that the smaller the conditional variance of the ambiguity, the higher the probability is of fixing the ambiguity correctly. Thus, for the integer bootstrapping method, it is better off to start with the ambiguity with the smallest variance, then the second smallest, then the third, and so on. The success rate can be used as a validation measure in the Bootstrapping ambiguity resolution method. Normally in Bootstrapping ambiguity resolution, a check must be made on the standard deviation of the float ambiguity to ensure it is small enough to yield a sufficiently high success rate.

3.3 Tests and Results

To show the effectiveness of both the Bootstrapping and LAMBDA ambiguity resolution techniques, the same 24-hour baseline data used in Chapter 2 is processed in kinematic mode with different ambiguity resolution strategies.

3.3.1 Results with LAMBDA

The data is processed with the software FLYKIN+TM (This software is discussed in detail in Chapter 4) using the LAMBDA ambiguity resolution module and position estimates given at every epoch. The observables used are the C/A pseudorange and WL carrier phase observables. FLYKIN+TM is a software package capable of processing GPS data in static or kinematic modes, and allows users to select from a wide range of processing options. However, it was stated in Chapter 1 of this thesis that the research is focused on normal RTK practices, so the software FLYKIN+TM was always used in kinematic mode.

The position domain results are presented in Figure 3.3. Green in the figure means that all ambiguities have been fixed, red means none of the ambiguities have been fixed, blue means all ambiguities except one have been fixed, and yellow means more than one ambiguity cannot be fixed. The overall position errors show the LAMBDA method works very well. This baseline is also processed with Bernese Software in batch processing mode. The Bernese software is well tuned for processing static data in batch mode and the ambiguity output from the Bernese software is assumed to be correct. The ambiguities output by Bernese are compared to the ambiguities output by FLYKIN+TM. Their difference in absolute value is shown in Figure 3.4. The difference is zero for the entire

data set, indicating that the ambiguities resolved with LAMBDA method is 100% accurate.

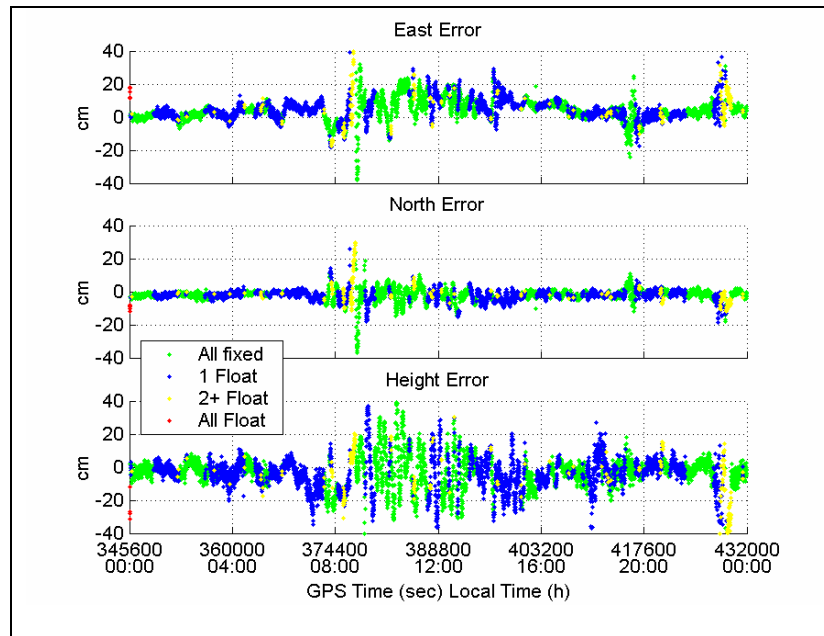


Figure 3.3 Position Errors with LAMBDA Method

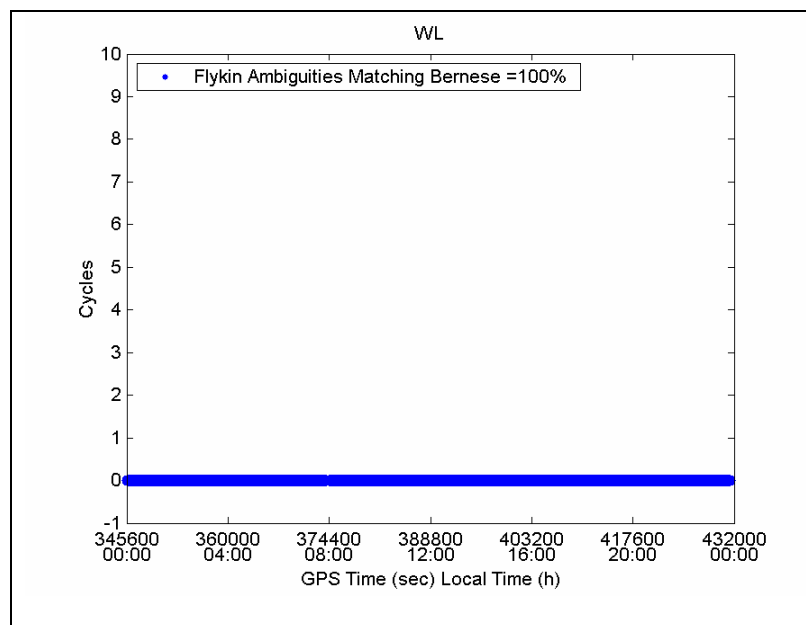


Figure 3.4 Ambiguity Difference between LAMBDA and Bernese Approaches

3.3.2 Results with Bootstrapping

To evaluate the performance of the Bootstrapping method, the data was also processed with FLYKIN+™ using the Bootstrapping ambiguity resolution module, and position estimates were again determined at every epoch. The position domain results are presented in Figure 3.5. It is clear that the position error is bounded very well, indicating that the Bootstrapping ambiguity resolution is functioning well in this case.

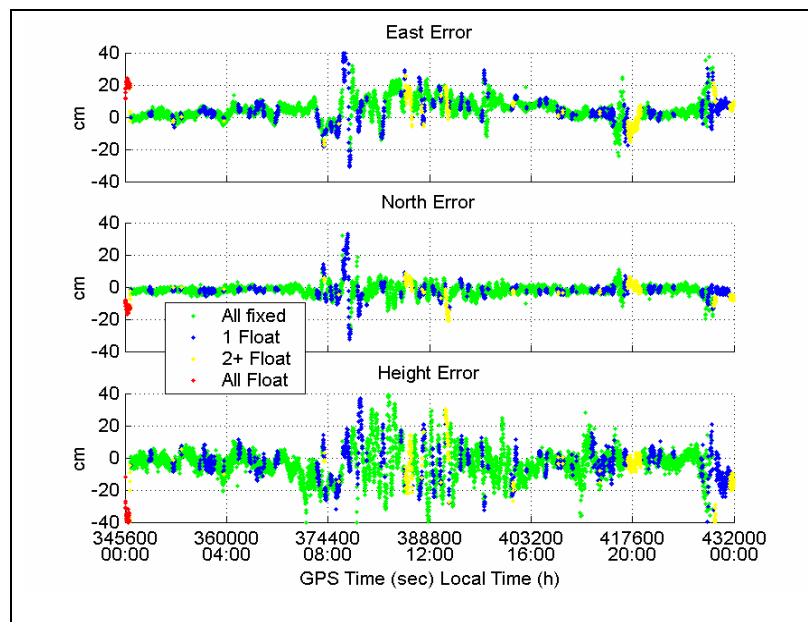


Figure 3.5 Position Errors with Bootstrapping Method

Figure 3.6 shows the difference between Bootstrapped ambiguities and Bernese generated ambiguities. The difference is zero for the entire data set, also indicating a 100% success rate for Bootstrapping ambiguity resolution method.

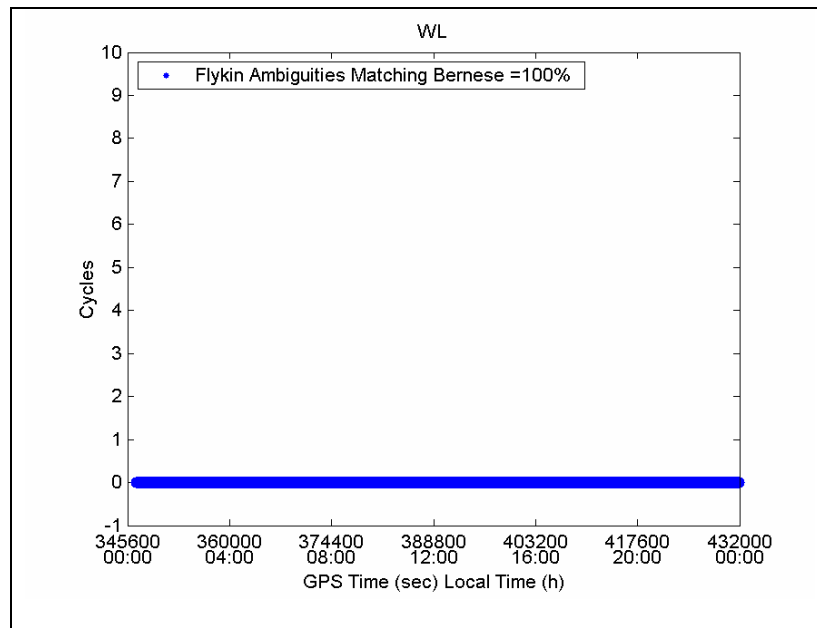


Figure 3.6 Ambiguity Differences between Bootstrapping and Bernese Approaches

Table 3.1 summarizes the performance for the LAMBDA and Bootstrapping ambiguity resolution methods for this data. Both methods result in the same position estimate RMS error in the north, east and up axes, which is understandable since Figure 3.4 and Figure 3.6 demonstrated that there are no inaccurately resolved ambiguities. In Table 3.1, “All Fixed Percentage” means the percentage of those epochs in the 24-hour period when all of the ambiguities are resolved to integers, and “All Float Percentage” means the percentage of those epochs in the 24-hour period when none of the ambiguities are resolved to integers. Table 3.1 reports 0.1% and 0.04% for the Bootstrapping and LAMBDA method in the “All Float Percentage” category respectively, which suggests a high efficiency for both the LAMBDA and Bootstrapping methods. In the “All Fixed Percentage” category, Bootstrapping reports 10% less than LAMBDA, which can be explained by the fact that a more rigorous constraint is enforced on the standard deviation of the float ambiguities in the Bootstrapping method.

Table 3.1 LAMBDA and Bootstrapping Comparison

Category		Bootstrapping	LAMBDA
RMS Error (cm)	North	9	9
	East	4	4
	Up	12	12
All Fixed Percentage		48%	58%
All Float Percentage		0.1%	0.04%

3.4 Suggested Ambiguity Resolution Method

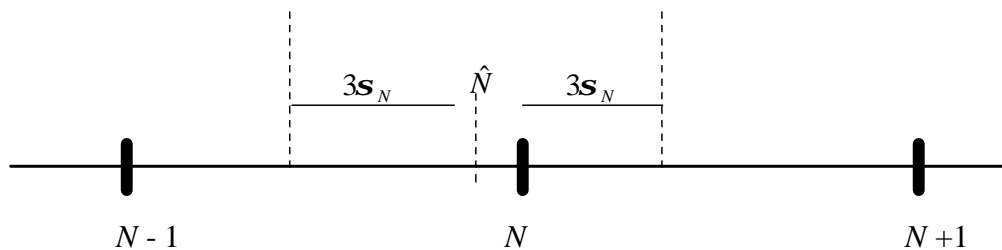
Teunissen (1998a) has proven that the success rate of using the LAMBDA method to estimate integer ambiguities is always greater than or equal to any other integer ambiguity estimator. Thus the LAMBDA method is a preferred method for ambiguity resolution. However since the validation procedure for the LAMBDA method employs a ratio test and this has turned out to have limitations which may cause problems. The above ratio test can provide a high degree of reliability, but it does not provide a high degree of efficiency, especially if there is frequent loss of tracking to some satellites. If a new satellite is included in a solution, the standard deviation for the ambiguity of the new satellite is usually very high, and this will push the result of the ratio test close to a value of one. More observations are needed to drive down the standard deviation of the newly included ambiguity parameter to increase the computed ratio. This is a loss of efficiency. The satellites that have been observed for an extended amount of time, and with their associated ambiguities fixed, should also have relatively small standard deviations. It

does not make sense then, to carry out the ambiguity resolution process for all the satellites when a new ambiguity parameter lowers the ratio value. In order to avoid this problem, a combined ambiguity resolution scheme is investigated and employed in the software FLYKIN+TM. First the software uses LAMBDA to solve for all the ambiguities. If the ratio does not exceed the threshold, then the software examines the float ambiguity value and the standard deviation of each individual ambiguity. If the standard deviation of an ambiguity is too large (for example: = 0.1 cycle), then the software will not fix this ambiguity, otherwise it carries out a search using the float ambiguity and its associated standard deviation via the procedures below. Assuming the value of the float ambiguity is \hat{N} , and the standard deviation of the ambiguity is \mathbf{s}_N , a search space (SS) is determined into which the integer ambiguity should fall. This search space is:

$$SS : [\hat{N} - 3\mathbf{s}_N, \hat{N} + 3\mathbf{s}_N]$$

Depending on the value of the float ambiguity, \hat{N} , and standard deviation, \mathbf{s}_N , there are three possible scenarios.

Scenario I: There is exactly one integer ambiguity in (SS) and the float ambiguity is very close to an integer.



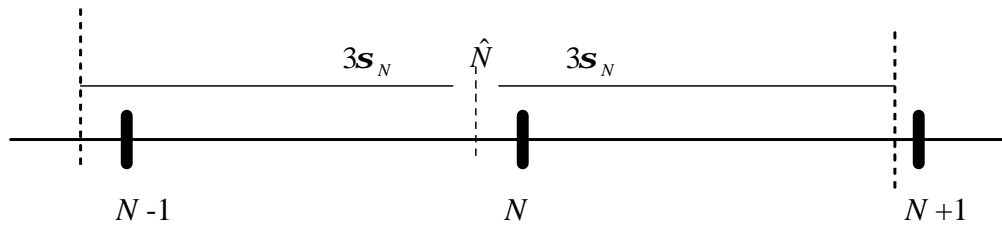
This is the ideal scenario. The only integer in (SS) is regarded as the correct ambiguity value.

Example:

$$\begin{cases} \hat{N} = 0.95 \\ \mathbf{s}_{\hat{N}} = 0.04 \end{cases} \Rightarrow (SS): [0.95 - 3 \times 0.04, 0.95 + 3 \times 0.04]$$

There is only one integer value, 1, within the (SS) . This float ambiguity has converged because the standard deviation of this float ambiguity is only 0.04. Unless there is cycle slip, the value of this float ambiguity will not change dramatically. Thus, 1 is deemed the correct integer ambiguity.

Scenario II: There is more than one integer ambiguity in (SS) because the standard deviation of the float ambiguity is too large.



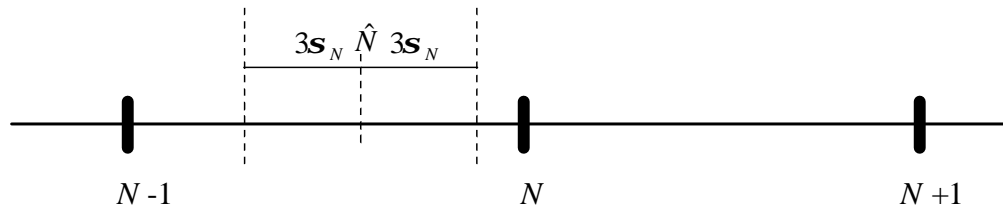
This is the case when the ambiguity has not been observed for enough time. The standard deviation is too large. More observations are needed to increase the precision of the float ambiguities.

Example:

$$\begin{cases} \hat{N} = 0.95 \\ \mathbf{s}_{\hat{N}} = 0.4 \end{cases} \Rightarrow (SS): [0.95 - 3 \times 0.4, 0.95 + 3 \times 0.4]$$

There are three integers $\{0, 1, 2\}$ in (SS) . It is highly risky to fix the ambiguity in this case.

Scenario III: The float ambiguity is far off any integer value.



This is the case when there are unmodelled error sources such as ionospheric error or multipath. It is safer to keep the ambiguity as a float value rather than to forcefully fix them with a high risk. Fixing to a wrong value is much worse than keeping the ambiguity float, as fixing incorrectly will introduce a large bias into the observations.

Example:

$$\begin{cases} \hat{N} = 0.55 \\ \mathbf{s}_{\hat{N}} = 0.04 \end{cases} \Rightarrow (SS): [0.55 - 3 \times 0.04, 0.55 + 3 \times 0.04]$$

There are no ambiguities in (SS) , and \hat{N} is nowhere near an integer; keep the ambiguities as float values and wait until the multipath or ionospheric error subsides.

The suggested ambiguity resolution method makes sense in practice. Usually it turns out that the ambiguity of the high elevation satellites will converge much faster than that of the low elevation satellites. It is reasonable to resolve the high elevation ambiguity first and leave the low elevation ambiguity float (Partial fixing). With fixing of high elevation satellite, the solution is strengthened and it is more efficient to fix the remaining float ambiguities.

This suggested ambiguity resolution technique is also implemented in the FLYKIN+™ software. It is recommended that for very short baseline RTK operations, this ambiguity resolution technique should be used. It is expected to be more efficient than the LAMBDA only method as the suggested algorithm can operate well in partial fixing mode. One important restriction applies to the suggested ambiguity resolution method. The combined method contains the Bootstrapping method, which is reliable only when the estimator that estimates the float ambiguity is unbiased or slightly biased. A Large bias due to unmodelled error sources like the high ionospheric error will bias the estimated float ambiguities and Bootstrapping will then result in erroneous integer ambiguities. It is recommended that this suggested ambiguity resolution approach should be tested extensively.

CHAPTER 4

AMBIGUITY RESOLUTION STRATEGIES

4.1 Introduction

Chapter 3 introduced the float filter, which serves as the starting point for ambiguity resolution. Once the float-valued ambiguities and the corresponding variance-covariance matrix are output from the float filter, an ambiguity resolution technique (LAMBDA, Bootstrapping, FASF, FARA, etc.) can be applied to resolve the correct integer ambiguities. However, how to generate the float-valued ambiguities and the corresponding variance-covariance matrix is not so straightforward.

It was shown in Chapter 3 that the float filter is implemented through a Kalman filter which contains both a dynamics model and a measurement model. The dynamics model dictates what states are estimated and the measurement model dictates what observations or observation combinations are used. The estimated states usually include position, velocity, ambiguities, and the DD ionospheric error (if estimated). The ambiguity states can be L1 ambiguity only, L2 ambiguity only, WL ambiguity only or any combination between L1, L2, and WL ambiguities. The observations can be L1 phase only, L2 phase only, L1 and L2 phase together, WL phase only, or IF phase only. The use of dual frequency GPS data facilitates a wide variety of possible dynamics and measurement

models. However, this “variety” also means that it is sometimes difficult to determine which dynamics and measurement models best fits an application. It is not clear whether they have the same ambiguity resolution and positioning performance or whether one is significantly better than the others.

In this chapter, eight processing strategies were formulated that combine different choices of observables (measurement model), parameterization schemes (dynamics model), and estimation models. All eight strategies were tested extensively in Chapter 5. This chapter will present the detailed formulation of each strategy.

4.2 Strategy Formulation

Table 4.1 summarizes all eight strategies in terms of ambiguities estimated and observables used, where N_1 is the L1 ambiguity, N_2 is the L2 ambiguity, N_{WL} is the WL ambiguity, and N_{IF} is the float valued IF ambiguity. CP_1 is the L1 carrier phase observable, CP_2 is the L2 carrier phase observable and P is the L1 C/A pseudorange observable. The P observable is used in every strategy. Chapter 2 has explained that the pseudorange observable is needed to speed up the convergence of the ambiguity states in the float filter.

Strategies 1 through 4 do not take the ionospheric error into account, i.e. the model assumes that it has been eliminated through the DD process. In contrast, Strategies 5 through 8 will deal with the ionospheric error by either removing it through forming the

IF observable (Strategies 5 and 6) or by estimating it with stochastic ionospheric modelling techniques (Strategies 7 and 8). For every strategy, the state vector always includes the three position states ($\mathbf{j}, \mathbf{l}, h$) and the three velocity states ($\dot{\mathbf{j}}, \dot{\mathbf{l}}, \dot{h}$). The velocity states are modelled as random walk processes. Each strategy also includes additional ambiguities states, determined by the parameterization schemes of the observations. The ambiguity states are modelled as random constants. In Strategies 7 and 8 where the DD ionospheric error is modelled and estimated, a first order Gauss-Markov process is used. Each of the strategies is discussed in detail below.

Table 4.1 Strategy Summary

Strategy	Ambiguity	Observables	Ionosphere
1	N_1	CP_1, P	Not Parameterized
2	N_{WL}	CP_1, CP_2, P	
3	N_1, N_2	CP_1, CP_2, P	
4	N_1, N_{WL}	CP_1, CP_2, P	
5	N_1, N_{WL} (IF Fixed)	CP_1, CP_2, P	Ionosphere-Free Combinations
6	N_{IF} (IF Float)	CP_1, CP_2, P	
7	N_1, N_2	CP_1, CP_2, P	Stochastic Ionosphere Modelling I_1
8	N_1, N_{WL}	CP_1, CP_2, P	

4.2.1 Strategy 1 (use CP_1 , CP_2 and P):

The observation equations for this strategy can be written as:

$$\begin{aligned}
 CP_1 &= \frac{\mathbf{r}}{I_1} + N_1 + e(cp_1) \\
 P &= \mathbf{r} + e(P)
 \end{aligned}
 \tag{4.1}$$

This is the simplest strategy, where only the L1 carrier phase and pseudorange observables are used. Correspondingly, only the L1 ambiguity is estimated. This is the typical scenario for most short baselines (say, < 5 km). The first advantage of this strategy is its simplicity, since only the L1 carrier phase observation is used and no observation combination is formed. The second advantage is its low noise and ionospheric error characteristics compared to WL and L2. Chapter 2 has shown that the ionospheric error and measurement noise on L1 in metres is the lowest compared to L2 and WL. If the L1 ambiguities are fixed correctly, then better position solution will be achieved compared to L2 and WL. The disadvantage is that this strategy will have problems resolving the L1 integer ambiguities in period of high ionospheric error, considering the relatively short wavelength of L1 carrier, 19 cm. If the ionospheric error is around or bigger than half of the wavelength, 10 cm, then this ambiguity resolution strategy can easily run into trouble. However, for most single frequency receivers, Strategy 1 is the only choice that can offer centimetre level positioning accuracy, but the success will be dependant on several factors including the ionospheric level.

4.2.2 Strategy 2 (use CP_1 , CP_2 and P):

The observation equations for this strategy can be written as:

$$\begin{aligned}
CP_{WL} &= CP_1 - CP_2 \\
N_{WL} &= N_1 - N_2 \\
CP_{WL} &= \frac{\mathbf{r}}{\mathbf{I}_{WL}} + N_{WL} + e(cp_{WL}) \\
P &= \mathbf{r} + e(P)
\end{aligned} \tag{4.2}$$

In this strategy, the WL carrier phase observable is used, and the WL ambiguity is estimated in the filter. Chapter 2 discussed the property of the WL observable. It is expected that Strategy 2 should have better ambiguity resolution performance than Strategy 1 considering the large wavelength (86cm) to ionospheric error (in cycles) ratio. However, it was also demonstrated in Chapter 2 that the ionospheric error in metres for the WL actually increased, plus the fact that the WL contains nearly six times the noise than the L1 in metres, so Strategy 2 is expected to give a position estimate which contains high noise and ionospheric error signature.

4.2.3 Strategy 3 (use CP_1 , CP_2 and P):

The observation equations for this strategy can be written as:

$$\begin{aligned}
CP_1 &= \frac{\mathbf{r}}{\mathbf{I}_1} + N_1 + e(cp_1) \\
CP_2 &= \frac{\mathbf{r}}{\mathbf{I}_2} + N_2 + e(cp_2) \\
P &= \mathbf{r} + e(P)
\end{aligned} \tag{4.3}$$

This strategy is similar to Strategy 1. However, besides the L1 ambiguities, additional L2 ambiguities are estimated in the filter using the L2 carrier phase observations. A dual

frequency receiver output both L1 and L2 carrier phase observables, thus it does not make sense to use only L1 data to estimate the positions as Strategy 1 does.

The first advantage of Strategy 3 is that more system redundancy is achieved with the inclusion of the L2 data. The second advantage is that, unlike Strategy 2, the carrier phase noise is kept minimum since no frequency combination is formed between L1 and L2. However, it was shown in Chapter 2 that L2 has more ionospheric error than either the L1 or the WL. It is expected that this strategy will suffer significantly from ionospheric error in periods of high ionospheric activity, while it is expected to perform better than Strategy 1 in periods of very low ionospheric error since there is an increase in system redundancy.

4.2.4 Strategy 4 (use CP_1 , CP_2 and P):

The observation equations can be written as:

$$\begin{aligned}
 CP_1 &= \frac{\mathbf{r}}{I_1} + N_1 + e(cp_1) \\
 CP_2 &= \frac{\mathbf{r}}{I_2} + N_1 - N_{WL} + e(cp_2) \\
 P &= \mathbf{r} + e(P)
 \end{aligned} \tag{4.4}$$

This strategy is very similar to the previous strategy except that the WL and L1 ambiguities are estimated in the filter rather than the L1 and L2 ambiguities. Compared to Strategy 1, this strategy has the same kind of advantages and disadvantages as Strategy 3. However, this strategy has an additional advantage brought by the parameterization

scheme in Equation (4.4): WL and L1 ambiguities are estimated in Equation (4.4) instead of the L1 and L2 ambiguities in Equation (4.3). It is expected that the WL ambiguities will converge very fast and be resolved to integers easily, while more data is needed to resolve the L1 ambiguities. Thus in this strategy, an attempt is first made to resolve the WL ambiguities; after that is done, an attempt is made to resolve the L1 ambiguities. It is expected that more data is needed for the L1 ambiguities to converge after the WL ambiguities are resolved since WL ambiguities are expected to converge much faster than L1 ambiguities. This strategy is included to compare the impact of different model parameterizations.

4.2.5 Strategy 5 (use CP_1 , CP_2 and P):

Strategy 5 is a cascading scheme and it involves two sets of observation equations. The first set of observation equations (Equation (4.5)) is the same as the one used in Strategy 2.

$$\begin{aligned} CP_{WL} &= \frac{\mathbf{r}}{\mathbf{I}_{WL}} + N_{WL} + e(cp_{WL}) \\ P &= \mathbf{r} + e(P) \end{aligned} \quad (4.5)$$

Equation (4.5) uses the WL observables to estimate the WL ambiguities. After the WL ambiguities are resolved, a modified IF observation $CP_1 - \frac{I_1}{I_2} CP_2 - \frac{I_1}{I_2} N_{WL}$ is formed and a new set of observation equations is constructed as shown below

$$CP_1 - \frac{I_1}{I_2} CP_2 - \frac{I_1}{I_2} N_{WL} = \frac{\mathbf{r}}{\mathbf{I}_{IF}} + \frac{I_2 - I_1}{I_2} N_1 + e(cp_{IF}) \quad (4.6)$$

where I_{IF} is the IF wavelength (48cm). Equation (4.6) uses the modified IF observation

$CP_1 - \frac{I_1}{I_2} CP_2 - \frac{I_1}{I_2} N_{WL}$ to estimate the N_1 ambiguity. It should be noted that in this case, the

effective L1 wavelength is $I_{IF} \frac{I_2 - I_1}{I_2}$ (10.7 cm) instead of I_1 (19 cm). The advantage of

this strategy is that it will not suffer from the ionospheric error given that this effect is removed. However, there are several disadvantages of this strategy. The first disadvantage is the noise characteristics of the modified IF observation

$CP_1 - \frac{I_1}{I_2} CP_2 - \frac{I_1}{I_2} N_{WL}$. Chapter 2 shows that the IF has a noise level which is three times

higher than on L1 in metres. It is thus expected that the position estimate of the strategy will show a strong noisy signature. The second disadvantage of this strategy is that the effective wavelength of N_1 is very small, only 10.7 cm. This will pose a problem when

trying to resolve the N_1 directly. N_1 may be resolved correctly provided that the combined residual tropospheric error and the position estimate error is not significant (< 5 cm). This condition may not be fulfilled easily in practice. The short wavelength of 10.7cm also means a much longer convergence time for the N_1 ambiguities is needed.

After the L1 ambiguities are estimated and resolved as integers, the ionosphere-free fixed (IF Fixed) position estimates can be computed and the ionospheric error can also be computed based on the L1 and L2 carrier phase observables using the following equation

$$I_1 = \frac{I_1 CP_1 - I_2 CP_2}{I_1 N_1 - I_2 N_2} \frac{I_1^2}{I_1^2 - I_2^2} \quad (4.7)$$

The term “IF Fixed” is derived because in this strategy, both L1 and L2 (or WL) ambiguities have been fixed to integer values. Blewitt (1989) discussed a similar approach to resolving ambiguities for long inter-station baselines.

4.2.6 Strategy 6 (use CP_1 , CP_2 and P):

The observation equations for this strategy can be written as:

$$\begin{aligned} CP_1 - \frac{I_1}{I_2} CP_2 &= \frac{\mathbf{r}}{I_{IF}} + N_{IF} + e(cp_{IF}) \\ P &= \mathbf{r} + e(P) \end{aligned} \quad (4.8)$$

In this strategy, the IF ambiguities N_{IF} are estimated using the IF observations. By nature, N_{IF} are floating values. This is a special strategy where ambiguities are estimated but need not be resolved to integers. The argument behind this strategy is that as long as all other observation errors (e.g. tropospheric error, satellite coordinates, multipath) are properly accounted for, the float-valued IF ambiguity should be errorless. The position estimates based on these float-valued IF ambiguities are named the “IF Float” solutions. This term is used because in this strategy no attempt is made to resolve the L1 and L2 (or WL) integer ambiguities. The advantage of this strategy is that no ambiguity resolution is needed and it is still expected to give a fair good position estimate since the ionospheric error is removed when forming the IF observation. The disadvantage of this strategy is its noise characteristics, as the IF observation is three times as noisy as L1 in metres.

4.2.7 Strategy 7 (use CP_1 , CP_2 and P):

The observation equation for this strategy is:

$$\begin{aligned}
 CP_1 &= \frac{\mathbf{r}}{I_1} + N_1 - I_1 + e(cp_1) \\
 CP_2 &= \frac{\mathbf{r}}{I_2} + N_2 - \frac{I_2}{I_1^2} I_1 + e(cp_2) \\
 P &= \mathbf{r} + I_1 + e(P) \\
 I_0 &= I_1 \\
 I_0 &\sim (0, \mathbf{s}_0^2)
 \end{aligned} \tag{4.9}$$

Chapter 2 has shown that a first order Gauss-Markov process is consistent with the observed temporal correlations for ionospheric error, thus it is feasible to model and estimate the ionospheric error in a Kalman filter. The previous state vector containing only position, velocity and ambiguity states in Strategies 1-6 is now expanded to include the DD ionospheric error, which is modelled as a first order Gauss-Markov process in this strategy.

The first advantage is that now the estimator in Strategy 7 is largely unbiased given the DD ionospheric error is modelled explicitly. It is expected that the position estimate will not be influenced by the ionospheric error. The other advantage of this strategy is that no frequency combination is made in modelling the ionospheric error between L1 and L2, unlike the previous two strategies where IF is formed to remove the ionospheric error, thus the observation noise is kept minimum. It is thus expected that the position estimate of this strategy will outperform the previous two strategies if ambiguities are resolved correctly in both Strategies 5 and 7. The advantage of this strategy is that the solution is weak since additional states are estimated in the filter. It is expected that the filter in this

strategy may take a longer time to converge compared to Strategies 3 and 4 even all three strategies use the observations of the same type and number. It is also expected that the filter may not distinguish between the N_1 and N_2 ambiguity states and the ionospheric error state at the initial filtering phase, causing extra delay in filter convergence and unreasonable DD ionospheric error estimate.

It is well known that the DD ionospheric error is usually bounded around zero. To help strengthen the solution and speed up the convergence, a pseudo-ionospheric error observable, I_0 , with a value of zero and variance of \mathbf{s}_0^2 is also added for each ionospheric error. The selection of the \mathbf{s}_0^2 is dependant on the highest level of the DD ionospheric error. This pseudo-observable will help constrain the DD ionospheric error to reasonable value during the initial phase of the filter, and force the filter to distinguish between the ionospheric error states and the ambiguity states. This strategy was first seen in (1997a) and applications of this strategy can be found in Odijk (2000).

4.2.8 Strategy 8 (use CP_1 , CP_2 and P):

The observation equations for this strategy are:

$$\begin{aligned}
 CP_1 &= \frac{\mathbf{r}}{I_1} + N_1 - I_1 + e(cp_1) \\
 CP_2 &= \frac{\mathbf{r}}{I_2} + N_1 - N_{wL} - \frac{I_2}{I_1^2} I_1 + e(cp_2) \\
 P &= \mathbf{r} + I_1 + e(P) \\
 I_0 &= I_1 \\
 I_0 &\sim (0, \mathbf{s}_0^2)
 \end{aligned} \tag{4.10}$$

This strategy is very similar to the Strategy 7 except that the WL and L1 ambiguities are estimated in the filter rather than the L1 and L2 ambiguities. Besides the advantages and disadvantages discussed in Strategy 7, this strategy has an additional advantage brought by the parameterization scheme in Equation (4.10): WL and L1 ambiguities are estimated in Equation (4.10) instead of L1 and L2 ambiguities in Equation (4.9). It is expected that the WL ambiguities will converge very fast and resolved to integers easily, while more data is needed to resolve the L1 ambiguities. Thus in this strategy, first an attempt is to resolve the WL ambiguities, after the WL ambiguities are resolved, an attempt is made to resolve the L1 ambiguities. It is expected that more data is needed for the L1 ambiguities to converge after the WL ambiguities are resolved since WL ambiguities are expected to converge much faster than L1 ambiguities. This strategy is included to compare the impact of different model parameterizations.

4.3 Software Realization

Previous sections examined various ambiguity resolution strategies. These processing strategies are implemented in the FLYKIN+TM software package. Before testing the strategies, it is appropriate to discuss some issues related to the FLYKIN+TM software development. The latest FLYKIN+TM is a powerful GPS processing software package and it outperforms its predecessor FLYKINTM (Lu et al., 1994) in many ways. Table 5.1 gives a comparison of these two versions.

Besides the differences shown in the table, the latest edition has some of the following advantages over its previous counterpart: The previous version used a fixed estimation model, which estimated position and velocity, and modelled the velocity as a random walk process; the user had no control of the states estimated and the model used. In the latest version of FLYKINTM, the user has the freedom of choosing which states are to be estimated, be they position, position + velocity, or position + velocity + acceleration. The user also has the freedom of choosing what model is to be used, be it Kalman filtering, or sequential least squares. Finally, users can now choose the observable or observation combination, such as pseudorange only, L1 phase only, L2 phase only, L1+L2 phase, or WL phase combination.

Table 4.2 Software Functionality

Functionality	FLYKIN+ TM	FLYKIN TM
Process data in kinematic mode	Yes	Yes
WL fixing	Yes	Yes
IF float	Yes	No
IF fixed	Yes	No
Process data in static mode	Yes	No
Estimate acceleration	Yes	No
Integrated real time/post mission	Yes	No
Height fixing	Yes	No
Stochastic ionosphere modelling	Yes	No

The latest FLYKIN+™ is developed based on the idea of Object-Oriented Programming (OOP). The benefits of OOP-style programming include code reusing and high modularization. In OOP, each object (a physical process, mathematical model, or a physical entity, etc.) is represented by a class, and similar objects are connected by virtue of inheritance. Specific to the domain of GPS software, the objects are raw observation data objects, satellite ephemeris objects, tropospheric delay model objects, and processing method (single point processing, single difference processing, double difference processing) objects. The software FLYKIN+™ used in this thesis is developed based on a GPS C++ library developed by the Navigation Lab at the Department of Geomatics Engineering, University of Calgary. To illustrate the OOP concept used in the FLYKIN+™ software, the troposphere class is used as an example as shown in Figure 4.1. There are numerous tropospheric delay models. The most frequently used is the modified Hopfield and Saastamoinen tropospheric delay model. By using the OOP style, the software can easily incorporate new models into the existing software with minimal change to the existing code.

Figure 4.1 shows the troposphere model class hierarchy. All the tropospheric models are derived from the same base class NTropoModel. This class encapsulates all the common functionalities of any troposphere model. There are several child classes of the base class NTropoModel. The class NhopfieldTropoModel implements the functionality specific to the modified Hopfield troposphere model. The class NsaasTropoModel implements the functionality specific to the Saastamoinen Model. If in the future a better troposphere model becomes available, a class called OtherTropoModel can be derived from the

NTropoModel to implement specific functionality of the new troposphere model. In this way, the change to the software module interface is minimized.

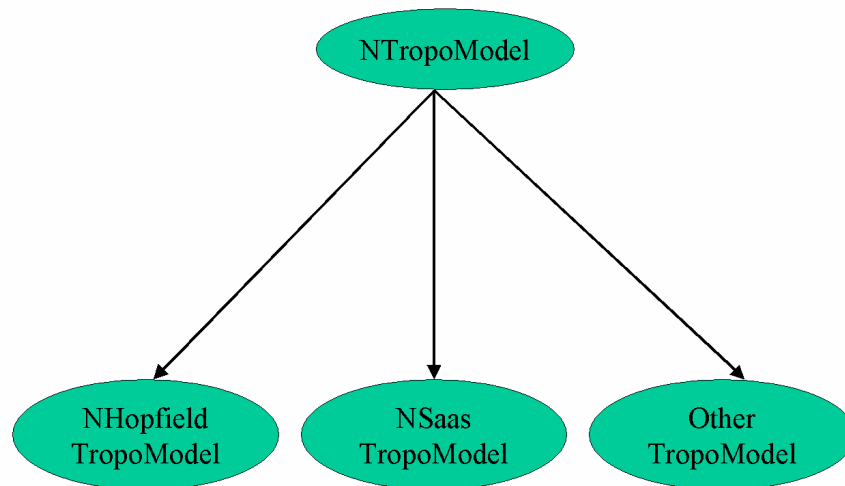


Figure 4.1 Tropospheric Delay Model Classes

To further illustrate the OOP programming style in FLYKIN+TM, another data handling class example is discussed next. Figure 4.2 shows the data handling class hierarchies. The class NUDData handles the undifferenced data object. It acts as a pre-processor to the single point positioning module. The class NSDData derives from the class NUDData and it acts as a pre-processor to the single differenced positioning module. The class NDDData derives from the class NSDData and it acts as a pre-processor to the double differenced positioning module.

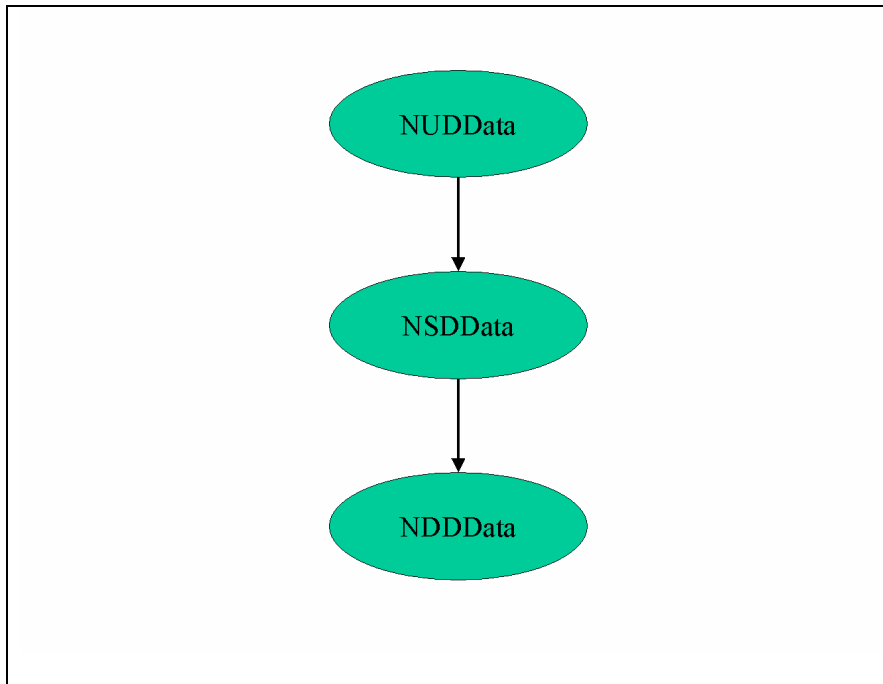


Figure 4.2 Data Handling Class

CHAPTER 5

SINGLE AND MULTIPLE REFERENCE STATION TESTS AND RESULTS

5.1 Introduction

In Chapter 4, eight different ambiguity resolutions strategies were introduced. This chapter tests these eight strategies in both single and multiple reference station scenarios. The test methodology and results for each scenario are presented below.

5.2 Single Reference Station Tests and Results

As stated in Chapter 1, the scope of this research is restricted to normal RTK practice, so a kinematic mode for the rover is assumed. The dynamics model and measurement model discussed in Chapter 3 are used. However, the reduction of real kinematic data is difficult due to the lack of reference trajectory (truth data). For easy comparisons of the position estimate, three static baselines have been selected and processed in a “simulated” kinematic mode. Because the data is static, a small spectral density ($0.0001 \text{ m}^2/\text{s}^3$) is set on the process noise that is driving the velocity states. This means the results are representative of one true kinematic case only when the rover has a constant velocity. For rovers that have significant accelerations, the results presented here are optimistic and they may not represent the real kinematic case. This means that a slight advantage is

gained from the fact that the rover receiver is actually static. All results shown here were obtained using the University of Calgary's new FLYKIN+™ software package described in the previous chapter.

In order to obtain a reference estimate for the L1 and L2 ambiguities, the data were first processed with the University of Bern's Bernese Software. The ambiguity estimates obtained from FLYKIN+™ can then be compared with those from Bernese to evaluate the performance of a given processing strategy. In total, two different tests were conducted. For both tests, FLYKIN+™ uses the LAMBDA technique to resolve the integer ambiguities.

In Test 1, the entire data set is processed with FLYKIN+™ with ambiguities and positions being estimated at each epoch. The rover position estimate is compared to the known position of the rover, and the RMS error is computed. Also, the integer ambiguities estimated by FLYKIN+™ are compared with those from Bernese.

In Test 2 the data set is divided into independent even intervals, and each interval is processed with FLYKIN+™ to check the ambiguity resolution performance and position accuracy for each strategy. Once the ambiguity is resolved, a fixed position solution is recorded and the software will re-initialize the filter and go to the beginning of next interval to try and resolve the ambiguities again. The purposes of Test 2 are to:

- 1) Determine how fast each strategy is able to resolve the ambiguities (time to fix ambiguities); and
- 2) Assess the accuracy of the fixed ambiguities (percentage of correctly fixed ambiguities).

In conjunction with this, this test will also help determine whether fixing WL first can reduce the position errors even if the L1 ambiguities cannot be fixed, although the ultimate goal is to fix the L1 ambiguities. Figure 5.1 shows the set-up for this purpose. In the figure, the upper bar chart represents Strategies 4 and 8 whereby the L1 and WL ambiguities are estimated. The lower bar chart represents Strategies 3 and 7 where the L1 and L2 ambiguities are estimated. The red segment (T2/T4) means that no integer ambiguities are resolved, and the yellow segment (T3) means only WL ambiguities are resolved (in Strategies 4 and 8 only). The green segment (the end) means that all ambiguities have been resolved. This test will compare whether the time needed to fix both L1 and WL (T1) is comparable to the time (T4) required to fix both L1 and L2 ambiguities. This test also will compare the position error RMS during T3 (only WL integer ambiguities are resolved) and T4 (both L1 and L2 ambiguities are not resolved).

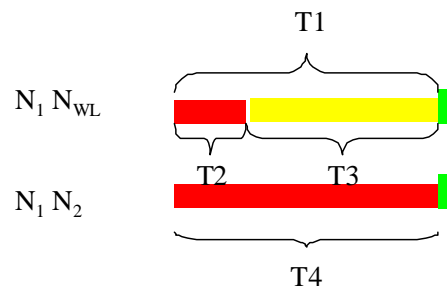


Figure 5.1 Test Set-up

Table 5.1 lists the variances of the different observations used in the processing of each strategy for all three baselines. To make the comparisons consistent, the variance given to the pseudoranges for all strategies is the same. The variance given to the L1 and L2 carrier phase for Strategies 1 to 6 is the same. The variance given to the L1 and L2 carrier phase for Strategies 7 and 8 is the same.

Table 5.1 Observation Standard Deviations

Strategy	Observation Standard Deviation			
	P (m)	CP_1 (cycle)	CP_2 (cycle)	I_0 (m)
1	0.5	0.04	N/A	N/A
2	0.5	0.04	0.04	N/A
3	0.5	0.04	0.04	N/A
4	0.5	0.04	0.04	N/A
5	0.5	0.04	0.04	N/A
6	0.5	0.04	0.04	N/A
7	0.5	0.01	0.01	\mathbf{s}_0
8	0.5	0.01	0.01	\mathbf{s}_0

Since Strategies 7 and 8 models the DD ionospheric error explicitly, the L1 and L2 phase observable variances are smaller than any of the other six strategies. The value of the ionospheric error pseudo-observables is zero. The standard deviation \mathbf{s}_0 for the pseudo-ionosphere observable for the first two baselines is 0.2 m and 0.3 m for the third baseline because the third baseline has a much higher ionospheric error than the first two.

5.2.1 Results

The test results are presented on a baseline-by-baseline basis following the order of the baseline lengths. The 13-km Calgary baseline is presented first.

I) Baseline I.

The first data processed is a 13km baseline in Calgary, Canada. The data set is 24 hours long with a sampling rate of 1Hz, collected in May 2002 with a pair of NovAtel Modulated Precision Clock (MPC) receivers. The cut-off elevation angle is 15° . The following figure depicts the DD ionospheric error on L1 for the 24-hour period which shows that the DD ionospheric error reaches 11 ppm.

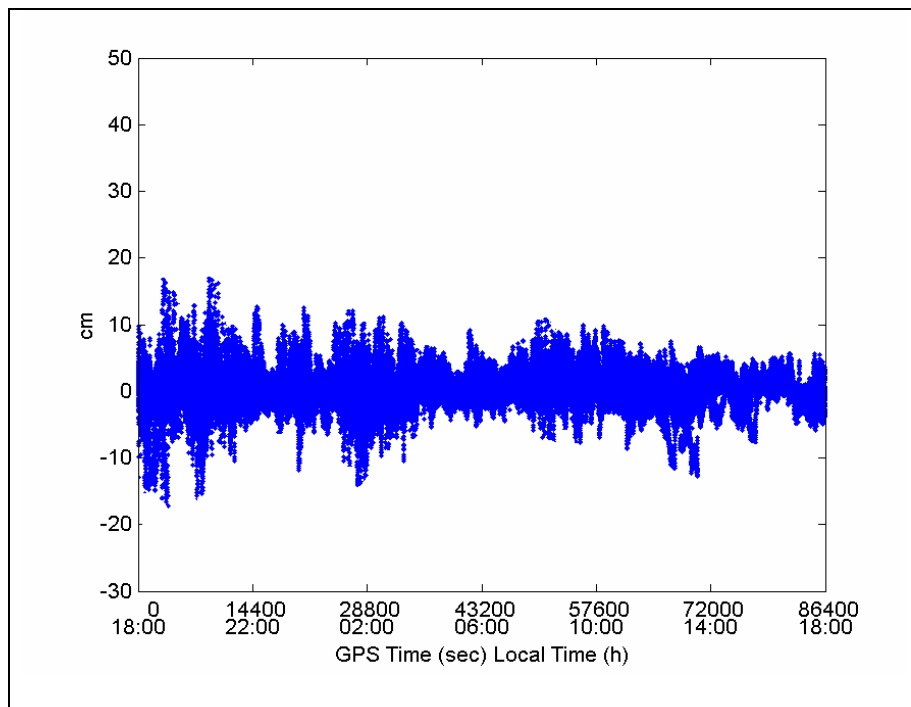


Figure 5.2 DD Ionospheric Errors on L1, 13 km Baseline

The following sub-sections analyze the results of the various strategies on a test-by-test basis.

1) Test 1 Result, 24-hour-run Test.

The left column of each strategy in Table 5.2 summarizes the position RMS error results and the left column of each strategy in Table 5.3 summarizes the ambiguity results for the eight strategies in Test 1. Strategies 5, 6, 7 and 8 clearly outperform Strategies 1, 2, 3 and 4. Strategies 1, 3, 4 where attempts are made to resolve the L1 ambiguities show the worst RMS position error in general, indicating the limitation of the L1 ambiguity resolution under an active ionosphere. Although Strategy 2 (WL) shows excellent ambiguity resolution performance (100% correct), it does not provide the least RMS error, as expected. The above Test 1 results are generated using a small spectral density on the process noise. To demonstrate the impact of the magnitude of the spectral density on positioning results, a larger spectral density of the process noise ($1 \text{ m}^2/\text{s}^3$, a typical value for most land vehicles) is used and Test 1 is performed again on the same baseline. The right column (shaded column) of each strategy in Table 5.2 summarizes the new position RMS error results and the right column (shaded column) of each strategy in Table 5.3 summarizes the new ambiguity results. In general, position and ambiguity results for each strategy become poorer because of the large spectral density used, as expected. However, the change of statistic is not significant. One can see that Strategies 2, 5 and 6 generates the same position and ambiguity results. Even though Strategy 8 resolves 0.3% of the L1 ambiguities wrong, it still generates the least RMS position errors among all the strategies. Therefore, the small process noise spectral density $0.0001 \text{ m}^2/\text{s}^3$ is used in all the following tests.

Table 5.2 24-hour-run Position Estimate RMS (cm) for Test Baseline 1

Axis	Strategy															
	1		2		3		4		5		6		7		8	
East	6	9	4	4	10	15	4	6	3	3	4	4	3	3	2	2
North	5	7	2	2	6	5	3	3	2	2	2	2	2	2	1	2
Height	16	19	6	6	26	21	8	9	4	4	4	4	3	5	3	4

Table 5.3 Percentage of Ambiguities Resolved Correctly (%)

Ambiguity	Strategy															
	1		2		3		4		5		6		7		8	
N_1	76.5	72.9	N/A	N/A	85.7	80.4	85.9	83.2	100	100	N/A	N/A	100	99.5	100	99.7
N_2	N/A	N/A	N/A	N/A	94.8	90.3	N/A	N/A	N/A	N/A	N/A	N/A	100	99.5	N/A	N/A
N_{wL}	N/A	N/A	100	100	N/A	N/A	97.3	96.8	100	100	N/A	N/A	N/A	N/A	100	100

1.1) Test 1, Strategy 1 Results

Figure 5.3 contains the position errors (top) and ambiguity errors (bottom) which are defined as the sum of absolute ambiguity difference as compared with the ambiguity output from Bernese.

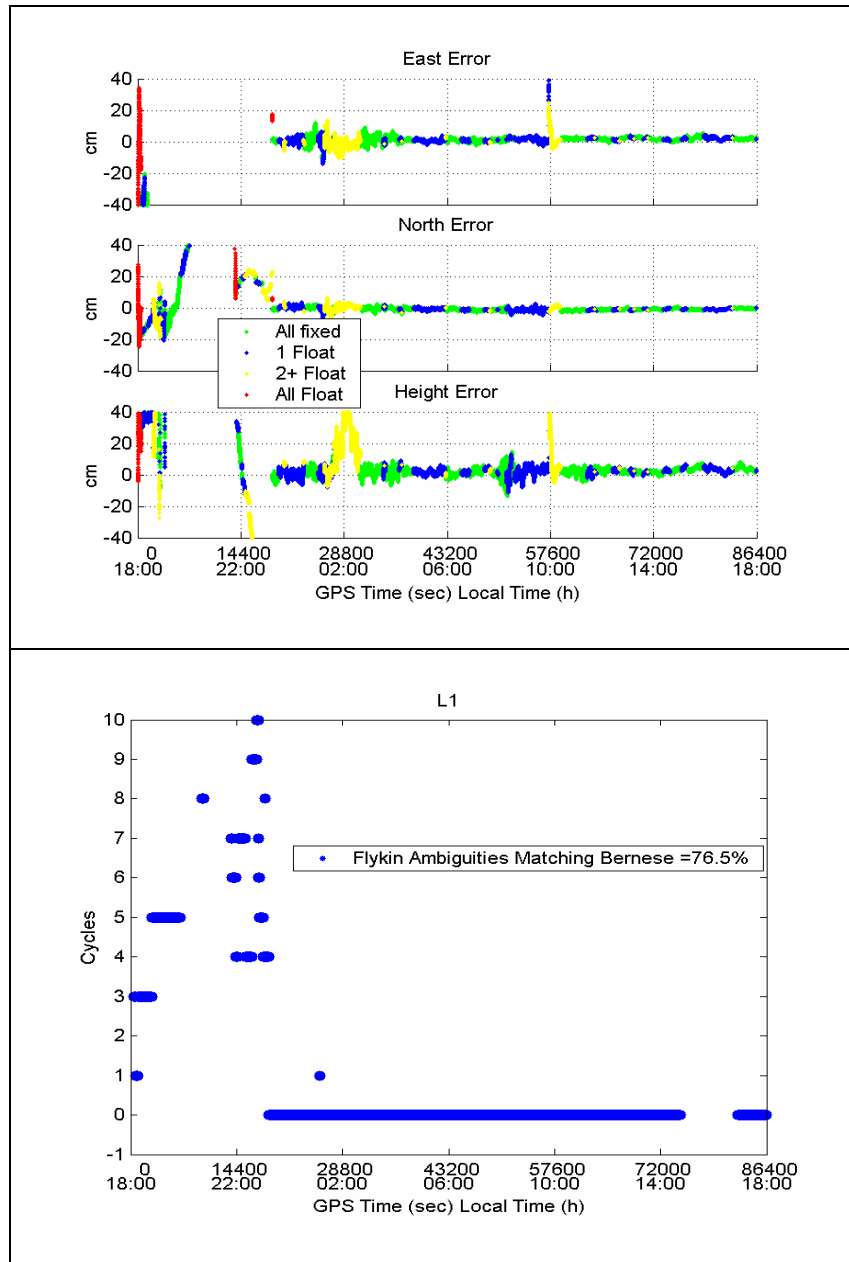


Figure 5.3 Position Errors and Ambiguity Comparison, Strategy 1

From the figure, it can be seen that the ambiguities are fixed correctly except from 18:00 to 02:00 local time, during which the ionospheric error is high. This result reinforces the fact that the ionosphere is the dominant error source hindering successful ambiguity resolution for L1. The poor ambiguity resolution performance during periods of high

ionospheric activity is coupled with poor position estimates. The top graph in Figure 5.3 and the ambiguity statistics in Table 5.3 also support these findings.

1.2) Test 1, Strategy 2 Results.

Figure 5.4 shows the position results for Test 1 using Strategy 2. Table 5.3 shows that the WL ambiguity is resolved 100% of the time correctly, despite the high ionospheric error at the beginning of the data. This is reasonable considering the large wavelength/ionosphere ratio (expressed in cycles) for WL. Although the WL ambiguities are resolved correctly, the position estimates are still influenced by the ionospheric error with errors up to 30-50 cm in some axes even when all ambiguities have been fixed correctly, as discussed above. Figure 5.4 clearly shows the position estimate variations caused by the ionosphere during the peak of ionospheric activity.

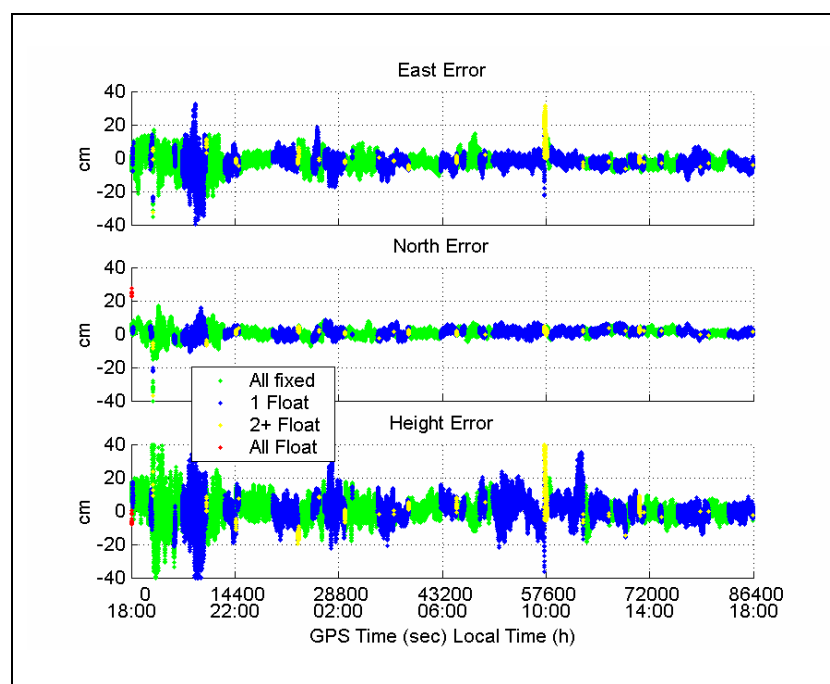


Figure 5.4 Position Errors, Strategy 2

1.3) Test 1, Strategy 3 Results.

Figure 5.5 shows the Test 1 results using Strategy 3. Ambiguity resolution for L1 and L2 is good after the beginning of the data set when the ionospheric error is high. This suggests that the introduction of L2 phase data still cannot help much during periods of high ionosphere if the ionospheric error is not modelled adequately.

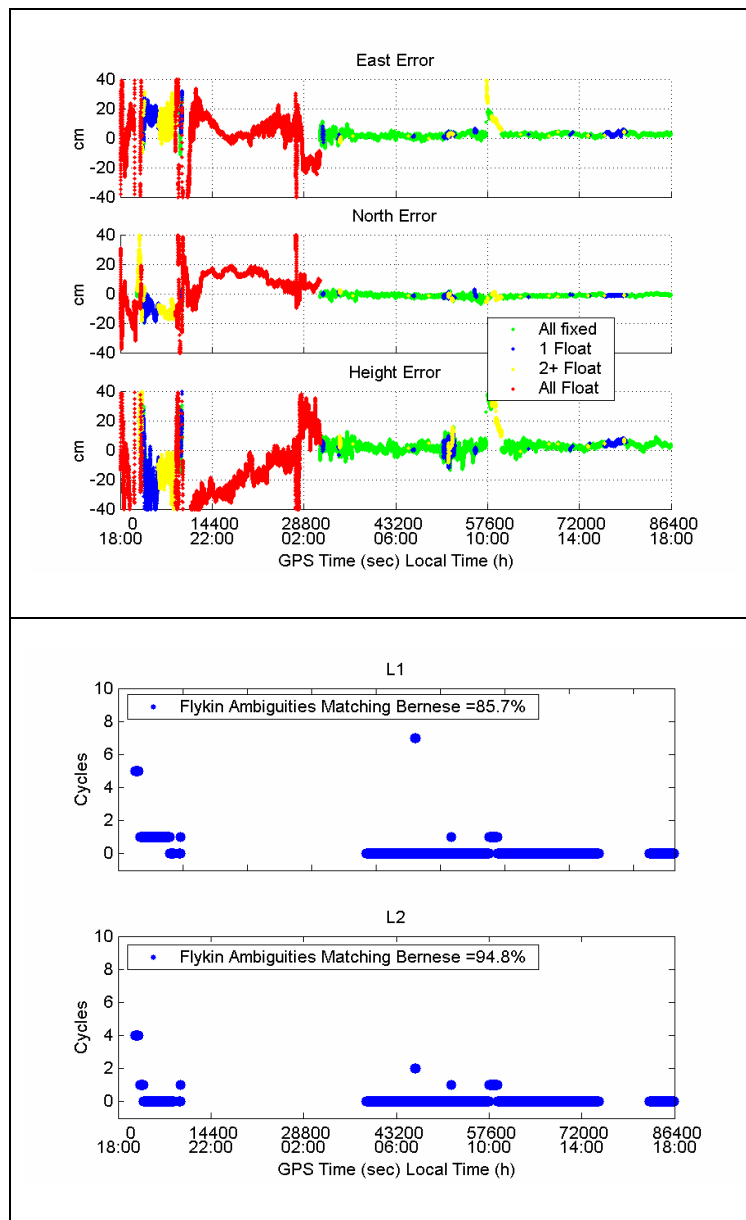


Figure 5.5 Position Errors and Ambiguity Comparison, Strategy 3

1.4) Test 1, Strategy 4 Results.

Figure 5.6 shows the position and ambiguity results for Test 1 using Strategy 4.

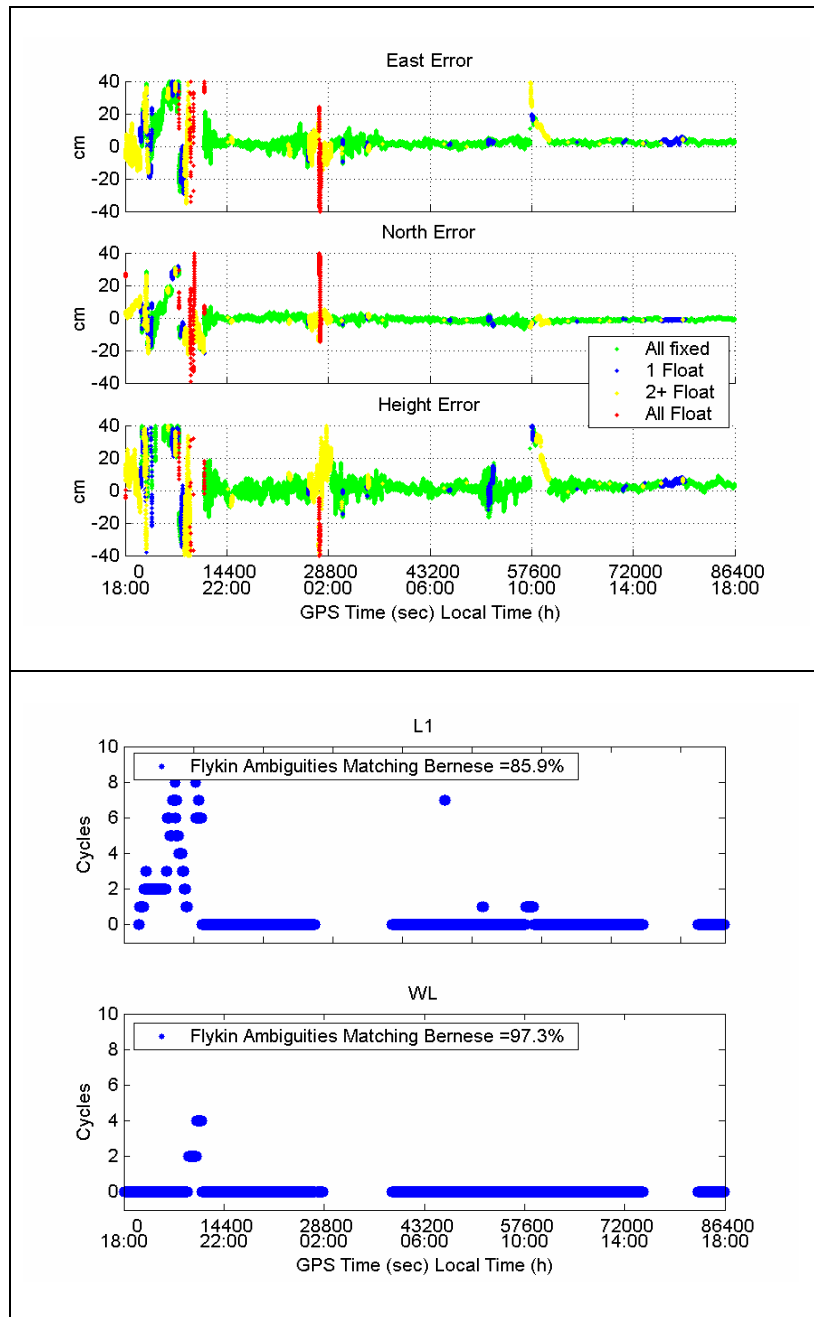


Figure 5.6 Position Errors and Ambiguity Comparison, Strategy 4

Recall that Strategy 4 used the same observations as Strategy 3 except that the L1 and WL ambiguities are estimated in the filter instead of the L1 and L2 ambiguities. As the

bottom graph in Figure 5.6 shows, although the WL ambiguities are fixed correctly at the beginning of the data set, a large quantity of L1 ambiguities are fixed incorrectly. This means that fixing of the WL ambiguities first during periods of high ionospheric activity does not aid the fixing of L1 ambiguities.

1.5) Test 1, Strategy 5 Results.

Figure 5.7 shows the position results for Test 1, Strategy 5.

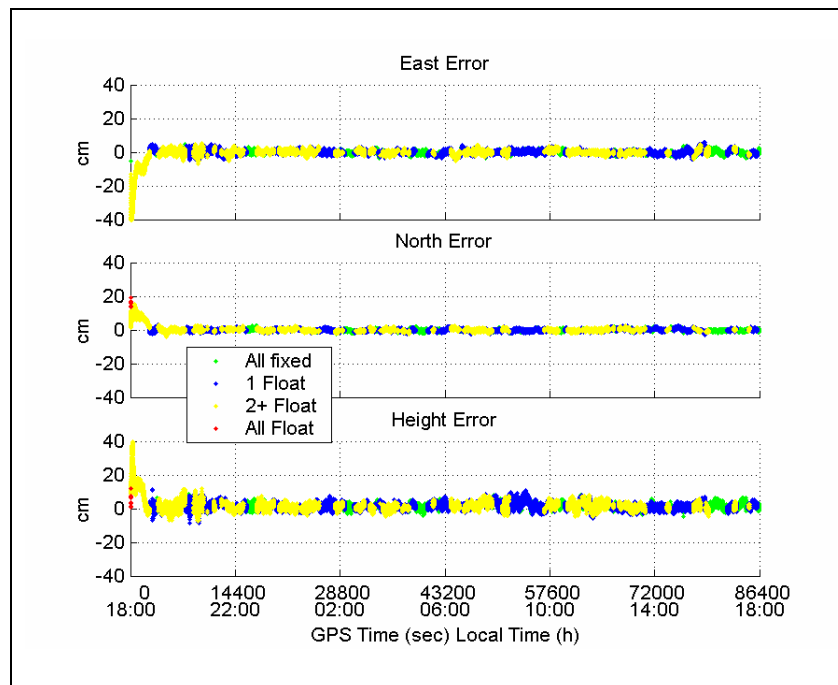


Figure 5.7 Position Errors, Strategy 5

Table 5.3 shows that the WL and L1 ambiguities for Strategy 5 are fixed correctly 100% of the time. The position error RMS values for Strategy 5 in Table 5.2 clearly outperform Strategies 1 through 4. Recall that this strategy uses a combination of L1 and L2 carrier phase observables. Although the ionospheric error is absent, the noise characteristic is evident in this strategy. Comparing the position error plots of both Figures 5.3, 5.5, 5.6

and 5.7 from 04:00 to 18:00 local time, when all three strategies fixed L1, L2 and WL ambiguities correctly most of the time, the position errors in Figure 5.7 shows a much noisier behavior, especially in height.

1.6) Test 1, Strategy 6 Results.

Figure 5.8 shows the position results for Test 1 using Strategy 5. Table 5.2 shows that the RMS of the position errors for Strategy 6 is worse than for Strategies 5, 7 and 8, but is still better than Strategies 1 through 4. In this Strategy, there is no risk of resolving the ambiguity to the wrong integer, thus it is a reliable method. However, there is one limitation with this method, namely the time needed for the ionosphere-free ambiguity to converge is significant. Figure 5.8 shows that it takes around 1 hour to converge based on the convergence of the position error towards zero.

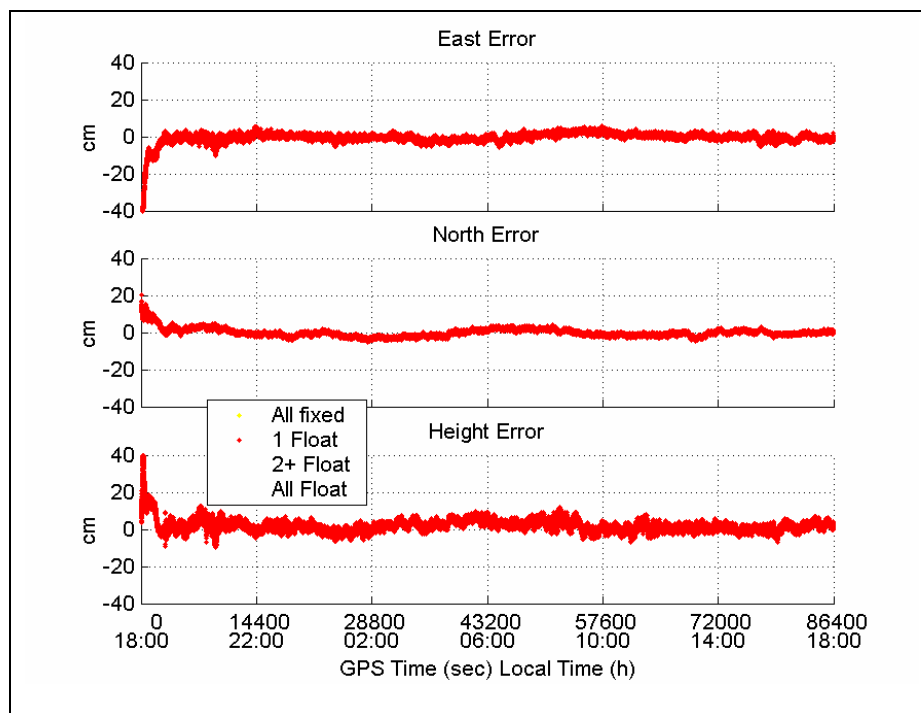


Figure 5.8 Position Errors, Strategy 6

1.7) Test 1, Strategy 7 Results.

Figure 5.9 shows the position results for Test 1 using Strategy 7. From the figure and Table 5.2, it can be seen that this strategy gives the best positioning performance compared to all previous strategies.

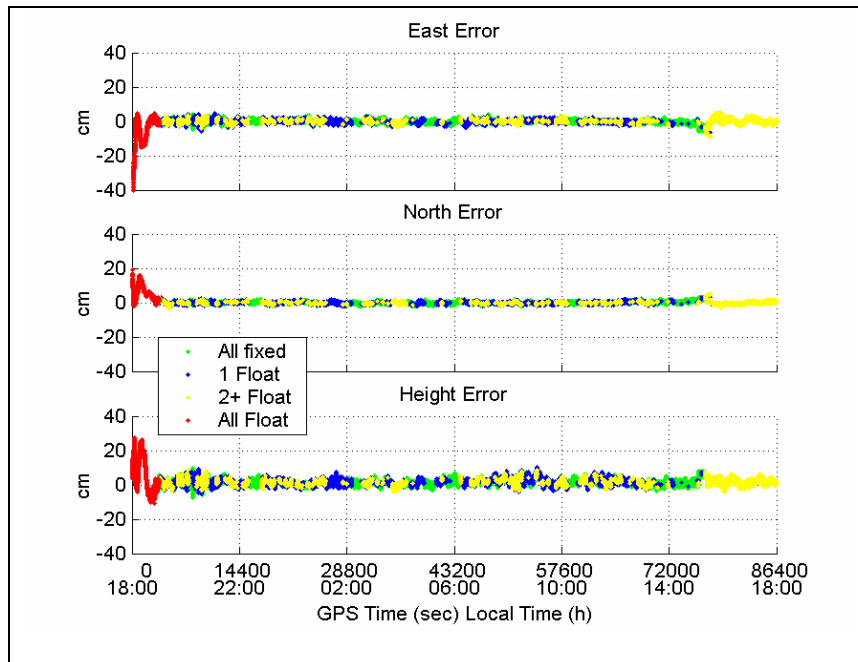


Figure 5.9 Position Errors, Strategy 7

1.8) Type 1, Strategy 8 Results.

Figure 5.10 shows the position results for Test 1 using Strategy 8. The observables used in this strategy are the same as in Strategy 7. The difference is that L1 and widelane ambiguities are estimated in the filter instead of L1 and L2 ambiguities. Figure 5.10 is very similar to Figure 5.9. The only obvious difference is that the position error of Strategy 8 is 50% smaller for the north and 100% for the east axes than that of Strategy 7. This is attributed to the fact that the widelane ambiguities can be fixed much faster than

the L1 ambiguities and the fixing of widelane ambiguities improves the position estimate.

See the results of Test 2 for more details.

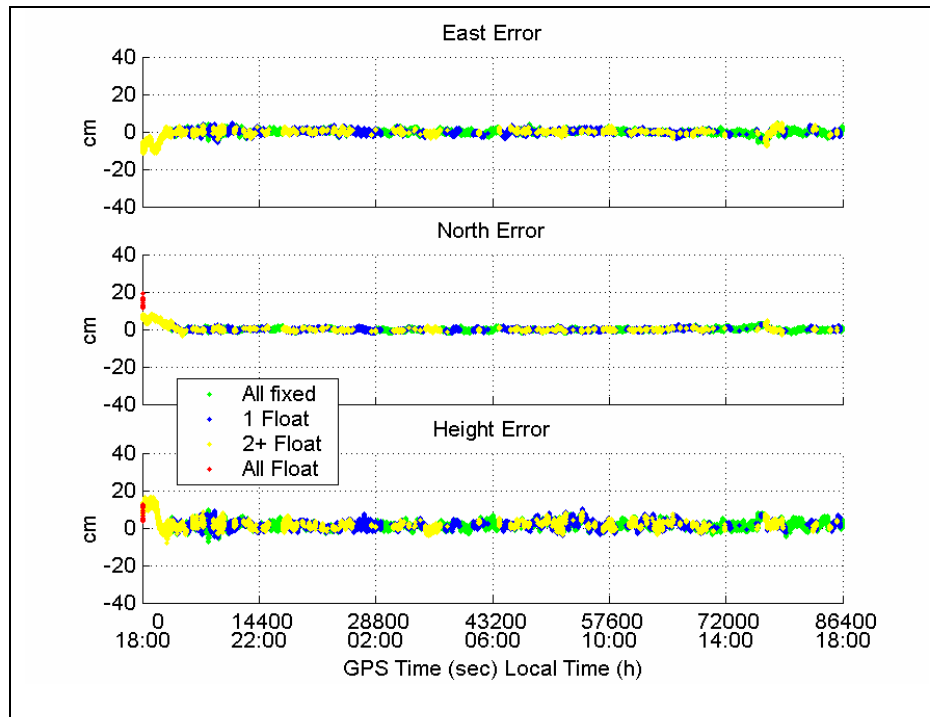


Figure 5.10 Position Errors, Strategy 8

2) Test 2 Result, 600-second-interval Tests.

In this test, the 24-hour data set is divided into equal 600-second intervals, and each interval is processed with FLYKIN+TM for all the strategies in Table 4.1 to assess the ambiguity resolution performance and position accuracy. Once the ambiguities are resolved, a fixed position solution is recorded and the FLYKIN+TM software will re-initialize the filter and go to the beginning of the next 600-second interval to try and resolve the ambiguities again.

Table 5.4 shows the 600-second-run statistics for all the strategies. The shaded block containing the statistics for the WL shows that the WL ambiguity is both reliable and stable in terms of time to fix and percentage correct. Also, comparing the statistics for Strategies 3 and 4, where the same observations are used, the only difference being that in Strategy 3, the L1 and L2 ambiguities are estimated in the filter, while in Strategy 4 the L1 and WL ambiguities are estimated. The statistics show that it takes comparable time to fix L1 ambiguities for both approaches (78 seconds for Strategy 3 and 80 seconds for Strategy 4) and the percentage correct is also comparable (93.5% for Strategy 3 and 91.9% for Strategy 4). The percentage fixed within the 600-second-interval is also comparable (83% for Strategy 3 and 80% for Strategy 4). The same is true for Strategies 7 and 8. Comparing the statistics for Strategies 7 and 8, where the same observations are used, the only difference being that in Strategy 7, the L1 and L2 ambiguities are estimated in the filter, while in Strategy 8 the L1 and WL ambiguities are estimated. The statistics show that it takes comparable time to fix L1 ambiguities for both approaches (216 seconds for Strategy 7 and 225 seconds for Strategy 8) and the percentage correct is also comparable (83% for Strategy 7 and 78.5% for Strategy 8). The percentage fixed within the 600-second-interval is also comparable (53% for Strategy 7 and 57% for Strategy 8).

For this data, estimating L1 and WL ambiguities in the same filter instead of L1 and L2 ambiguities does not bring much improvement as far as L1 ambiguity resolution is concerned.

Table 5.4 600-second-run Statistics, 13 km Baseline

Measure	Strategy						
	1	2	3	4	5	7	8
N_1 FWI ¹	76%	N/A	83%	80%	27%	53%	57%
N_1 PCFA ²	77.6%	N/A	93.5%	91.9%	52%	83%	78.5%
N_1 MTTF ³	277 s	N/A	78 s	80 s	530 s	216 s	225 s
N_2 FWI	N/A	N/A	83%	N/A	N/A	53%	N/A
N_2 PCFA	N/A	N/A	93.5%	N/A	N/A	83%	N/A
N_2 MTTF	N/A	N/A	87	N/A	N/A	219	N/A
N_{wl} FWI	N/A	99%	N/A	99%	99%	N/A	99%
N_{wl} PCFA	N/A	97.4%	N/A	96.4%	97.4%	N/A	98.7%
N_{wl} MTTF	N/A	30 s	N/A	30 s	30 s	N/A	32 s

¹ FWI: Fixed Within 600-s Interval (%)

² PCFA: Percentage of Correctly Fixed Ambiguities (%)

³ MTTF: Mean Time To Fix (s)

However, estimating L1 and widelane ambiguities in the filter instead of L1 and L2 ambiguities does have a benefit in the position domain. Table 5.5 shows the position error RMS for Strategies 3, 4, 7, and 8. The position error for Strategies 4 and 8 after the WL ambiguities are resolved are significantly lower than for Strategies 3 and 7 where both L1 and L2 ambiguities cannot be resolved. Therefore estimating WL and L1 ambiguities instead of L1 and L2 has a benefit on position estimation provided that the WL ambiguity

resolution is reliable and fast. Another phenomenon worth noting is the overall position accuracy improvement of the stochastic ionosphere modelling which can be seen by comparing the RMS position error between Strategies 3, 4 and Strategies 7, 8.

Table 5.5 Position RMS (cm) for 600-second-run, 13 km Baseline

Axis	Strategy			
	3	4	7	8
	No Ambiguity Fixed	Only WL Ambiguity Fixed	No Ambiguity Fixed	Only WL Ambiguity Fixed
East	37	8	19	5
North	16	5	13	3
Height	51	20	26	6

II) Baseline II

This second baseline was collected on February 7, 2002 from the Campania network in Italy. Dual frequency data were collected at a rate of 1 Hz for 24 hours. The cut-off elevation angle is also 15 degrees. The data were processed once for each of the strategies listed in Table 4.1. As shown in Figure 5.11, the ionospheric error on L1 at the beginning and end of the data set is small, 2-5 ppm, while it is very high in the middle of the data (08:00 16:00 local time), up to 15 ppm.

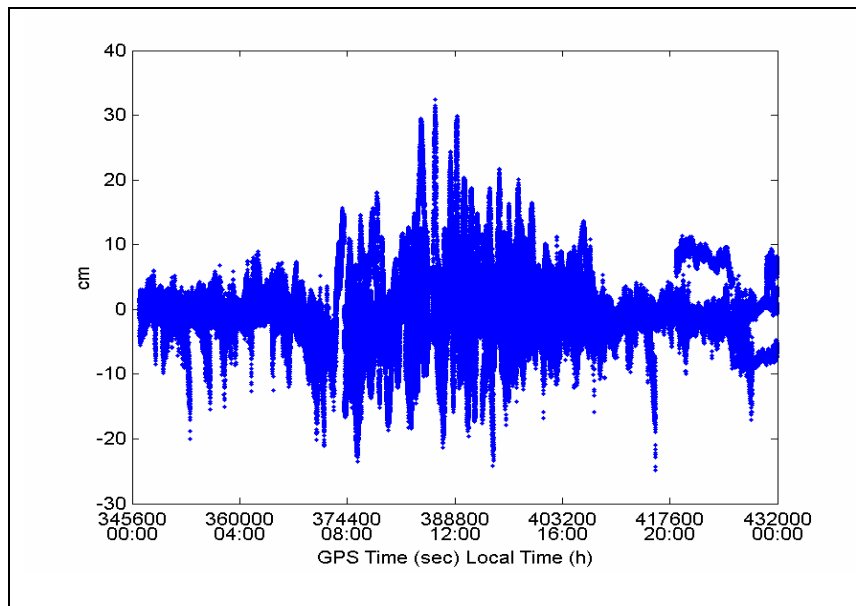


Figure 5.11 DD Ionospheric Errors on L1, 26 km Baseline

The following sub-sections analyze the results of the various strategies on a test-by-test basis.

1) Test 1 Result, 24-hour-run Tests.

Table 5.6 summarizes the position RMS and Table 5.7 summarizes the ambiguity result for the eight strategies in Test 1. Again, Strategies 5, 6, 7 and 8 outperform Strategies 1, 2, 3 and 4. Strategies 1, 3, 4 where attempts are made to resolve the L1 ambiguities show the worst position RMS error in general, due to the limitation of the L1 ambiguity resolution under active ionosphere. Although Strategy 2 (WL) shows excellent ambiguity resolution performance (100% correct), the RMS position error is dwarfed compared to the last four strategies. This is the expected behaviour of WL.

Table 5.6 24-hour-run Position Estimate RMS (cm) for Test Baseline 2

Axis	Strategy							
	1	2	3	4	5	6	7	8
East	35	9	13	11	4	5	2	2
North	16	4	12	16	2	4	2	1
Height	33	12	27	34	9	11	6	3

Table 5.7 Percentage of Ambiguities Resolved Correctly (%), 26 km Baseline

Ambiguity	Strategy							
	1	2	3	4	5	6	7	8
N_1	69.5	N/A	97.4	92	100	N/A	100	100
N_2	N/A	N/A	98.1	N/A	N/A	N/A	100	N/A
N_{wL}	N/A	100	N/A	100	100	N/A	N/A	100

1.1) Test 1, Strategy 1 Results

Figure 5.12 contains the position errors (top) and ambiguity errors (bottom). From the figure, it can be seen that the ambiguities are fixed correctly except from 08:00 to 16:00 local time, during which the ionospheric error is high. This result reinforces the fact that the ionosphere is the dominant error source hindering successful ambiguity resolution for L1. The bad ambiguity resolution performance during periods of high ionospheric

activity is coupled with bad position estimates. The top graph in Figure 5.12 and the statistics in Table 5.7 also support these findings.

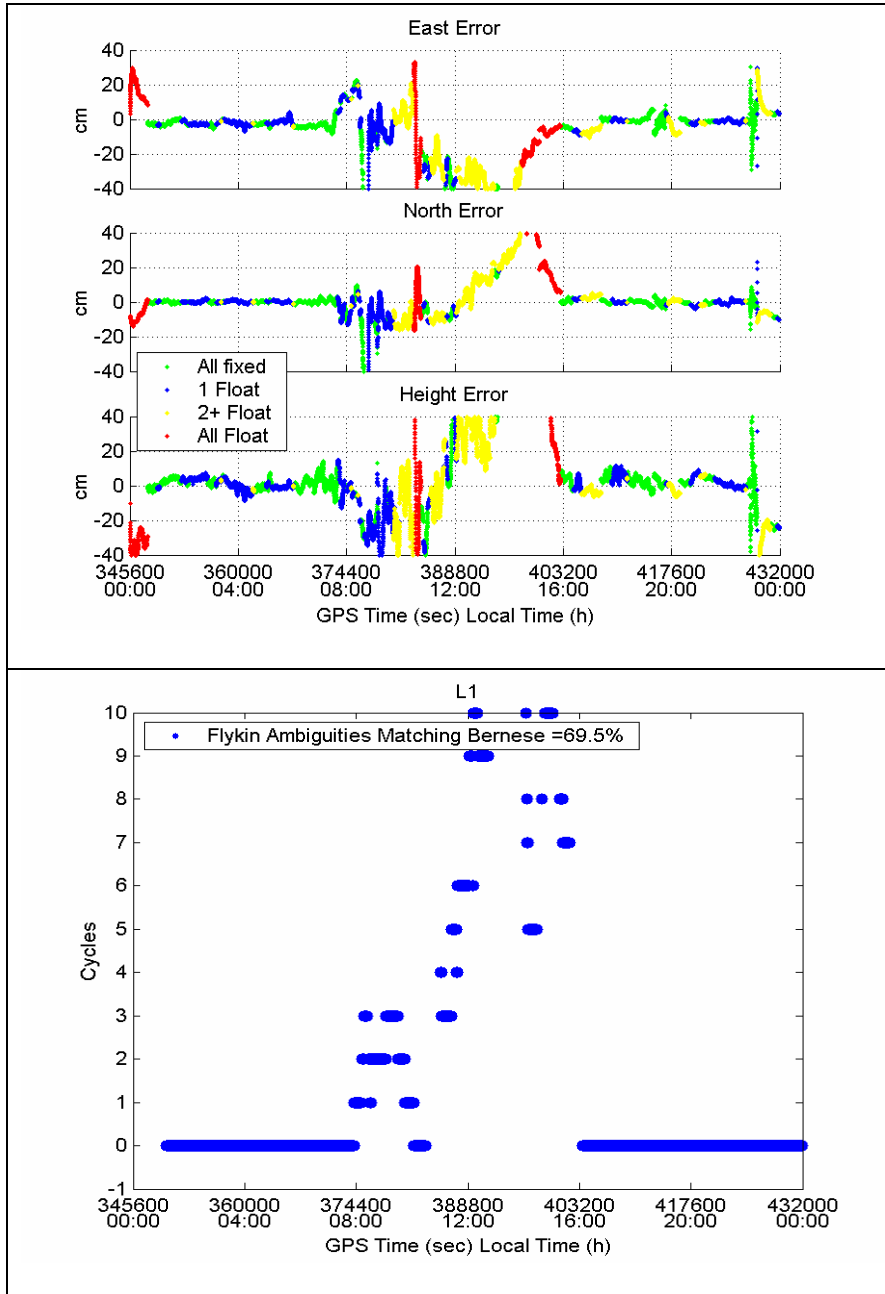


Figure 5.12 Position Errors and Ambiguity Comparison, Strategy 1

1.2) Test 1, Strategy 2 Results.

Figure 5.13 shows the position result for Test 1 using Strategy 2. Table 5.7 shows that the WL ambiguity is resolved 100% correctly, despite the high ionosphere in the middle of the data. This is reasonable considering the long wavelength of the WL, relative to the ionospheric error (expressed in cycles). Although the WL ambiguities are resolved correctly, the position estimate is still influenced by the ionospheric error with errors up to 40cm in all three axes even when all ambiguities have been fixed correctly, as discussed above. Figure 5.13 clearly shows the position estimate variations caused by the ionosphere during the period of high ionospheric activity.

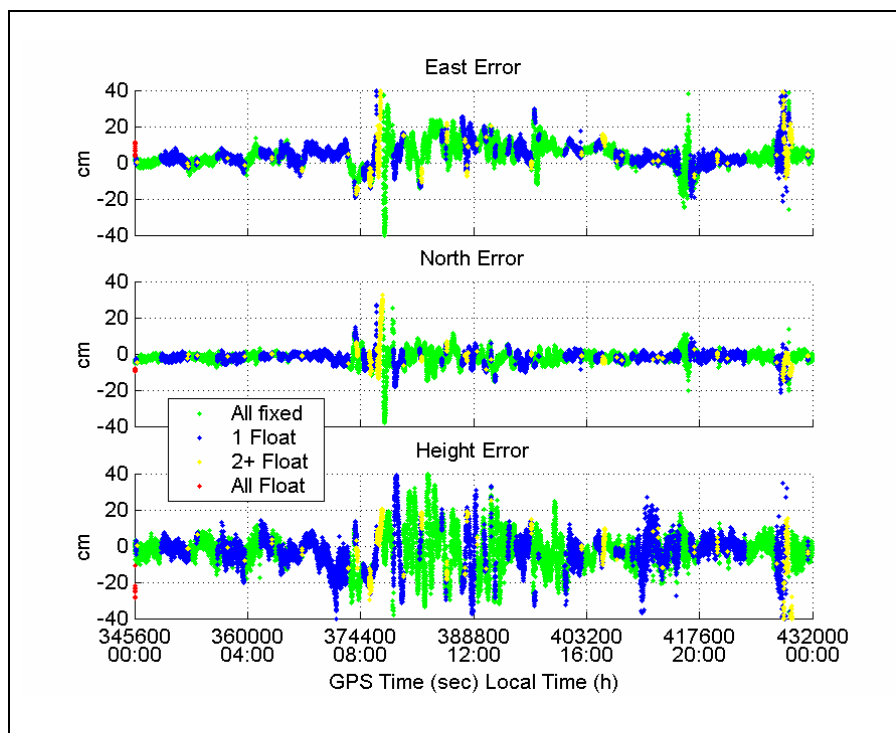


Figure 5.13 Position Errors, Strategy 2

1.3) Test 1, Strategy 3 Results.

Figure 5.14 shows the Test 1 results using Strategy 3. Ambiguity resolution for L1 and L2 is good at the beginning and end of the data set when the ionospheric error is small. However, errors become evident starting at 08:00 local time when the ionospheric

activity increases. This suggests that the introduction of L2 phase data still cannot help much during periods of high ionosphere if the ionospheric error is not modelled adequately.

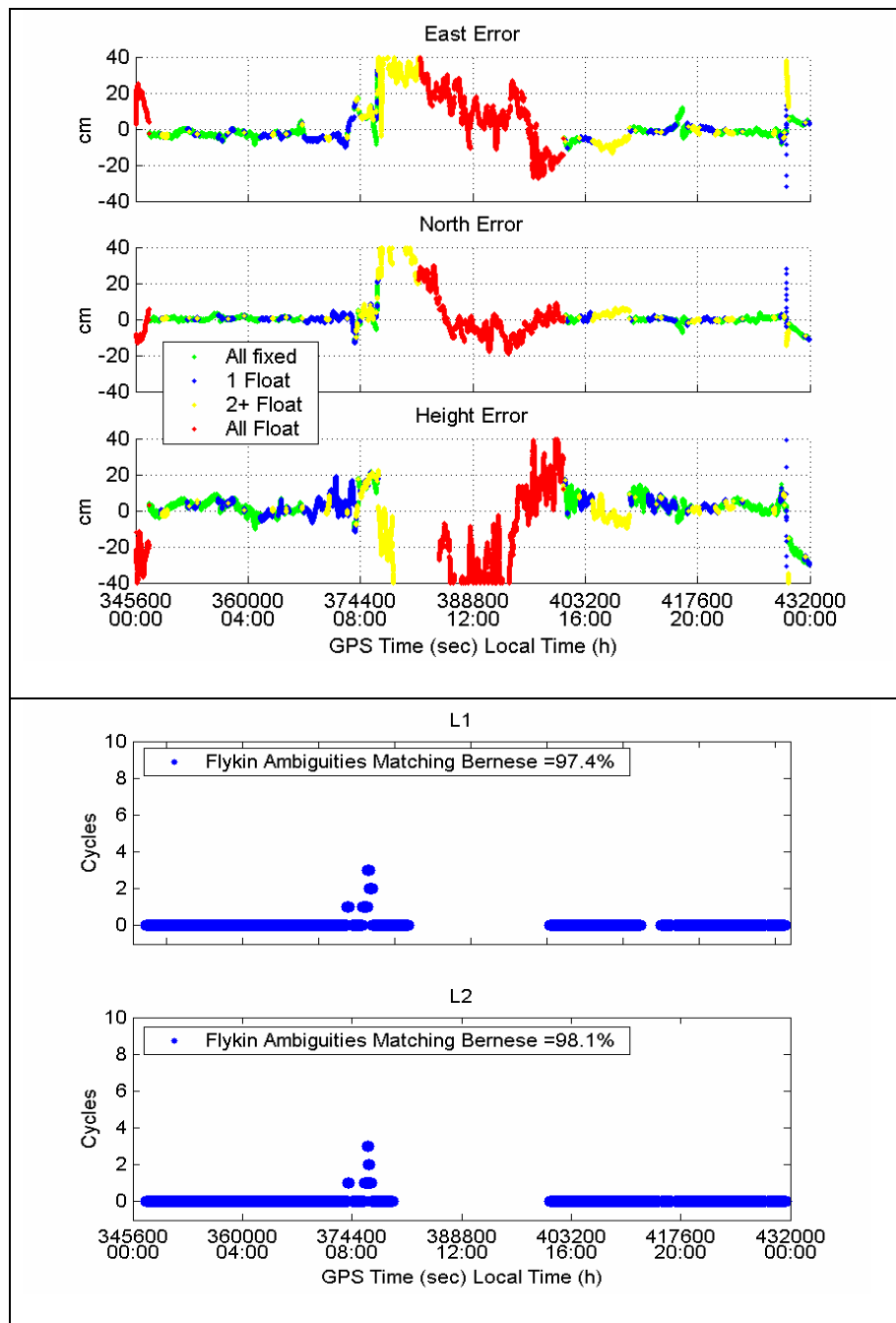


Figure 5.14 Position Errors and Ambiguity Comparison, Strategy 3

1.4) Test 1, Strategy 4 Results.

Figure 5.15 shows the position and ambiguity results for Test 1 using Strategy 4.

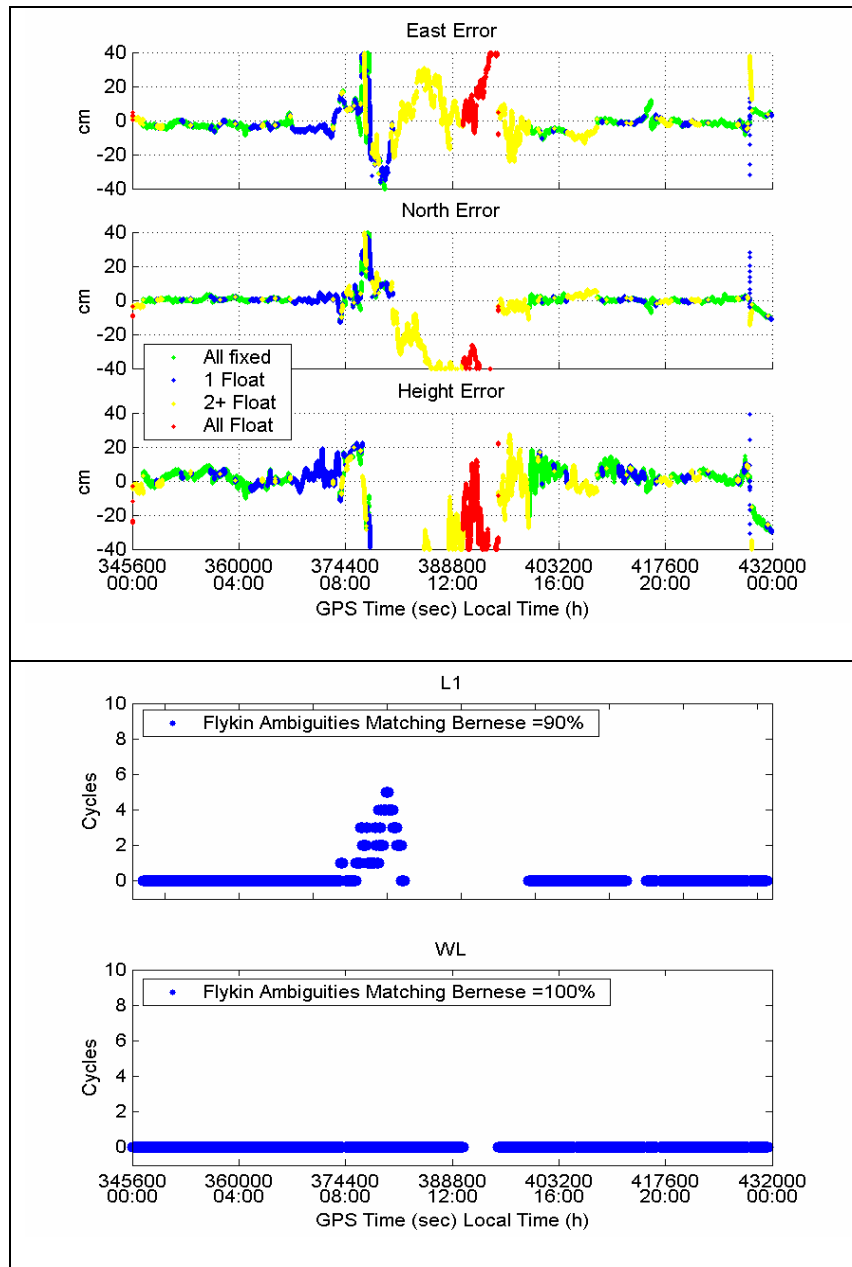


Figure 5.15 Position Errors and Ambiguity Comparison, Strategy 4

Recall that Strategy 4 used the same observations as Strategy 3 except that the L1 and WL ambiguities are estimated in the filter instead of the L1 and L2 ambiguities. As the

bottom graph in Figure 5.15 shows, although the WL ambiguities are fixed correctly 100% of the time, the percentage of L1 ambiguities fixed correctly is lower than for Strategy 3. This means that fixing of the WL ambiguities first during periods of high ionospheric activity does not significantly aid the fixing of L1 ambiguities. Comparing these results to Strategy 3 shows fewer L1 ambiguities are fixed correctly and the position error is larger.

1.5) Test 1, Strategy 5 Results

Figure 5.16 shows the position results for Test 1, Strategy 5.

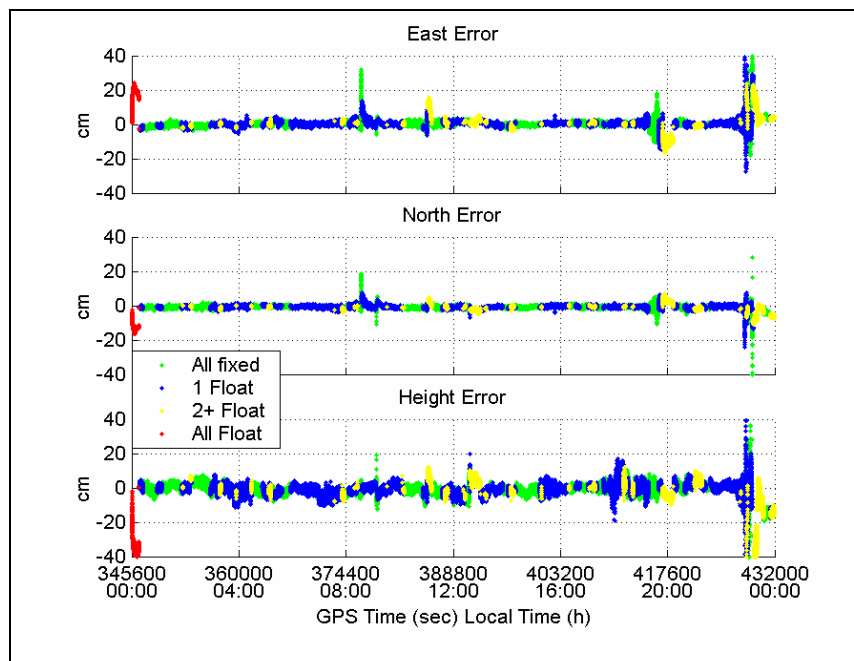


Figure 5.16 Position Errors, Strategy 5

Table 5.7 shows that the WL and L1 ambiguities for Strategy 5 are fixed correctly 100% of the time. The position error RMS values for Strategy 5 in Table 5.6 clearly outperforms Strategies 1 through 4. Recall that this strategy uses a combination of L1 and L2 carrier phase observables. Although the ionospheric error is absent, the noise

characteristic is evident in this strategy. Comparing the position error plots of both Figures 5.15 and 5.16 from 00:00 to 08:00 local time and 16:00 to 00:00, when both strategies fixed L1 and WL ambiguities correctly, the position errors in Figure 5.16 shows a much noisier behavior than that of Figure 5.15.

1.6) Test 1, Strategy 6 Results.

Figure 5.17 shows the position results for Test 1 using Strategy 5. Table 5.6 shows that the RMS of the position errors for Strategy 6 is worse than for Strategies 5, 7 and 8, but is still better than Strategies 1 through 4. In this Strategy, there is no risk of resolving the ambiguity to the wrong integer, thus it is a reliable method. However there is one limitation with this method, namely the time needed for the ionosphere-free ambiguity to converge is significant. Figure 5.17 shows that it takes around 2 hours to converge based on the convergence of the position error towards zero.

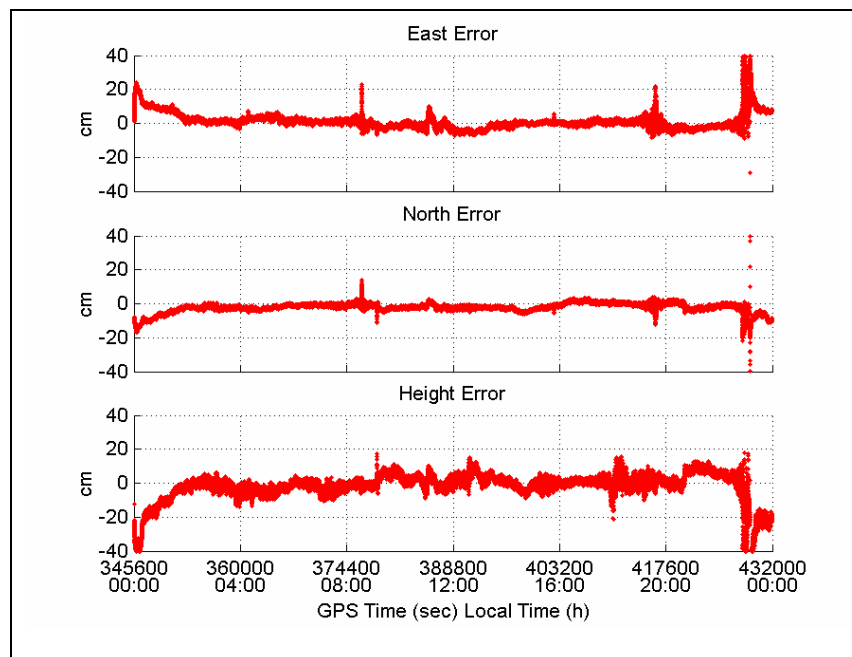


Figure 5.17 Position Errors, Strategy 6

1.7) Test 1, Strategy 7 Results.

Figure 5.18 shows the position results for Test 1 using Strategy 7. From the figure and Table 5.7, it can be seen that this strategy gives the best positioning performance compared to all previous strategies.

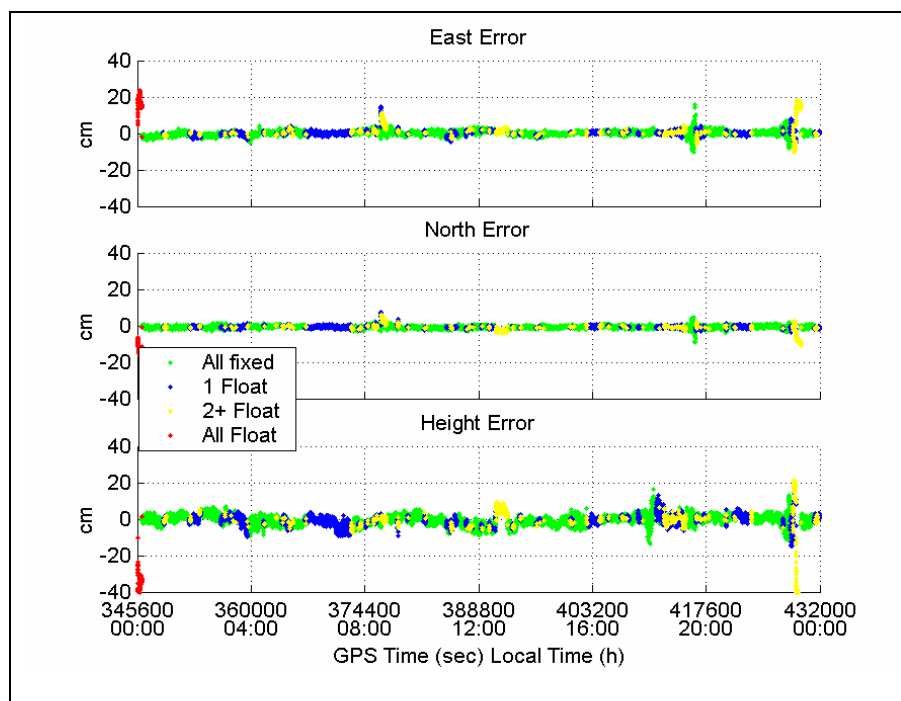


Figure 5.18 Position Errors, Strategy 7

1.8) Type 1, Strategy 8 Results.

Figure 5.19 shows the position results for Test 1 using Strategy 8. The observables used in this strategy are the same as in Strategy 7. The difference is that L1 and widelane ambiguities are estimated in the filter instead of L1 and L2 ambiguities. Figure 5.19 is very similar to Figure 5.18. The only obvious difference is that the position error of

Strategy 8 is 50% smaller than that of Strategy 7 for the north and east axes. Again, this is attributed to the fact that the widelane ambiguities can be fixed much faster than the L1 ambiguities and the fixing of widelane ambiguities improves the position estimate.

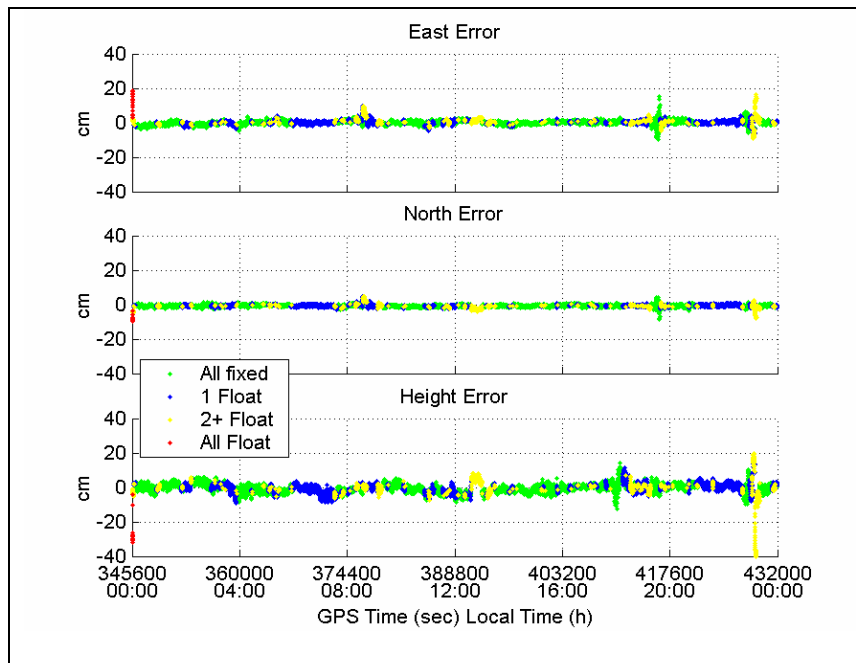


Figure 5.19 Position Errors, Strategy 8

2) Test 2 Result, 600-second-interval Tests.

In this test, the 24-hour data set is divided into equal 600-second intervals, and each interval is processed with FLYKIN+TM for all the strategies in Table 4.1 to assess the ambiguity resolution performance and position accuracy. Once the ambiguity is resolved, a fixed position solution is recorded and the FLYKIN+TM software will re-initialize the filter and go to the beginning of next 600-second interval to try and resolve the ambiguities again.

Table 5.8 shows the 600-second-run statistics for all the strategies. The shaded block containing the statistics for the WL shows that the WL ambiguity is both reliable and stable in terms of time to fix and percentage correct. Also, comparing the statistics for Strategies 3 and 4, where the same observations are used, the only difference being that in Strategy 3, the L1 and L2 ambiguities are estimated in the filter, while in Strategy 4 the L1 and WL ambiguities are estimated. The statistics show that it takes comparable time to fix L1 ambiguities for both approaches (116 seconds for Strategy 3 and 113 seconds for Strategy 4) and the percentage correct is also comparable (94% for Strategy 3 and 90% for Strategy 4). The percentage of fixing the L1 ambiguities within the 600-second interval is also comparable (54% for Strategy 3 and 47 for Strategy 4). The same is true for Strategies 7 and 8. Comparing the statistics for Strategies 7 and 8, where the same observations are used, the only difference being that in Strategy 7, the L1 and L2 ambiguities are estimated in the filter, while in Strategy 8 the L1 and WL ambiguities are estimated. The statistics show that it takes comparable time to fix L1 ambiguities for both approaches (144 seconds for Strategy 7 and 155 seconds for Strategy 8) and the percentage correct is also comparable (90% for Strategy 7 and 91% for Strategy 8). The percentage fixed within the 600-second-interval is also comparable (70% for Strategy 7 and 68% for Strategy 8).

For this data, estimating L1 and WL ambiguities in the same filter instead of L1 and L2 ambiguities does not bring much improvement as far as L1 ambiguity resolution is concerned.

Table 5.8 600-second-run Statistics, 26 km Baseline

Measure	Strategy						
	1	2	3	4	5	7	8
N_1 FWI	44%	N/A	54%	47%	26%	70%	68%
N_1 PCFA	36%	N/A	94%	90%	78%	90%	91%
N_1 MTTF	244 s	N/A	116 s	113 s	326 s	144 s	155 s
N_2 FWI	N/A	N/A	54%	N/A	N/A	70%	N/A
N_2 PCFA	N/A	N/A	95%	N/A	N/A	91%	N/A
N_2 MTTF	N/A	N/A	116 s	N/A	N/A	144 s	N/A
N_{wL} FWI	N/A	99%	N/A	93%	99%	N/A	99%
N_{wL} PCFA	N/A	100%	N/A	98%	100%	N/A	100%
N_{wL} MTTF	N/A	17 s	N/A	19 s	17 s	N/A	17 s

However, estimating L1 and widelane ambiguities in the filter instead of L1 and L2 ambiguities does have a benefit in the position domain. Table 5.9 shows the position error RMS for Strategies 3, 4, 7, and 8. The position errors of Strategies 4 and 8 in all three axes after the WL ambiguities are resolved are significantly lower than for Strategy 3 and Strategy 7 where both L1 and L2 ambiguities cannot be resolved. Therefore estimating WL and L1 ambiguities instead of L1 and L2 has a benefit on position estimation provided that the WL ambiguity resolution is reliable and fast. Again there is overall position accuracy improvement brought by the stochastic ionosphere modelling comparing the position RMS between Strategies 3, 4 and Strategies 7, 8 in Table 5.9.

Table 5.9 Position RMS (cm) for 600-second-run, 26 km Baseline

Axis	Strategy			
	3	4	7	8
	No Ambiguity Fixed	Only WL Ambiguity Fixed	No Ambiguity Fixed	Only WL Ambiguity Fixed
East	49	18	15	9
North	26	8	11	5
Height	76	15	27	12

III) Baseline III

This baseline was collected on the same day and from the same network as baseline II. However, the baseline length is much longer in this case, 43 km. The cut-off elevation angle is 15 degrees. Figure 5.20 shows the estimate of the DD ionospheric error on L1 for the 24-hour period. The DD ionospheric error goes as high as 50 cm for certain satellites during the peak of the ionospheric activity.

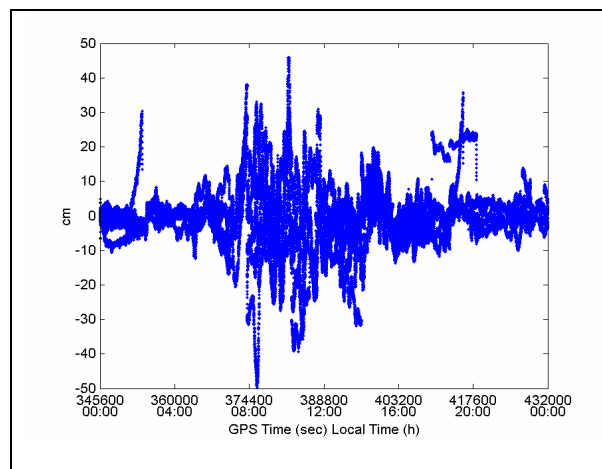


Figure 5.20 DD Ionospheric Errors on L1, 43 km Baseline

1) Test 1 Result, 24-hour-run Tests.

Table 5.10 summarizes the position RMS and Table 5.11 summarizes the ambiguity result for the eight strategies in Test 1. Once again, Strategies 5, 6, 7 and 8 clearly outperform Strategies 1, 2, 3 and 4. Strategies 1, 3, 4 where attempts are made to resolve the L1 ambiguities show the worst position RMS error in general, indicating the limitation of the L1 ambiguity resolution under active ionosphere. Although Strategy 2 (WL) shows excellent ambiguity resolution performance (100% correct), it does not provide the least RMS error, as expected.

Table 5.10 24-hour-run Position Estimate RMS (cm) for Test Baseline 3

Axis	Strategy							
	1	2	3	4	5	6	7	8
East	12	10	25	22	8	5	5	2
North	13	11	19	15	6	4	3	2
Height	22	14	35	43	14	6	9	5

Table 5.11 Percentage of Ambiguities Resolved Correctly (%), 43 km Baseline

Ambiguity	Strategy							
	1	2	3	4	5	6	7	8
N_1	57	N/A	51.6	70.1	83	N/A	99.8	100
N_2	N/A	N/A	51.4	N/A	N/A	N/A	99.8	N/A
N_{WL}	N/A	100	N/A	90.2	100	N/A	N/A	100

For this baseline, however, Strategy 5 only resolved L1 ambiguities 83% correctly, which may be attributed by the fact that the baseline length is too long in this case (43km) and

the residual tropospheric error cannot be neglected any more. The following results are presented on a strategy-by-strategy basis.

1.1) Test 1, Strategy 1 Results.

Figure 5.21 contains the L1-solution position errors (top) and ambiguity errors (bottom).

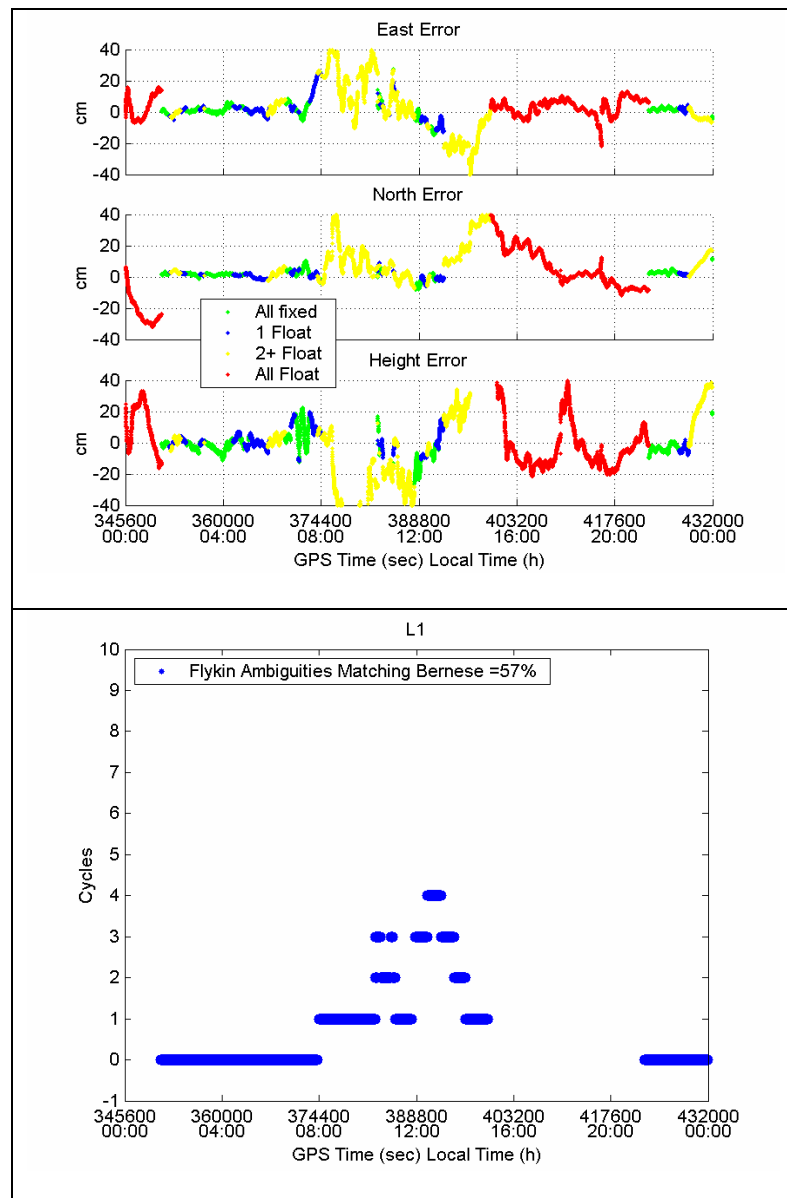


Figure 5.21 Position Errors and Ambiguity Comparison, Strategy 1

From the figure, it can be seen that the ambiguities are fixed correctly except from 08:00 to 16:00 local time, during which the ionospheric error is high. This result is in agreement with previous L1 results in that the Strategy 1 ambiguity resolution is bad during periods of high ionospheric error. Poor position performance comes as a direct result of bad ambiguity resolution. The top graph in Figure 5.21 and the statistics in Table 5.11 also support these findings.

1.2) Test 1, Strategy 2 Results.

Figure 5.22 shows the position results for Test 1 using Strategy 2. Table 5.11 shows that the WL ambiguity is resolved 100% of the time correctly, despite the high ionospheric activity in the middle of the data. Although the WL ambiguities are resolved 100% correctly, the position estimate is still influenced by the ionospheric error with large errors at the middle in all three axes. Figure 5.22 clearly shows the position estimate variations caused by the ionosphere during the period of high ionospheric activity.

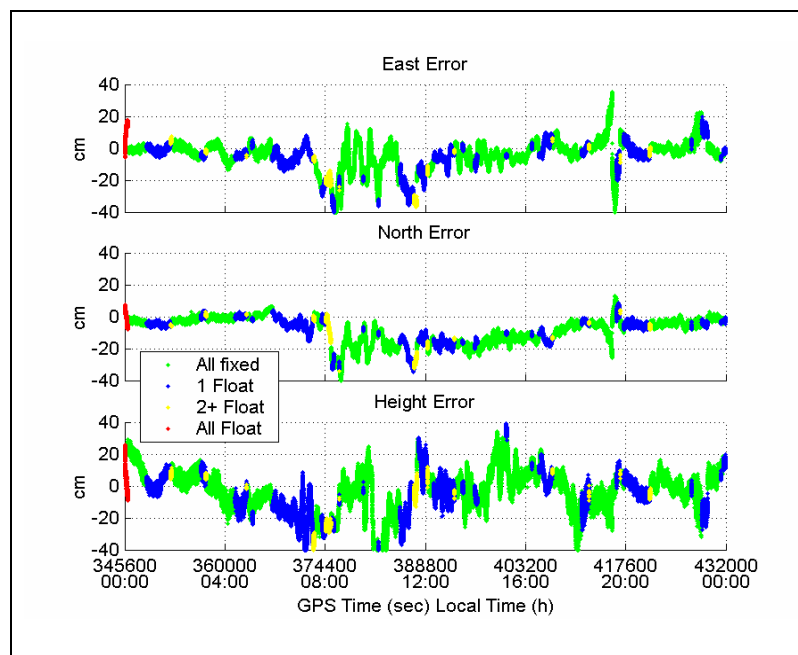


Figure 5.22 Position Errors, Strategy 2

1.3) Test 1, Strategy 3 Results.

Figure 5.23 shows the Test 1 results using Strategy 3.

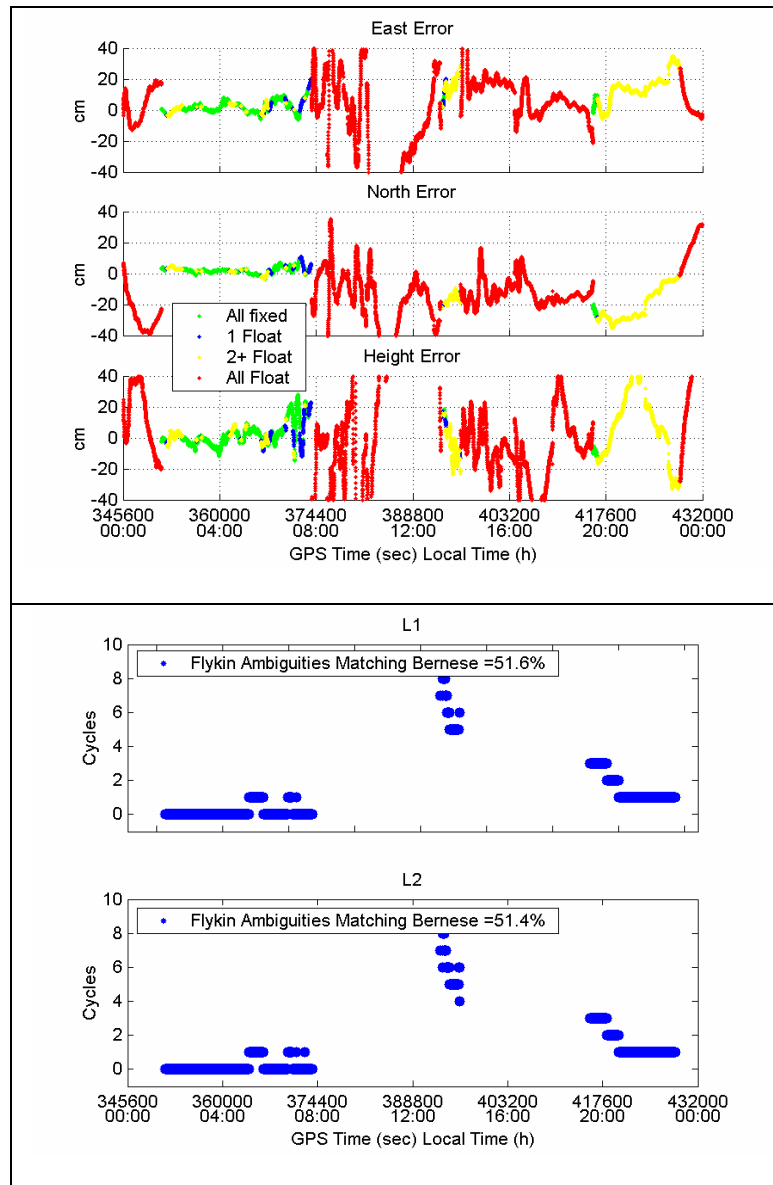


Figure 5.23 Position Errors and Ambiguity Comparison, Strategy 3

Ambiguity resolution for L1 and L2 is good at the beginning and end of the data set when the ionospheric error is small. However, errors become evident starting at 08:00 local time when the ionospheric activity increases. This suggests that the introduction of the L2

phase data still cannot help much during periods of high ionospheric activities if the ionospheric error is not modelled adequately.

1.4) Test 1, Strategy 4 Results.

Figure 5.24 shows the position and ambiguity results for Test 1 using Strategy 4.

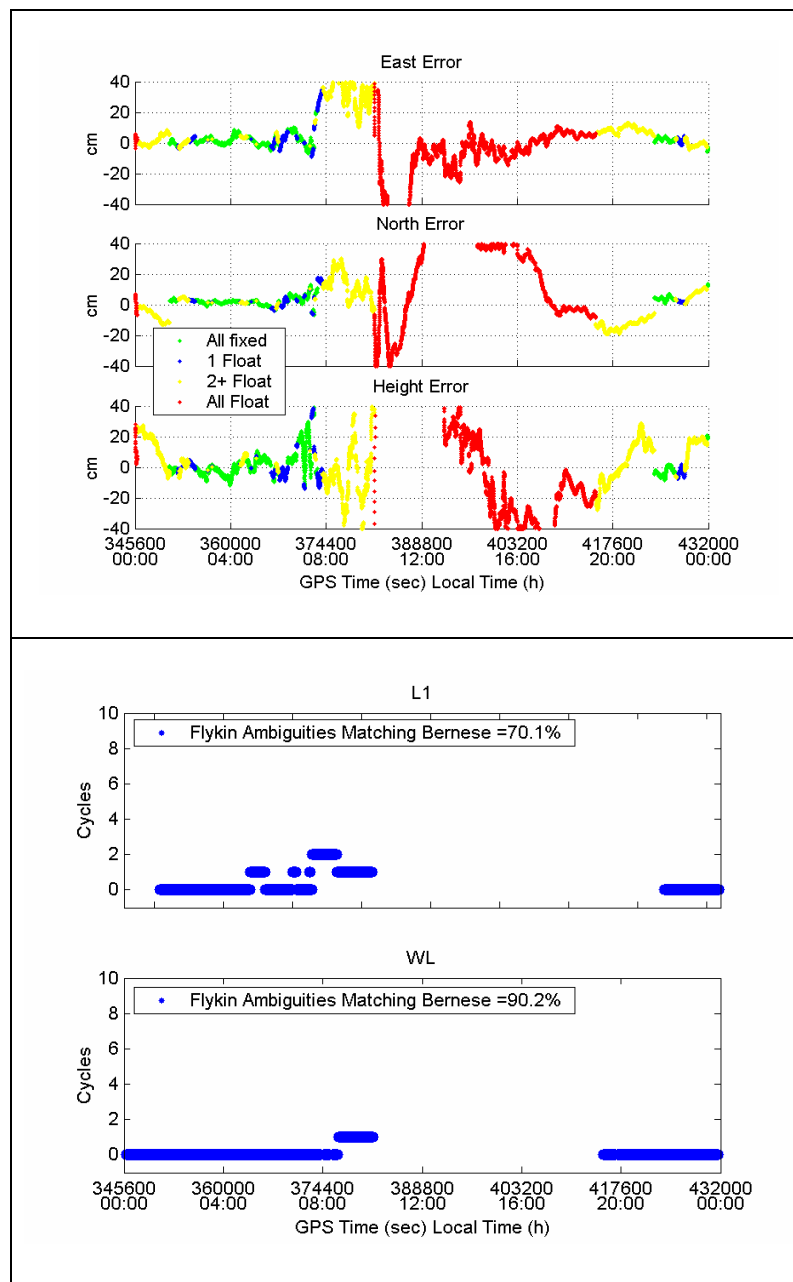


Figure 5.24 Position Errors and Ambiguity Comparison, Strategy 4

Recall that Strategy 4 used the same observations as Strategy 3 except that the L1 and WL ambiguities are estimated in the filter instead of the L1 and L2 ambiguities. As the bottom graph in Figure 5.24 shows, both the WL and L1 ambiguities suffer from the ionosphere from the middle of the data set.

1.5) Test 1, Strategy 5 Results.

Figure 5.25 gives the position results for Test 1, Strategy 5.

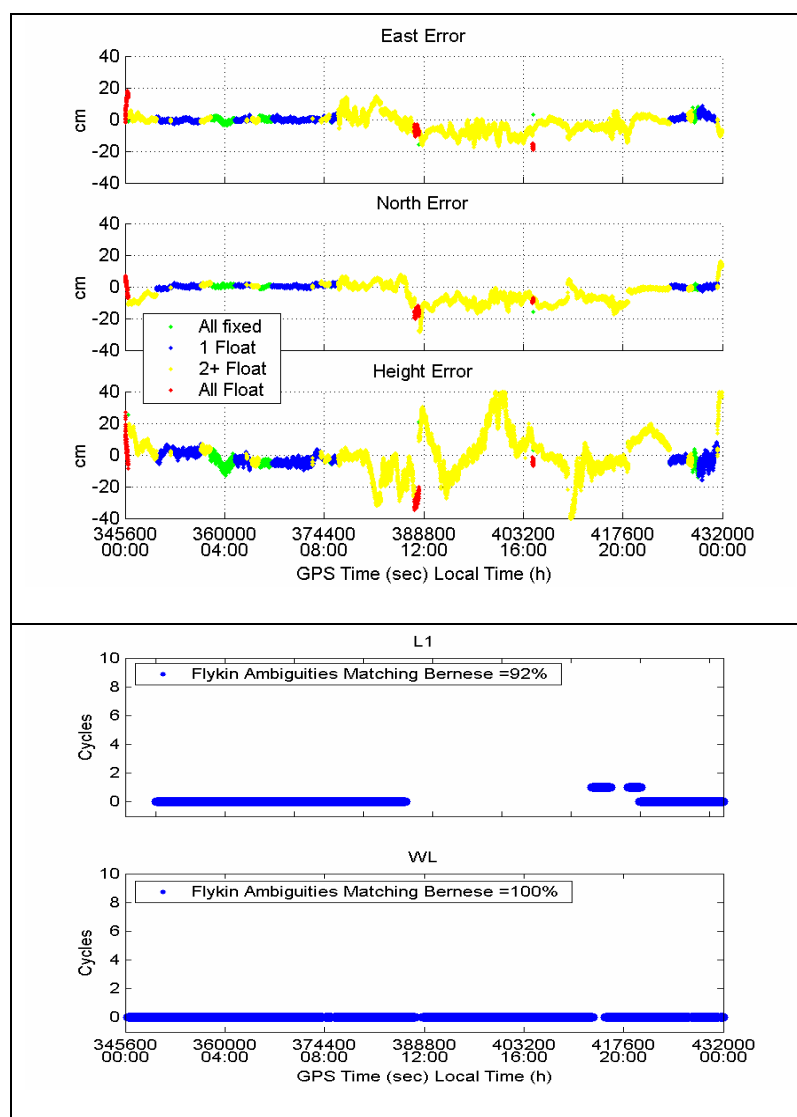


Figure 5.25 Position Errors and Ambiguity Comparison, Strategy 5

Figure 5.25 shows that the WL ambiguities for Strategy 5 are fixed correctly 100% and 83% of the time for the L1 ambiguities. The position error RMS values for Strategy 5 in Table 5.10 clearly outperform Strategies 1 through 4. This time the L1 ambiguities are fixed for 83% of the time, not 100%. The possible reason is that in this case, the residual tropospheric error can not be neglected due to the much longer baseline length, i.e. 43 km.

1.6) Test 1, Strategy 6 Results.

Figure 5.26 shows the position results for Test 1 using Strategy 6. Table 5.10 shows that the RMS of the position errors for Strategy 6 is better than Strategies 1 through 4. Nevertheless, this time Strategy 6 gives better RMS than Strategy 5 because there is 17% wrong L1 ambiguity fixes for Strategy 5.

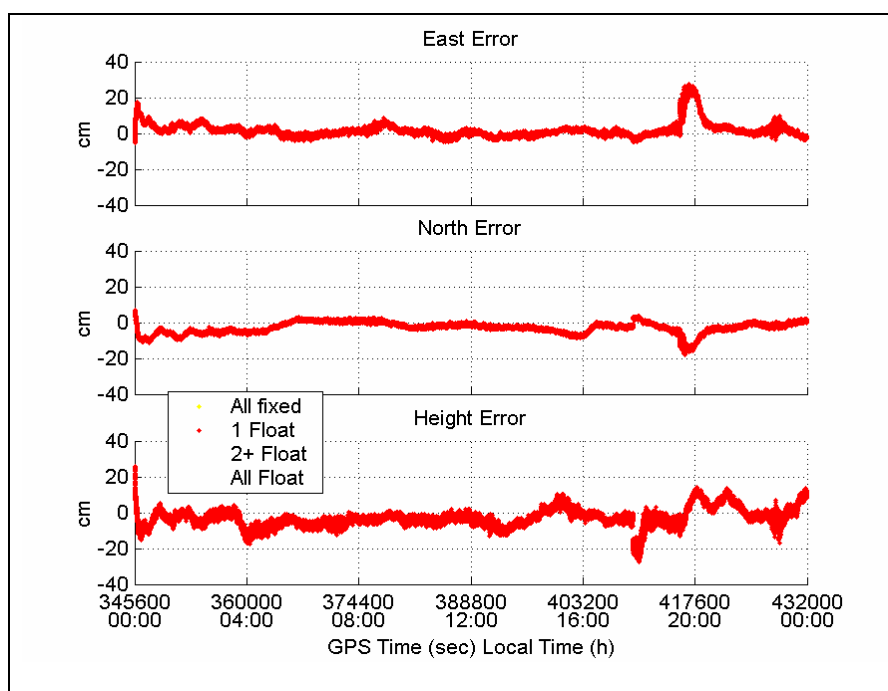


Figure 5.26 Position Errors, Strategy 6

In this Strategy, there is no risk of resolving the ambiguity to the wrong integer, thus it is a reliable method. However there is one limitation with this method, namely the time needed for the ionosphere-free ambiguity to converge is significant. Figure 5.26 shows that it takes around 1 hour to converge based on the convergence of the position error towards zero.

1.7) Test 1, Strategy 7 Results.

Figure 5.27 shows the position results for Test 1 using Strategy 7. From the figure and Table 5.11, it can be seen that this strategy gives the best positioning performance compared to all previous strategies.

1.8) Test 1, Strategy 8 Results.

Figure 5.28 shows the position results for Test 1 using Strategy 8. The observables used in this strategy are the same as in Strategy 7. The difference is that L1 and widelane ambiguities are estimated in the filter instead of L1 and L2 ambiguities. Figure 5.28 is very similar to Figure 5.27. The only obvious difference is that the position error of Strategy 8 is much smaller than that of Strategy 7 for the north and east axes. This is explained by two reasons. First, Strategy 7 has two 0.2% incorrect L1 and L2 ambiguity fixes. Second, in Strategy 8, the widelane ambiguities can be fixed much faster than the L1 ambiguities and the fixing of widelane ambiguities improves the position estimate accuracy.

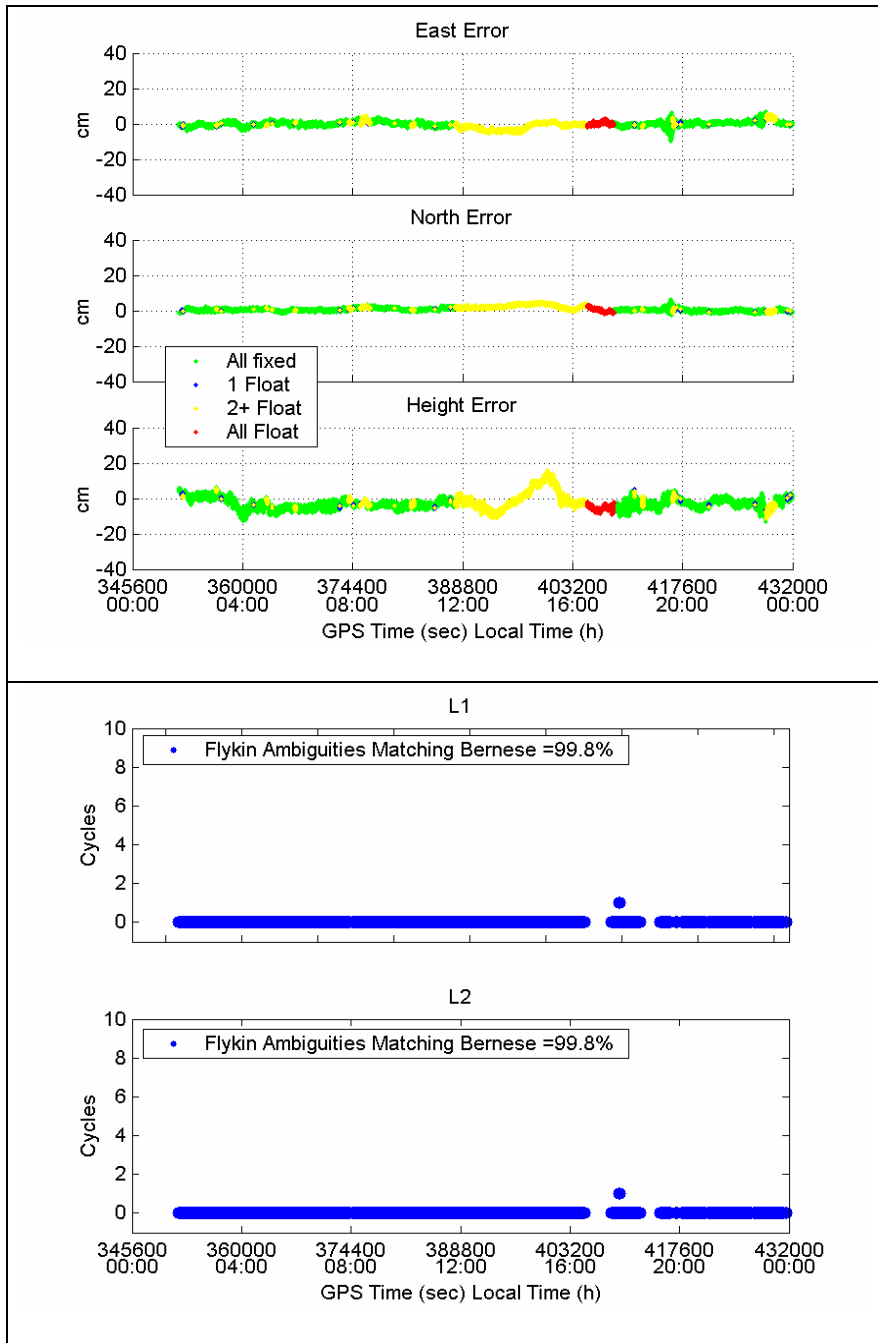


Figure 5.27 Position Errors and Ambiguity Comparison, Strategy 7

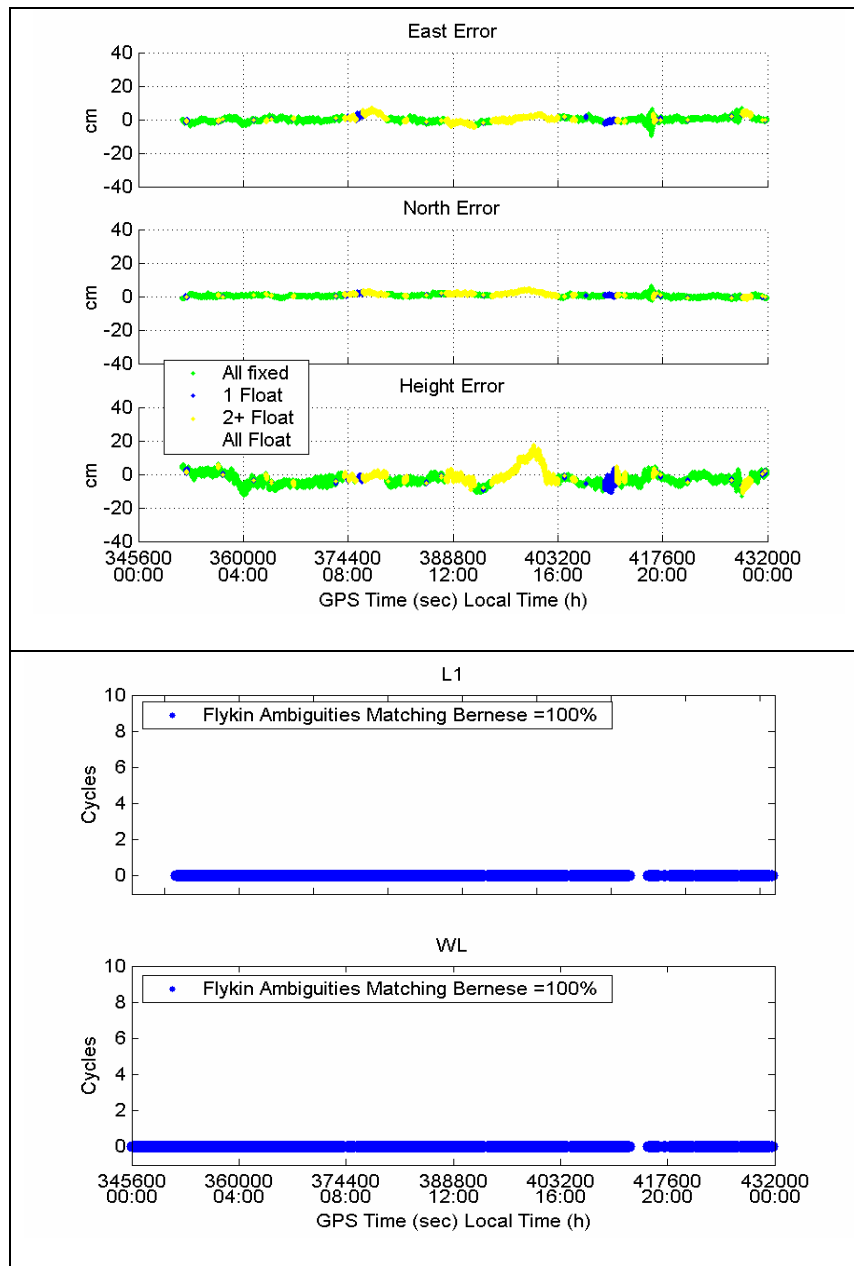


Figure 5.28 Position Errors and Ambiguity Comparison, Strategy 8

2) Test 2 Result, 900-second-interval Tests.

In this test, the 24-hour data set is divided into equal 900-second intervals, and each interval is processed with FLYKIN+TM for all the strategies in Table 4.1 to assess the

ambiguity resolution performance and position accuracy. A 900-second interval instead of 600-second is chosen because extra time is needed for the filter to converge, given the much longer baseline length this time. Once the ambiguity is resolved, a fixed position solution is recorded and the FLYKIN+TM software will re-initialize the filter and go to the beginning of next 900-second interval to try and resolve the ambiguities again.

Table 5.12 shows the 900-second-run statistics for all the strategies. The shaded block containing the statistics for the WL shows that the WL ambiguity is both reliable and stable in terms of time to fix and percentage correct. Also, comparing the statistics for Strategies 3 and 4, where the same observations are used, the only difference being that in Strategy 3, the L1 and L2 ambiguities are estimated in the filter, while in Strategy 4 the L1 and WL ambiguities are estimated. The statistics show that it takes comparable time to fix L1 ambiguities for both approaches and the percentage correct is also comparable. The same is true for Strategies 7 and 8. It can be concluded that estimating L1 and WL ambiguities in the same filter, instead of L1 and L2 ambiguities, does not bring much improvement in terms of L1 ambiguity resolution for this data set.

Table 5.12 900-second-run Statistics, 43 km Baseline

Measure	Strategy						
	1	2	3	4	5	7	8
N_1 FWI ¹	31%	N/A	13%	19%	27%	35%	32%
N_1 PCFA ²	43%	N/A	84%	79%	68%	74.2%	75%
N_1 MTTF ³	337 s	N/A	165 s	154 s	340 s	274 s	281 s
N_2 FWI	N/A	N/A	13%	N/A	N/A	35%	N/A
N_2 PCFA	N/A	N/A	84%	N/A	N/A	74.2%	N/A
N_2 MTTF	N/A	N/A	165 s	N/A	N/A	274 s	N/A
N_{wL} FWI	N/A	80%	N/A	82%	80%	N/A	97%
N_{wL} PCFA	N/A	100%	N/A	96%	100%	N/A	100%
N_{wL} MTTF	N/A	133 s	N/A	92 s	133 s	N/A	54 s

However, estimating L1 and WL ambiguities in the filter instead of L1 and L2 ambiguities does have a benefit in the position domain. Table 5.13 shows the position error RMS for Strategies 3, 4, 7, and 8. The position error after the WL ambiguities are resolved are significantly lower than for Strategy 3 where both L1 and L2 ambiguities cannot be resolved. Therefore estimating WL and L1 ambiguities instead of L1 and L2 has a benefit on position estimation provided that the WL ambiguity resolution is reliable and fast.

Table 5.13 RMS Position (cm) for 900-second-run, 43 km Baseline

Axis	Strategy			
	3	4	7	8
	No Ambiguity Fixed	Only WL Ambiguity Fixed	No Ambiguity Fixed	Only WL Ambiguity Fixed
East	38	27	9	6
North	25	13	12	13
Height	65	41	18	11

5.3 Multiple Reference Station Tests and Results.

Previous sections in this chapter tested eight different ambiguity resolution strategies. It was found that the last four strategies (Strategies 5, 6, 7 and 8) gave better ambiguity resolution and positioning performance than the first four strategies (Strategies 1, 2, 3 and 4) because the former takes the ionospheric error into account through either forming the IF combination or stochastic ionosphere modelling. This means that in order to achieve optimal ambiguity resolution performance under an active ionosphere, the rover can not implement the two widely used Strategies 1 and 2. Instead the rover has to implement a complicated algorithm such as Strategy 5, 6, 7 and 8. This may not be feasible for all users.

There is an emerging alternative technique that can predict the ionospheric error and then correct such errors using a network of GPS reference stations. The network models the ionospheric error and transmits the corrections to the rover, so the rover can have

improved ambiguity resolution and positioning performance even with Strategies 1, 2, 3 and 4 because the ionospheric error has been properly taken into account by the network.

Driven by the demand of high precision positioning from the civil community, the use of a GPS multiple reference station network to generate carrier phase observation corrections, to compensate the differential errors over a large area and increase the maximum distance at which reliable ambiguity resolution can go ahead, has been under intensive research in recent years (Wanninger, 1995; Han and Rizos, 1996b; Wubben et al., 1996; Raquet, 1998). According to Fotopoulos (2000), the methods developed up to date can be classified into four categories.

- Partial derivative algorithms (Wubben et al., 1996; Varner et al., 1997)
- Linear interpolation algorithms (Wanninger, 1995; Gao et al., 1997; Han and Rizos, 1996b)
- Condition adjustment algorithm (Raquet, 1998)
- Virtual reference station algorithm (Wanninger, 1995, van der Marel, 1998)

Among all mentioned methods, the one derived at the University of Calgary by Raquet (1998), is one of the most rigorous from an optimal estimation theory point of view (Fortes, 2002). This method is referred to as MultiRef in this thesis and it is schematically illustrated in Figure 5.29. The four reference stations at each corner collect measurements and transmit these measurements to the control centre (The one shown in the middle of the figure). The central GPS reference station will generate carrier phase corrections

based on these measurements. These corrections are then transmitted to the user (ship, surveyor, etc...) to facilitate a real time carrier phase based positioning.

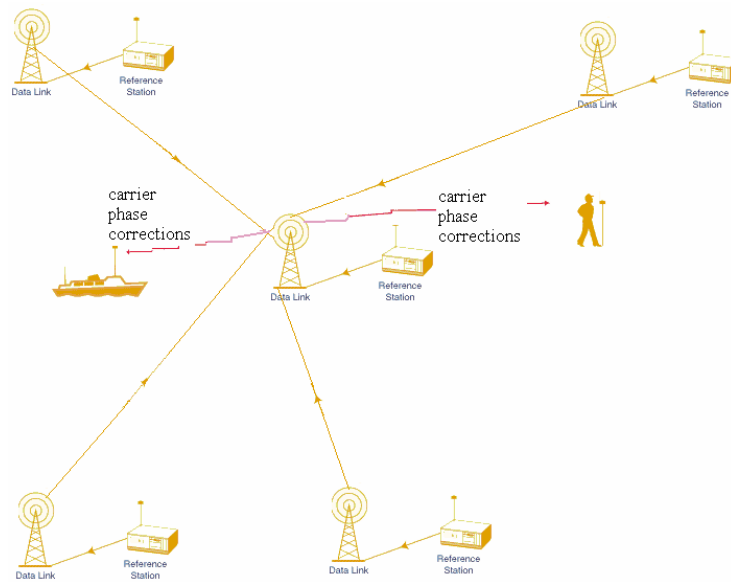


Figure 5.29 A GPS MultiRef Network

The MultiRef approach is based on Least-Squares collocation (Fortes, 2002). By estimating the differential errors between those reference receivers, the differential errors between the rover station and any reference station can be predicted, thus corrections can be applied to the raw observables at the rover to compensate these differential errors. With fewer differential errors, the rover, in theory, should have a higher probability in successfully resolving integer ambiguities and providing high accuracy position estimates.

MultiRef was initially designed for real-time operation. A lot of results have been presented in the past to show the effectiveness of the MultiRef approach in post mission.

Fotopoulos (2000) has conducted research on the correction generation and dissemination scheme, and tested these schemes with data from the Swedish Network. However, no real time test was carried out. Another objective of this thesis is to develop a real time system and evaluate the performance of the system in real conditions. The real time test is explained below.

5.3.1 Test Setup

Figure 5.30 shows the real time test set-up where the GPS reference stations are enclosed in the ellipse. Each reference station makes measurement and sends the measurements to a control centre using high bandwidth Internet with TCP/IP protocol. The control centre then processes data from all the reference stations, solving the integer ambiguities between the reference stations and generating corrections.

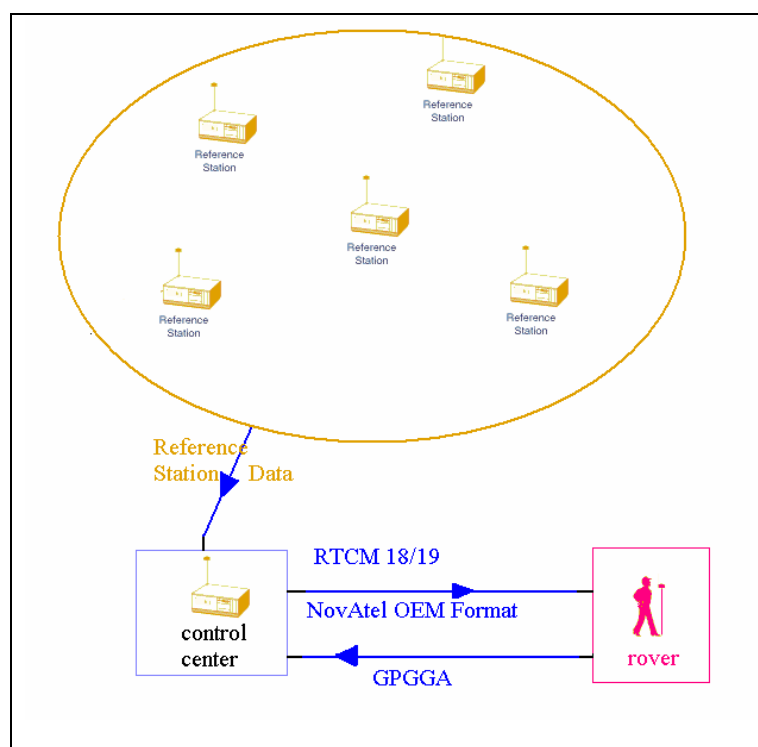


Figure 5.30 Real Time Test Flow Chart

In the present case the real time test is carried out as follows: The rover sends an NMEA 0183 message GPGGA to the control centre via the Internet using TCP/IP protocol. The GPGGA message contains the approximate position of the rover. Based on this approximate rover position, the control centre will generate the corrections for this rover position and apply the corrections to a Virtual Reference Station's (VRS) observation data and send the corrected VRS observation to the rover in NovAtel OEM format via the Internet.

A small MultiRef network has been set up in Calgary, Alberta (Figure 5.31). This network consists of six stations with a NovAtel MPC receiver employed at each station. The raw data collected at each station is sent to a control centre located in the Department of Geomatics Engineering Satellite Observatory. Two reference stations (MPC4 and MPC5) are set up very close to each other. The reason is that MPC5 will eventually be deployed somewhere around Cochrane near Calgary. The longest baseline in this Network is 24.3 km. The size of the Calgary network is small, which leads the magnitude of the most corrections to be under 2 cm.

In this test, the university station MPC-UofC is excluded from the MultiRef network and used as a rover. The nearest reference station to the rover MPC-UofC is 5.4km. Under the MultiRef environment, it does not matter which reference station acts as the reference to do position estimate for the MPC-UofC rover because of the data encapsulation effect of the MultiRef. An epoch-by-epoch RTK solution is computed for the station MPC-UofC.

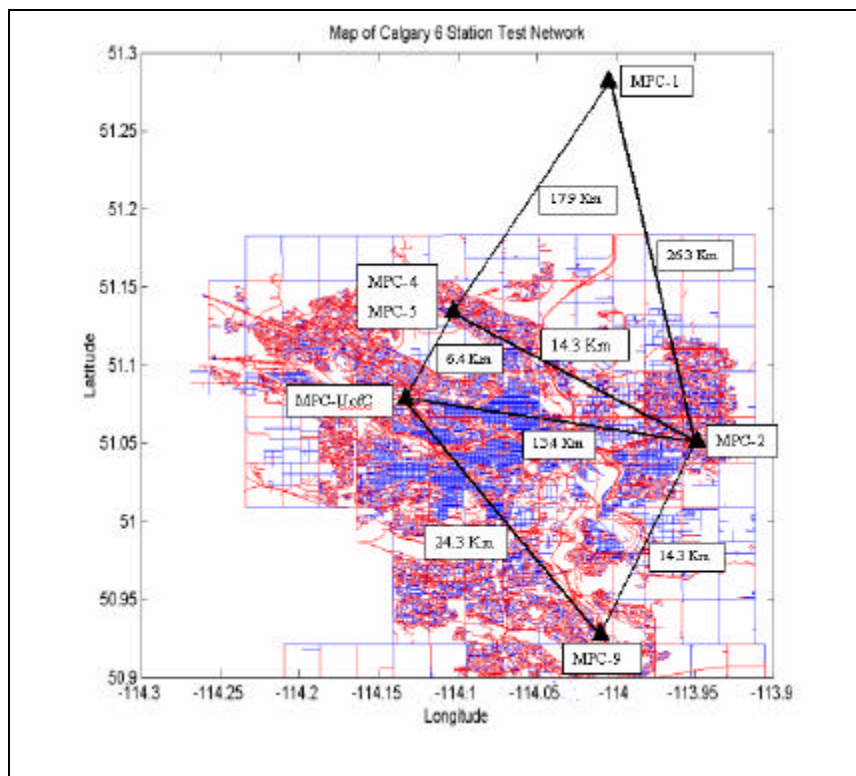


Figure 5.31 Calgary MultiRef Network Configuration

The ambiguity resolution strategies used are Strategies 1, 2, 3, 4, 7 and 8. Each strategy was run for one hour consecutively in real time generating a position solution at every second. The cut-off elevation angle is 5 degrees and at least five satellites are observed for the entire test period. The position error plots for each strategy are shown in Figures 5.32 to 5.37. The position statistics are shown in Table 5.14 to Table 5.19 for each strategy.

5.3.2 Results

1) Result for Strategy 1

The 1-hour position error for Strategy 1 is shown in Figure 5.32. There are several red dots (float solution) at the beginning due to the filter convergence. The L1 ambiguities are resolved within thirty seconds. The distance of the rover to the closest reference station is 6.4km. Considering the time of the day this test is carried out (13:30-14:30 local time), this indicates very good performance of MultiRef approach in real time. The blue segment in the plot is caused by one float ambiguity that just entered the solution.

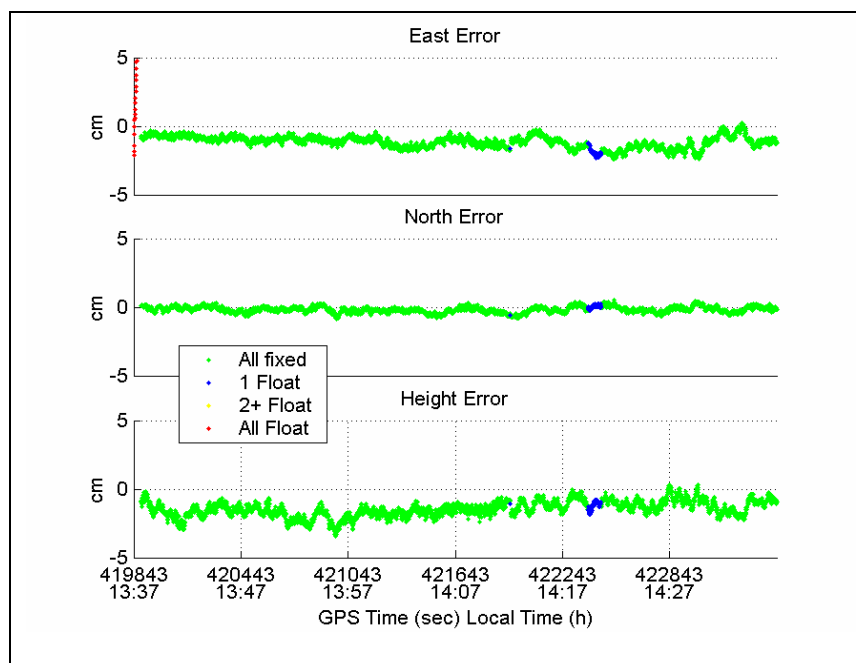


Figure 5.32 Real Time Position Errors with Strategy 1

Table 5.14 shows the position RMS error for Strategy 1. The RMS for the All Fixed (All the ambiguities have been fixed) case is 1 cm, 0 cm and 2 cm for east, north and up axis.

During 96.8% of all the epochs in this 1-hour test, all ambiguities are fixed.

Table 5.14 RMS Position Errors, Strategy 1

RMS (cm)												
Axis	All Points (100%)			All Fixed (96.8%)			Partial Fixed (2.1%)			All Float (1.1%)		
	Min	Max	RMS	Min	Max	RMS	Min	Max	RMS	Min	Max	RMS
East	-2	8	1	-2	0	1	-2	0	2	-2	8	5
North	-1	42	4	-1	0	0	-1	0	0	40	42	41
Height	-3	37	4	-3	0	2	-2	0	1	30	37	35

2) Result for Strategy 2

The 1-hour position error for Strategy 2 is shown in Figure 5.33. The noise property of Strategy 2 (WL) is clearly shown in this figure. Float ambiguities (blue) cause large position variations in the middle of the test. Table 5.15 shows the position RMS error for Strategy 2. The RMS for the All Fixed case is 3 cm, 2 cm and 3 cm for east, north and up axis. All ambiguities are fixed 71.4% of the time. This relatively low percentage compared to all other strategies is caused by the long time span of the float ambiguity in the middle of the 1-hour test.

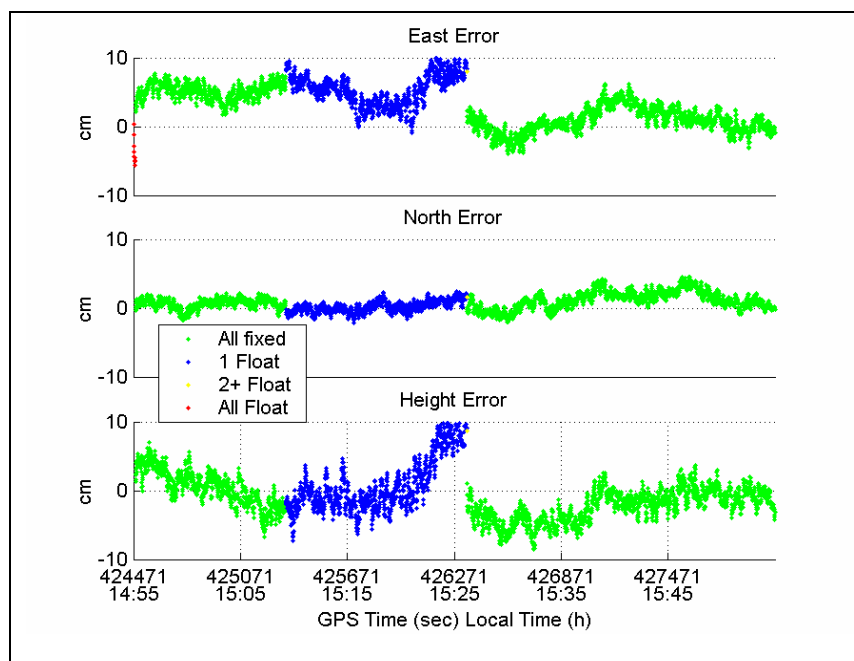


Figure 5.33 Real Time Position Errors with Strategy 2

Table 5.15 RMS Position Errors, Strategy 2

RMS (cm)												
Axis	All Points (100%)			All Fixed (71.4%)			Partial Fixed (28.2%)			All Float (0.3%)		
	Min	Max	RMS	Min	Max	RMS	Min	Max	RMS	Min	Max	RMS
East	-6	10	4	-4	8	3	-1	10	6	-6	0	4
North	-2	28	2	-2	5	2	-2	2	1	24	28	26
Height	-7	27	4	-7	9	3	-5	15	5	19	27	21

3) Result for Strategy 3

The 1-hour test position error for Strategy 3 is shown in Figure 5.34. Table 5.16 shows the position RMS error for Strategy 3. The RMS for the All Fixed case is 1 cm, 0 cm and

3 cm for east, north and up axis. During 99.1% of all the epochs in this 1-hour test, all ambiguities are fixed, and the remaining 0.9% contains epochs when no ambiguities are fixed when the filter is converging.

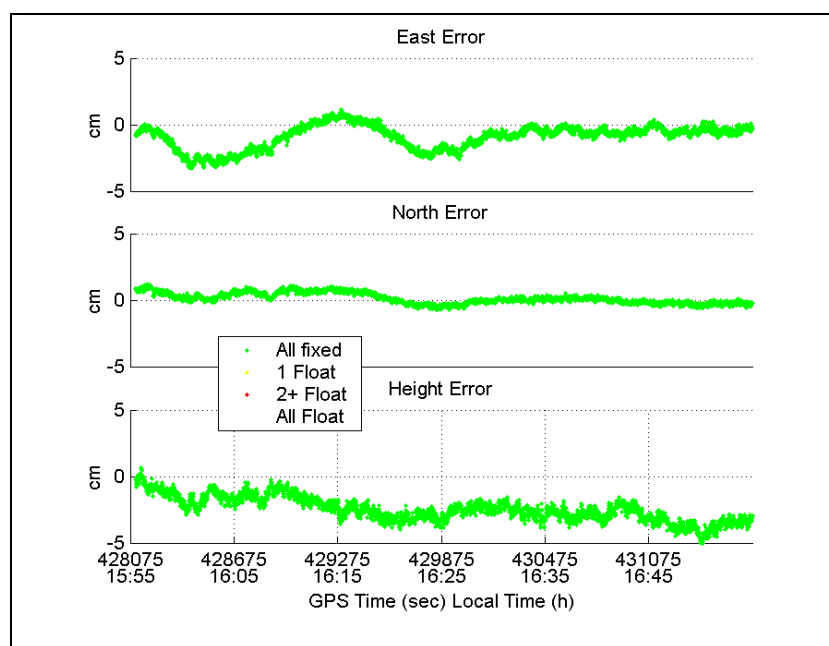


Figure 5.34 Real Time Position Errors with Strategy 3

Table 5.16 RMS Position Errors, Strategy 3

RMS (cm)												
Axis	All Points (100%)			All Fixed (99.1%)			Partial Fixed (0%)			All Float (0.9%)		
	Min	Max	RMS	Min	Max	RMS	Min	Max	RMS	Min	Max	RMS
East	-17	1	2	-3	1	1	N/A	N/A	N/A	-17	-15	16
North	-1	24	2	-1	1	0	N/A	N/A	N/A	20	24	22
Height	-21	1	3	-5	1	3	N/A	N/A	N/A	-21	-17	19

4) Result for Strategy 4

The 1-hour position error for Strategy 4 is shown in Figure 5.35. Table 5.17 shows the position RMS error for Strategy 4. The RMS for the All Fixed case is 1 cm, 1 cm and 3 cm for east, north and up axis. During 99.1% of all the epochs in this 1-hour test, all ambiguities are fixed, and the remaining 0.9% contains epochs when no ambiguities are fixed when the filter is converging.

Table 5.17 RMS Position Errors, Strategy 4

RMS (cm)												
Axis	All Points (100%)			All Fixed (99.1%)			Partial Fixed (0%)			All Float (0.9%)		
	Min	Max	RMS	Min	Max	RMS	Min	Max	RMS	Min	Max	RMS
East	-5	1	1	-2	1	1	N/A	N/A	N/A	-5	-1	4
North	-1	16	2	-1	2	1	N/A	N/A	N/A	12	16	14
Height	-5	44	5	-5	0	3	N/A	N/A	N/A	41	44	43

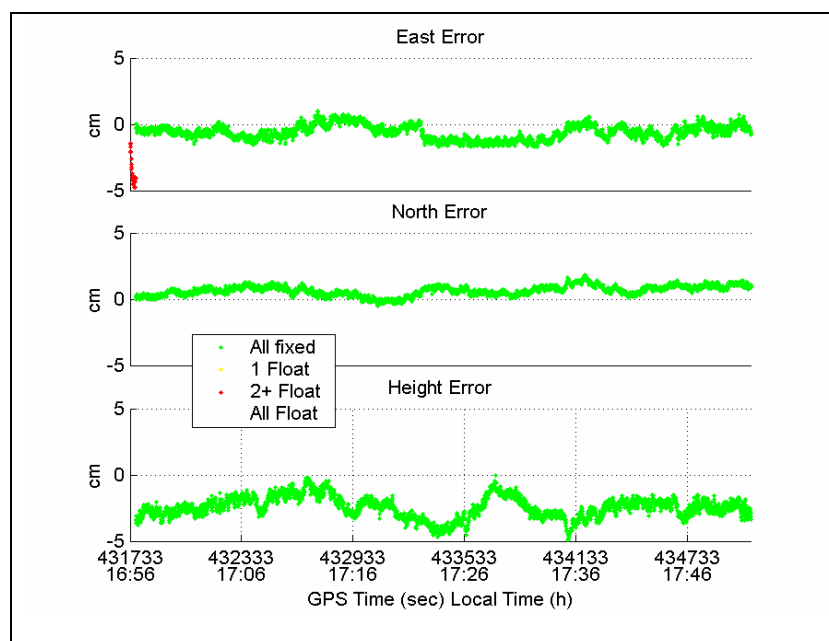


Figure 5.35 Real Time Position Errors with Strategy 4

5) Result for Strategy 7

The 1-hour position error for Strategy 7 is shown in Figure 5.36. Table 5.18 shows the position RMS error for Strategy 7. The RMS for the All Fixed case is 1 cm, 1 cm and 3 cm for east, north and up axis. During 98.9% of all the epochs in this 1-hour test, all ambiguities are fixed, and during 0.2% of all the epochs, there is not ambiguity being fixed. The remaining 0.9% contains epochs when all but one ambiguity is fixed.

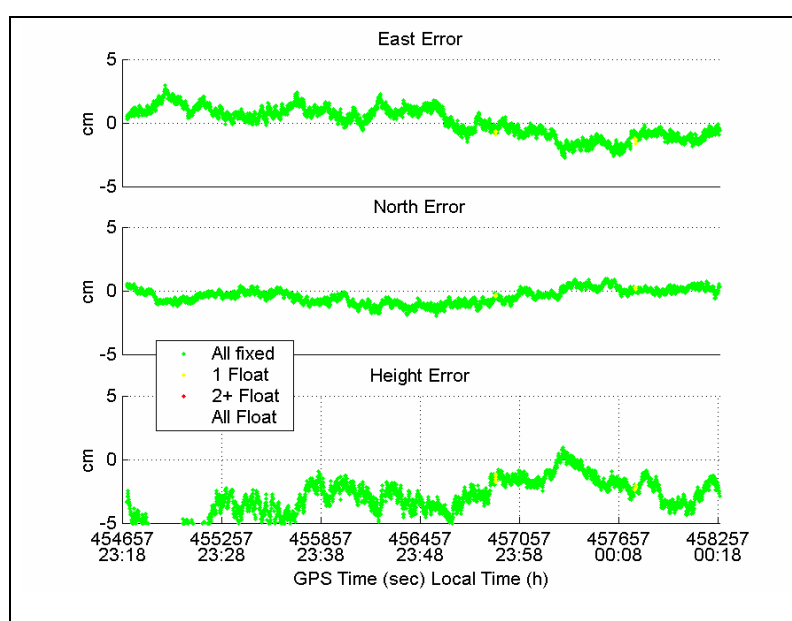


Figure 5.36 Real Time Position Errors with Strategy 7

Table 5.18 RMS Position Errors, Strategy 7

Axis		RMS (cm)										
		All Points (100%)			All Fixed (98.9%)			Partial Fixed (0.2%)			All Float (0.9%)	
Min	Max	RMS	Min	Max	RMS	Min	Max	RMS	Min	Max	RMS	
East	-3	18	2	-3	3	1	-2	0	1	12	18	16
North	-2	26	2	-2	1	1	0	0	0	24	26	25
Height	-44	1	5	-8	1	3	-2	0	2	-44	-39	43

6) Result for Strategy 8

The 1-hour position error for Strategy 8 is shown in Figure 5.37. Table 5.19 shows the position RMS error for Strategy 8. The RMS for the All Fixed case is 1 cm, 0 cm and 2 cm for east, north and up axis. All the ambiguities are fixed 98.9% of the time.

Table 5.19 RMS Position Errors, Strategy 8

RMS (cm)												
Axis	All Points (100%)			All Fixed (98.9%)			Partial Fixed (0.2%)			All Float (0.9%)		
	Min	Max	RMS	Min	Max	RMS	Min	Max	RMS	Min	Max	RMS
East	-2	29	3	-2	1	1	-1	0	1	22	29	28
North	-1	42	4	-1	1	0	0	0	0	38	42	38
Height	-33	1	4	-5	1	2	-2	0	1	-33	-31	32

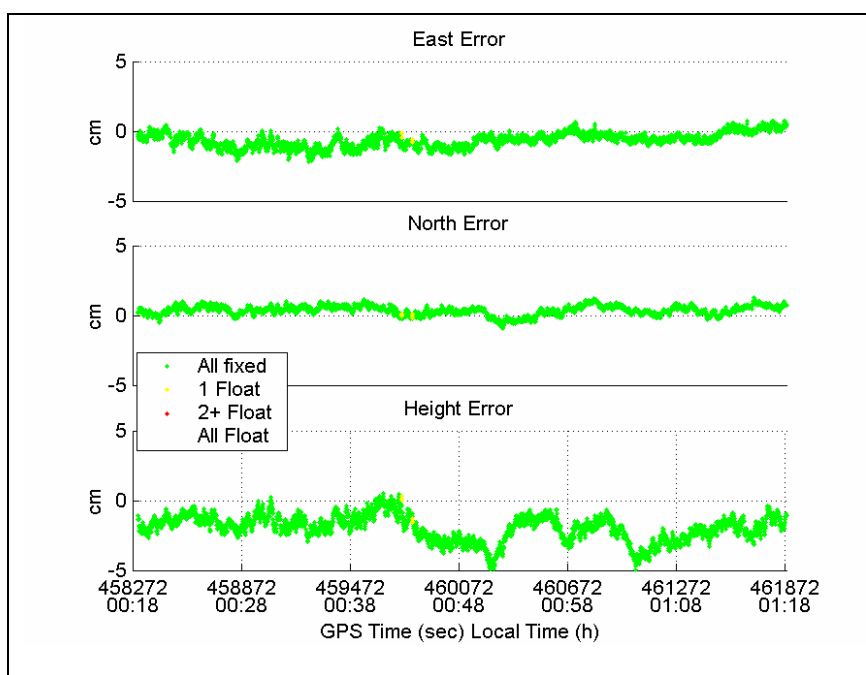


Figure 5.37 Real Time Position Errors with Strategy 8

5.4 Summary

Based on the tests and results achieved in this chapter, the following summaries can be made:

1. WL ambiguity is both reliable and easier to resolve than the L1 and L2 ambiguities. In periods of high ionospheric activity, the ionospheric bias is actually amplified in the WL observable in units of metres, thus WL combinations do not necessarily give the optimal position results in terms of accuracy.
2. During periods of high ionospheric activity, in order to achieve an optimal position solution, the ionospheric bias must be dealt with explicitly by either forming the IF observable or through stochastic modelling.
3. Estimating L1 and WL ambiguities in the same filter, instead of L1 and L2 ambiguities, does not help to resolve the L1 ambiguities faster or more accurately, but it can decrease the position errors if the WL is fixed correctly. This is relative to the strategies where the L1 and L2 ambiguities remain as floating values. Results may be different for very short baselines where the ionosphere is less significant.
4. Stochastic ionospheric modelling gives the best positioning results among all of the strategies used for this data set.

5. In Strategy 5 (IF Fixed), the WL ambiguities are usually fixed quickly, while the L1 ambiguities require a longer time to fix because of their reduced wavelength (10.7cm). This may hinder the real time use of Strategy 5. Nevertheless, even if the L1 ambiguities are not fixed, an ionosphere-free float solution results, which, as demonstrated by Strategy 6, can still give reasonable position estimates.

6. This chapter also presented a system to evaluate the MutliRefTM approach in real time conditions. For each strategy, test results are impressive with position RMS values less than 3 cm in All Fixed cases for all three axes. The results obtained clearly show that the system works very well. Considering the baseline between the nearest reference station to this 'rover' is 6.4 km, the effectiveness of the MultiRefTM approach is demonstrated.

CHAPTER 6

CONCLUSIONS AND RECOMMENDATIONS

This research investigated various ambiguity resolution strategies. It gave a detailed analysis of the impact of observation types and combinations, and model parameterization on carrier phase ambiguity resolution and position accuracy under operational conditions. The thesis began with a thorough investigation into the differential error sources for carrier phase relative positioning. It stated that for medium baselines, the differential ionospheric error is usually the dominant error source preventing the user from achieving successful ambiguity resolution, and high precision position results. To examine the impact of the differential ionospheric error on ambiguity resolution, a total of eight ambiguities resolution strategies were implemented in the FLYKIN+TM software package. All those eight strategies have been tested using three baselines from Calgary, Canada and Campania, Italy. The baseline length ranges from 10 km to 43 km. All of the data was collected near the peak of the 11-year sunspot cycle and the differential ionospheric error reaches as high as 15 ppm for some baselines. This thesis also presented a system to evaluate the MutliRefTM approach in real time conditions. Test results are impressive with RMS position values less than 3 cm in All Fixed cases for all three axes.

Based on the tests and results achieved in this chapter, the following conclusions can be made:

1. The selection of the observation types and combinations, and model parameterization, and estimation model directly impact carrier phase ambiguity resolution and positioning accuracy under active ionospheric conditions.
2. WL ambiguities are both reliable and easy to resolve. It was demonstrated that WL ambiguities are fixed 100% of the time correctly for all three baselines. Tables 5.4, 5.8 and 5.12 have shown that the mean time to fix the WL ambiguities is much shorter than the mean time to fix the L1 or L2 ambiguities.
3. In periods of high ionospheric activity, the ionospheric bias is actually amplified in the WL observable in units of metres, thus WL combination does not necessarily give the optimal position results in terms of accuracy. Tests in Chapter 5 have shown that position errors under active ionosphere can reach more than 50 cm even the WL ambiguities are fixed correctly.
4. Estimating L1 and WL ambiguities in the same filter, instead of L1 and L2 ambiguities, does not help to resolve the L1 ambiguities faster or more accurately. This is relative to the strategies where the L1 and L2 ambiguities remain as floating values. It was demonstrated in Tables 5.4, 5.8 and 5.12 that the mean time to fix the L1 ambiguities is comparable.

5. Estimating L1 and WL ambiguities in the same filter, instead of L1 and L2 can decrease the position errors if the WL is fixed correctly. It was demonstrated in Tables 5.5, 5.9 and 5.13 that the position RMS errors in Strategies 4 and 8 after the WL ambiguities are fixed correctly are significantly better than the position errors in Strategies 3 and 7 when both L1 and L2 ambiguities are not fixed.
6. During periods of high ionospheric activity, in order to achieve an optimal position solution, the ionospheric bias must be dealt with explicitly by either forming the IF observable or through stochastic modelling. It was demonstrated that the performance of Strategies 1, 2, 3 and 4 (in which the ionospheric error is assumed to be absent) are largely dependant on the DD ionospheric errors. They are capable of centimetre positioning under a low DD ionospheric error condition. However, this capability is severely compromised with an increased DD ionospheric error.
7. The stochastic ionosphere modelling strategies gives the best position estimate compared to all others. Less than 10 cm position RMS errors are reported by the stochastic ionosphere modelling strategies for all three baselines.
8. The real-time system implemented has clearly demonstrated centimetre level positioning accuracy capability for the Calgary Network. All the strategies tested reported less than 3 cm RMS position error.

Based on the results and conclusions of this research, the following recommendations regarding the use and further investigations of various ambiguity resolution strategies can be made:

1. The test results for various ambiguity resolution strategies in Chapter 5 show that Strategies 7 and 8 (the two stochastic ionosphere modelling strategies) gives better positioning results than Strategies 5 and 6 (the two ionosphere free combination strategies). Further research can be done to explain this phenomenon.
2. The test results in Chapter 5 are based on certain input parameters. These input parameters include data rate, observation variances, the magnitude of the noise spectral density driving the velocity and position states, and the magnitude of the pseudo-ionosphere observable variance. The impact of these input parameters on the output is not investigated in this thesis. The relation between these input parameters and output parameters is important, as it is expected that the slight change in the input parameters should not significantly change the output.
3. The author implements a suggested ambiguity method in the software FLYKIN+TM. Very limited tests have been done to test the efficiency of this method. It is recommended that this method should be tested more extensively for RTK applications.
4. The detection of multiple cycle slips at the same epoch is very critical for the success of any kinematic software. There is a large possibility that multiple cycle

slips will occur at the same time. One obvious example is that there is a cycle slip on the reference satellite. The appendix of this thesis has shown the basic measures to detect and remedy the cycle slips. More work is required in this area to increase the robustness of the FLYKIN+™ software.

Overall, this thesis clarifies the pros and the cons of all the introduced ambiguity resolution strategies. With this knowledge, the ambiguity resolution process can be better understood and the optimal scheme for an application can be chosen.

REFERENCES

- Allison, T. (1991), Multi-observable Processing Techniques for Precise Relative Positioning, In Proceedings of ION GPS 91, The 4th International Technical Meeting of the Satellite Division of the Institute of Navigation, Albuquerque, New Mexico, September 11-13, pp. 715-725.
- Axelrad et al. (1996), GPS Navigation Algorithms, in Global Positioning System: Theory and Applications Volume 1, Eds. Parkinson, B., Spiker, J., Axelrad, P, Enge, P., American Institute of Aeronautics and Astronautics, pp. 409-433.
- Behr, J.A., and Hudnut, K.W. (1998), Monitoring Structural Deformation at Pacoima Dam, California Using Continuous GPS, In Proceedings of the 11th International Technical Meeting of the Satellite Division of the Institute of Navigation (ION GPS-98), Nashville, TN, pp. 59-68.
- Blewitt, G. (1989), Carrier Phase Ambiguity Resolution for the GPS Applied to Geodetic Baselines up to 2000km, *Journal of Geophysical Research*, Vol. 94, No. B8, pp. 10187-10203.
- Bock, Y. (1996), Medium Distance GPS Measurement, in GPS for Geodesy, Eds P.J.G.Teunissen, A. Kleusberg, Springer, pp. 337-377.

Braasch, M.S. (1996), Multipath Effects, in Global Positioning System: Theory and Applications Volume 1, Eds. Parkinson, B., Spiker, J., Axelrad, P, Enge, P., American Institute of Aeronautics and Astronautics, pp. 547-568.

Brown, R.G. and Hwang, P.Y.C. (1992), Introduction to Random Signals and Applied Kalman Filtering, 2nd Ed. John Wiley & Sons, Inc., New York.

Cannon, M.E. (1991), Airborne GPS/INS with an Applications to Aerotriangulations, UCSE Reports No. 20040, Department of Surveying Engineering, University of Calgary.

Cannon, M.E. (2002), GPS Positioning, ENGO 561 Lecture Notes, Department of Geomatics Engineering, The University of Calgary, Calgary, Alberta

Chen, D and Lachapelle, G (1994), A Comparison of the FASF and Least-Squares Search Algorithms for On-the-Fly Ambiguity Resolution. Journal of the Institute of Navigation, Vol. 42, No.2, pp.371-390.

Colombo, O.L. (1998), Long-Distance Kinematic GPS, in GPS for Geodesy, Eds P.J.G.Teunissen, A. Kleusberg, Springer, pp. 537-567.

Counselman, C.C. et al. (1981), Miniature interferometer terminals for earth surveying: ambiguity and multipath with the Global Positioning System. IEEE Transactions on Geoscience and Remote Sensing, GE-19(4), pp. 244-252.

U.S. Department of Defense (2001), Global Positioning System Standard Positioning Service Performance Standard, USA.

Euler, H.J. and Landau, H (1992), Fast GPS Ambiguity Resolution On-The-Fly for Real-time Applications. In Proceedings of 6th Geodetic Symposium on Satellite Positioning, pp. 650-729.

FAA, Specifications for the Wide Area Augmentation System, FAA-E-2892C (draft), 1997.

Fortes, L.P.S. (2002), Optimizing the Use of GPS Multi-Reference Stations for kinematic Positioning. Ph.D. thesis, Department of Geomatics Engineering, University of Calgary, Calgary, Alberta, Canada.

Fotopoulos, G. (2000), Parameterization of DGPS Carrier Phase Errors Over A Regional Network of Reference Receivers. MSc thesis, Department of Geomatics Engineering, University of Calgary, Calgary, Alberta, Canada.

Frei, E (1991), GPS-Fast Ambiguity Resolution Approach "FARA": theory and application. Paper presented at XX General Assembly of the IUGG, IAG-Symposium GM ¼, Vienna, August 11-24.

Gao, Y., Li, Z., and McLellan, J. (1997), Carrier Phase Based Regional Area Differential GPS for Decimetre-Level Positioning and Navigation. In Proceedings of the 10th International Technical Meeting of the Satellite Division of the Institute of Navigation (ION GPS 97), pages 1305-1313, Kansas City, Missouri.

Goad, C.C. (1992), Robust Techniques for Determining GPS Phase Ambiguities, Proc 6th Geodetic Symposium on Satellite Positioning, pp. 246-254.

Han, S. and Rizos, C. (1996a), Integrated Method for Instantaneous Ambiguity Resolution Using New Generation GPS Receivers, IEEE PLANS'96, pp. 254-261, Atlanta.

Han, S. and Rizos, C. (1996b), GPS network design and error mitigation for Real-Time Continuous Array Monitoring Systems. In Proceedings of the 9th International Technical Meeting of the Satellite Division of the Institute of Navigation (ION GPS-96), Kansas City, Missouri, pp.1827-1836.

- Hatch, R. (1982), The Synergism of GPS Code and Carrier Phase Measurements. In Proceedings of the 3rd Geodetic Symposium on Satellite Positioning, Las Vegas, New Mexico, Vol 2, pp. 1213-1231.
- Hatch, R (1989), Ambiguity Resolution in the Fast Lane, ION GPS 89, In Proceedings of ION GPS-89, Colorado Springs, Colorado, September 27-29, pp. 45-50.
- Hatch, R. (1990), Instantaneous Ambiguity Resolution. In Kinematic Systems in Geodesy, Surveying, and Remote Sensing, Eds Schwarz, KP, Springer, pp. 299-308.
- Hatch, R. (1991), Ambiguity Resolution while Moving-Experimental Results. In Proceedings of ION GPS 91, Albuquerque, New Mexico, September, pp. 707-713.
- Hegarty et al. (2001), Scintillation Modelling for GPS-Wide Area Augmentation System Receivers, Radio Science, Vol. 36, No. 5, pp. 1221-1231.
- Hopfield, H.S. (1970), Tropospheric Effect on Electromagnetically Measured Range: Prediction from Surface Weather Data, Applied Physics Laboratory, Johns Hopkins University, Baltimore, MD.
- Hopfield, H.S. (1972), Tropospheric Range Error Parameters-Further Studies, Applied Physics Laboratory, Johns Hopkins University, Baltimore, MD.

IGS (2001), IGS Product Table. International GPS Service, <http://igsb.jpl.nasa.gov/components/prods.html>, extracted on Dec 18th, 2002.

Kaplan, D (1996): Understanding GPS Principles and Applications, Artech House Publishers, Boston, pp. 351.

Klobuchar, J.A. (1986), Design and Characteristics of the GPS Ionospheric time-delay algorithm for single-frequency users. In Proceedings of PLANS'86-Position Location and Navigations symposium, Las Vegas, Nevada, November, pp 280-286.

Klobuchar, J.A. et al. (1995), Potential Ionospheric Limitations to GPS Wide Area Augmentations System. In Navigation, Journal of the Institute of Navigation, Vol 42. 1995.

Klobuchar, J.A. (1996), Ionospheric Effects on GPS. In Global Positioning System, Theory and Application, Vol 1, Eds, Parkinson, B. and Spilker, J., American Institute of Aeronautics and Astronautics, Inc., pp. 485-514.

Lachapelle, G. (2000), GPS Theory and Applications. ENGO625 Lecture Notes, Department of Geomatics Engineering, The University of Calgary.

Langley, R.B. (1996), GPS Receivers and the Observables, in GPS for Geodesy, Eds P.J.G.Teunissen, A. Kleusberg, Springer, pp. 181-182.

Lanyi, G. (1984), Tropospheric Delay Effects in Radio Interferometry, Telecommunications and Data Acquisition Progress Rep., Jet Propulsion Lab, Pasadena, CA.

Liu, G. (2001), Ionosphere Weighted Global Positioning System Carrier Phase Ambiguity Resolution, MSc. Thesis, Department of Geomatics Engineering, University of Calgary, Calgary.

Lu, G. (1995), Development of a GPS Multi-Antenna System for Attitude Determination, Ph.D. thesis, Department of Geomatics Engineering, The University of Calgary.

Lu, G., Cannon, M.E., Chen, D., and G. Lachapelle (1994), FLYKINTM Operator's Manual, version 2.0. Department of Geomatics Engineering, The University of Calgary.

Odijk, D. (2000), Stochastic Modelling of the Ionosphere for Fast GPS Ambiguity Resolution, In Geodesy Beyond 2000, IAG General Assembly, Eds. K.P. Schwarz, Springer Verlag, Berlin, 2000, Vol. 121, pp. 387-392.

Parkinson, B.W. (1996), GPS Error Analysis, in Global Positioning System: Theory and Applications Volume 1, Eds. Parkinson, B., Spiker, J., Axelrad, P., Enge, P., American Institute of Aeronautics and Astronautics, pp. 469-483.

Raquet, J. (1998), Development of a Method for Kinematic GPS Carrier-Phase Ambiguity Resolution Using Multiple Reference Receivers. Ph.D. Thesis, University of Calgary, Department of Geomatics Engineering Report Number 20116, Calgary 1998.

Roulston, A. et al. (2000), An Evaluation of Various GPS Satellite Ephemerides, In Proceedings of ION GPS 00, Salt Lake City, pp. 45-54.

Saastamoinen, J. (1972), Atmospheric Correction for the Troposphere and stratosphere in Radio Ranging of Satellites, Geophysical Monograph 15, American Geophysical Union, Washington DC.

Schaer, S. (1999), Mapping and Predicting the Earth's Ionosphere Using the Global Positioning System, Ph.D. Dissertation, Astronomical Institute, University of Berne, Berne, Switzerland.

Seeber, G. (1993) Satellite Geodesy, Foundations, Methods, and Applications. Walter de Gruyer.

Skone, S. (1998), Wide Area Ionosphere Grid Modelling in the Auroral Region, Ph.D. thesis, Department of Geomatics Engineering, University of Calgary, Calgary, AB

- Skone, S. (2001), Atmospheric Effects on Satellite Navigation Systems. ENGO 699.56
Lecture Notes, Department of Geomatics Engineering, The University of Calgary,
2001.
- Spilker, J.J., Jr. (1994), Tropospheric Effects on GPS, in Global Positioning System:
Theory and Applications Volume 1, Eds. Parkinson, B., Spiker, J., Axelrad, P, Enge,
P., American Institute of Aeronautics and Astronautics, pp. 517-546.
- Teunissen, P.J.G. (1993), Least squares estimation of the integer GPS ambiguities, Paper
presented at the General Meeting of the IAG at Beijing, P.R.China, August 8-13.
- Teunissen, P.J.G. (1997) The Geometry-Free GPS Ambiguity Search Space with a
Weighted Ionosphere, Journal of Geodesy, Vol. 71, No. 6, pp. 370-383.
- Teunissen, P.J.G. (1998a), Success Probability of integer GPS ambiguity rounding and
bootstrapping, Journal of Geodesy, Springer-Verlag 1998, Vol 72, pp.606-612.
- Teunissen, P.J.G. (1998b), GPS for Geodesy, 2nd Edition, Springer, Eds Teunissen P.J.G.
and Kleusberg, A.
- Universität Bern (2000), Bernese GPS Software Version 4.2 Manual, Astronomisches
Institut, Universität Bern, Bern, Switzerland.

- van der Marel, H. (1998), Virtual GPS Reference Stations in the Netherlands, In Proceedings of ION GPS 98, Nashville, pp. 49-58.
- Varner, C. and Cannon, M.E. (1997), The Application of Multiple Reference Stations and the Determinations of Multipath and Spatially Decorrelating Errors. In Proceedings of the National Technical Meeting of the Institute of Navigation (ION NTM-97), Santa Monica, California, pp. 323-333.
- Wanninger, L. (1993), Effects of Equatorial Ionosphere on GPS, in GPS World, Advanstar Communication, pp. 48-54.
- Wanninger, L. (1995), Improved ambiguity resolution by regional differential modelling of the ionosphere. In Proceedings of the 8th International Technical Meetings of the Satellite Division of the Institute of Navigation (ION GPS-95), Palm Springs, California, pp. 55-62.
- Wells, D., Beck, N., Delikaraoglou, D., Kleusberg, A., Kraviswisky, E.J., Lachapelle, G., Langley, R., Nakiboglu, M., Schwarz, K.P., Tranquilla, J.M., and Vanicek, P. (1986), Guide to GPS Positioning. Canadian GPS Associates, Fredericton, 1986.
- Wubbena, G. et al. (1996), Reducing Distance Dependent Errors for Real-Time Precise DGPS Applications by Establishing Reference Station Networks. In Proceedings of ION GPS 96, Kansas City, September 1996. pp. 1845-1852.

APPENDIX: QUALITY CONTROL IN GPS CARRIER PHASE POSITIONING

GPS signals travel an average distance of 20200 km to reach the receiver. During this long journey, the signal attenuation due to the atmosphere results in various measurement biases, such as troposphere error and ionosphere error. The magnitude of these errors is generally dependent on the elevation angle of the satellite. The higher the elevation, the less those biases are. Because of this, the elevation dependant variance-covariance modelling is employed in the software. A mapping function is used to relate the precision of the measurement made at the zenith direction to any elevation. The simplest mapping function is $\sin(E)$, where E is the elevation angle.

Besides the atmospheric biases, the measurement is also susceptible to blunders. The most two common blunders are carrier phase cycle slips and code multipath. In carrier phase based double differenced positioning, the code multipath is generally less critical than carrier phase cycle slips, as the precision of the carrier phase far outweighs that of the code observables. Carrier phase cycle slips are very critical in carrier phase based positioning as undetected cycle slips will cause a discrepancy between measurement and states being estimated and will lead to large position error. Cycle slips can occur as a consequence of several reasons, such as obstruction between receiver antenna and satellite, high dynamics of the receiver carrier, and ionospheric scintillation, to name a few. The detection of the cycle slip used in the software FLYKIN+TM is based on the Kalman filter's innovation sequence testing (Teunissen, 1998b).

Figure A1 shows a standard linearized Kalman filter loop. The innovation sequence v is generated by subtracting the predicted measurement from the actual measurement. A property of the Kalman filter is that if the system driving noise is white, then innovation sequence v will follow a zero mean Gaussian distribution with dispersion C_v , namely

$$v \sim (0, C_v) \quad (1)$$

Based on the property of the innovation sequence, two hypotheses can be made.

$$\begin{aligned} H_0 : E\{v\} &= 0 \\ H_1 : E\{v\} &= \nabla \end{aligned} \quad (2)$$

where ∇ represents the model error vector (cycle slips, multipath, etc.).

Based on the null hypothesis H_0 and the alternative hypothesis H_1 , a test statistic can be constructed. The test statistic reads

$$t = \frac{v^T C_v^{-1} v}{m} \quad (3)$$

where m is the number of observables in the Kalman filter.

The expectation of this test statistic is 1 if the null hypothesis is true. Thus if the following inequality holds true, then the alternative hypothesis will be accepted instead of the null hypothesis.

$$T > F_a(m, \infty, 0) \quad (4)$$

where F is the fisher distribution with the chosen significance level \mathbf{a} .

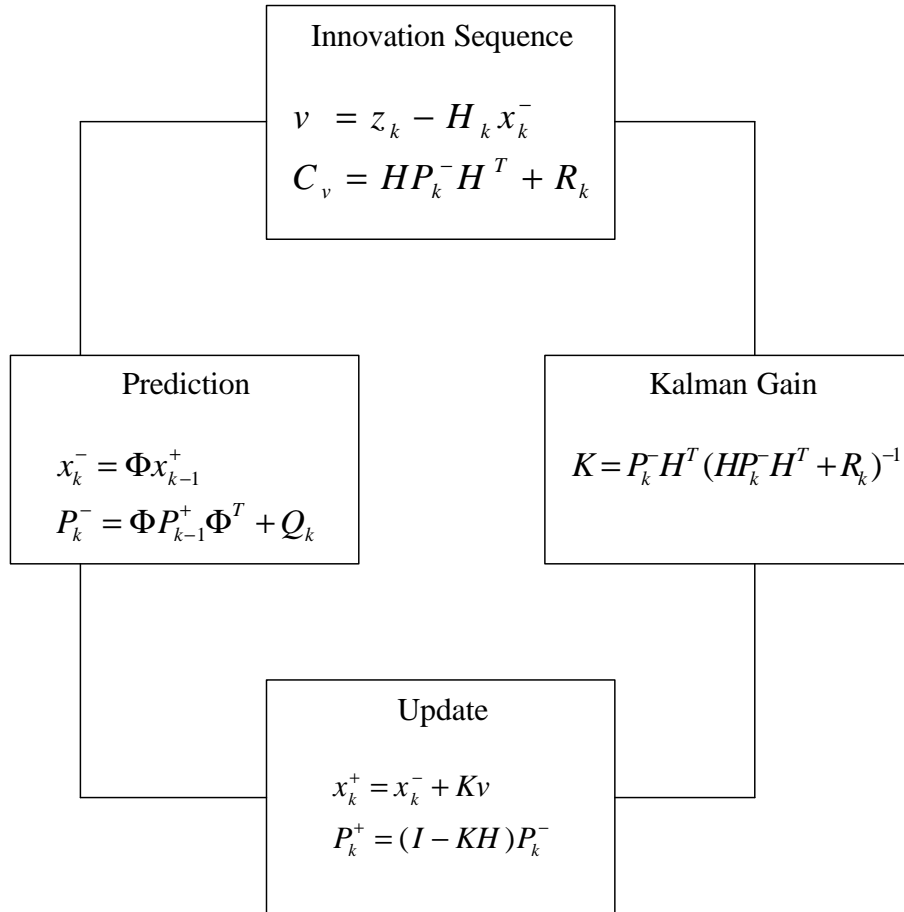


Figure A1 Linearized Kalman Filter Loop

If the test statistic alerts that the null hypothesis is wrong and the alternative hypothesis should be used, then further steps are needed to identify which observable is the problem. Another test statistic should be used. Assume that there is only one observable bias at one epoch, this statistic reads

$$t^k = \frac{c_k^T C_v^{-1} v}{\sqrt{C_v^{-1}[k][k]}} \quad (5)$$

where $c_k = \{0, 0, \dots, 0, 1, \dots, 0, 0\}$ means the k th observable is tested against possible measurement biases. t^k follows a $N(0,1)$ distribution if all the observables at this epoch are free of any biases. This test is repeated for every observable $k = 1, 2, \dots, m$. The largest $|t^k|$ will indicate the most likely biased observable. The test statistics is then compared with the critical value of $N_{\alpha/2}(0,1)$, where α is the chosen level of significance. If the largest $|t^k|$ exceeds the critical value, then that observable is to be rejected. The power of this test statistics is dependant on its minimum detectable bias (MDB), which reads

$$MDB = \sqrt{\frac{I_0}{C_v^{-1}[k][k]}} \quad (6)$$

where I_0 is a function of the chosen level of significance α , the power of the test β , and the degrees of freedom in the estimation model.

A numerical example is shown below to demonstrate this method. A three-minute single frequency GPS data was processed. Figure A2 shows the sky plot during that three-minute interval. The data have been analyzed and no actual carrier phase cycle slip was found. Six artificial cycle slips were added to the data at GPS Time 21, 41, 61, 81, 101, and 121. The magnitude of these artificial cycle slips is all -1. Both baseline and ambiguity states were estimated using L1 carrier phase observable. The level of significance, α , was chosen as 0.001 and the power of the test β was set to 0.8 for the

test. The identification results are depicted in Figure A3. The six spikes represent that all of the cycle slips were correctly identified.

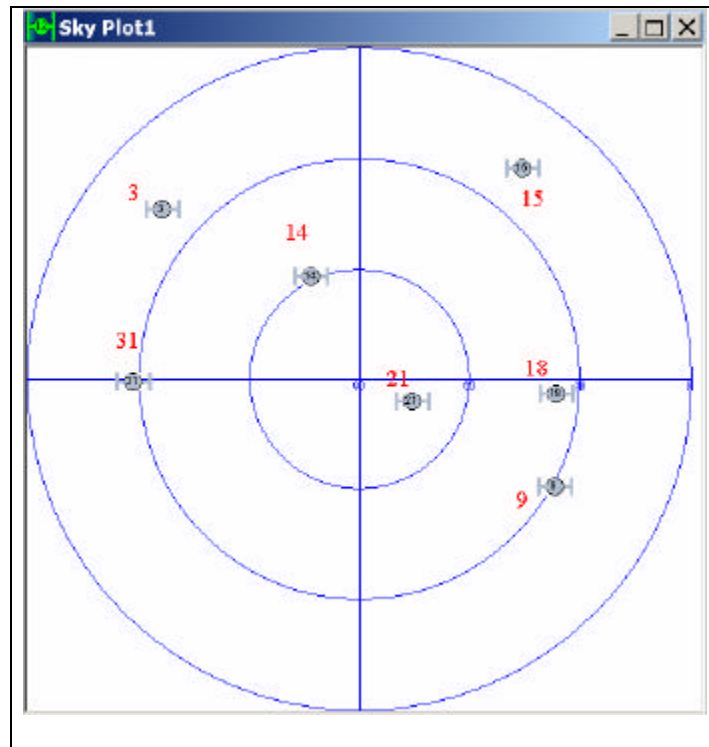


Figure A2 Sky Plot

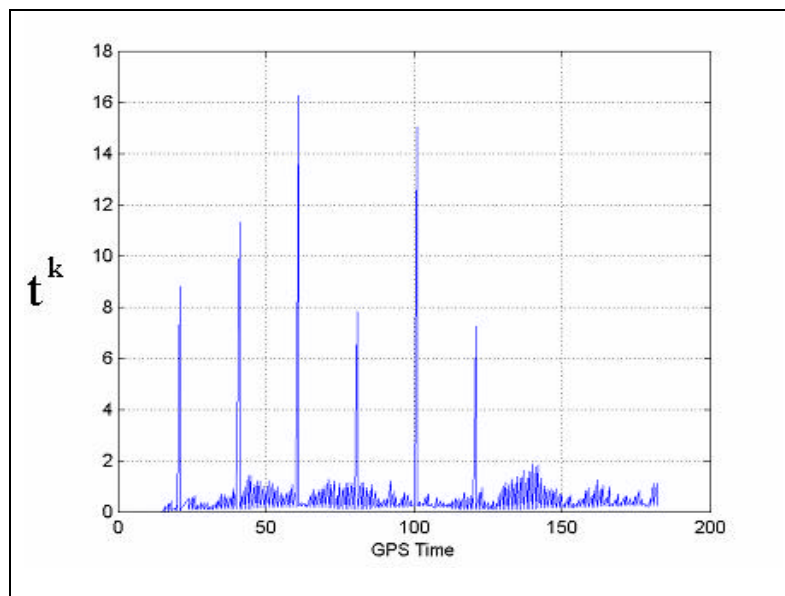


Figure A3 Test Statistics t^k versus GPS Time

Table A1 shows the simulated cycle slip N , its estimated value \hat{N} and the MDB. MDB is dependant on many factors, such as the precision of the measuring equipment and the geometry. It is clear that from the table that the MDB is highly correlated with the elevation. The higher the satellite elevation is, the smaller the MDB is.

Table A1 Carrier Phase Cycle Slips Detection Summary

Epoch(sec)	PRN	N (cycle)	\hat{N} (cycle)	MDB(cycle)	Elevation
21	3	-1	-1.00	0.47	19
41	9	-1	-0.95	0.35	29
61	14	-1	-1.03	0.26	59
81	15	-1	-1.05	0.56	17
101	18	-1	-1.02	0.28	36
121	31	-1	-0.95	0.54	29

This innovation test usually assumes that there is at most one cycle slip at the same epoch. If there are two cycle slips at the same epoch, this method may not give correct results. To demonstrate this, the same data was used. Instead of adding one cycle slip at one epoch, two simultaneous cycle slips were added to two different satellites. The magnitude of these cycle slips is all -1 . The table below shows the actual cycle slip and corresponding epochs.

Table A2 Simulated Cycle Slips

Epoch(sec)	PRN	N (cycle)	PRN	N (cycle)
21	3	-1	9	-1

41	9	-1	14	-1
61	14	-1	15	-1
81	15	-1	18	-1
101	18	-1	31	-1
121	31	-1	3	-1
121	21	-1	N/A	N/A

The table below shows the identification process. The identification result is not good at all. For example, at epoch 21, it is PRN 3 and PRN 9 that contains the cycle slips, while the innovation test reports PRN 31 to contain a cycle slip. The cycle slip of PRN 9 is detected at epoch 24, which is 4 epochs past the actual time. The cycle slip of PRN 3 is never detected. Another interesting thing to note is that at epoch 141 a cycle slip with magnitude of -1 is added to the reference PRN 21 (which means all the DD ambiguities suffer from cycle slips). The innovation sequence statistics report that PRN 14 is biased at epoch 141 and PRN 9 is biased at epoch 142. The limitation of this innovation testing is clearly exemplified.

Table A3 Detected Cycle Slips

Epoch	PRN Identified	\hat{N} (cycle)	MDB
21	31	1.82	0.57
24	9	-0.4	0.43
41	14	-1.48	0.26

42	9	-0.83	0.46
61	14	-0.75	0.26
62	15	-1.06	0.65
81	9	1.02	0.35
82	14	-0.38	0.35
101	18	-1.15	0.27
102	15	-0.72	0.74
121	14	0.24	0.26
141	14	0.9	0.26
142	9	-0.48	0.47